

Let it flow

Hemodynamics of pulmonary artery
stenosis in congenital heart disease

Let it flow - Hemodynamics of pulmonary artery stenosis in congenital heart disease
Maartje Conijn

ISBN: 978-94-6458-149-2

Provided by thesis specialist Ridderprint, ridderprint.nl

Printing: Ridderprint

Layout and design: Rowen Aker, persoonlijkproefschrift.nl

Copyright 2021 © Maartje Conijn

The Netherlands. All rights reserved. No parts of this thesis may be reproduced, stored in a retrieval system or transmitted in any form or by any means without permission of the author.

Let it flow

Hemodynamics of pulmonary artery stenosis in
congenital heart disease

Laat het stromen

Hemodynamica van pulmonaal arterie stenose bij aangeboren
hartafwijkingen
(met een samenvatting in het Nederlands)

Proefschrift

ter verkrijging van de graad van doctor aan de
Universiteit Utrecht
op gezag van de
rector magnificus, prof.dr. H.R.B.M. Kummeling,
ingevolge het besluit van het college voor promoties
in het openbaar te verdedigen op

donderdag 2 juni 2022 des middags te 2.15 uur

door

Maartje Conijn

geboren op 19 juni 1991
te Sint-Oedenrode

Promotoren:

Dr. J.M.P. Breur

Prof. dr. F. Haas († 2022)

Copromotor:

Dr. G.J. Krings

Financial support by the Dutch Heart Foundation for the publication of this thesis is gratefully acknowledged.

Table of contents

Chapter 1	General introduction and thesis outline	7
Part I		
Chapter 2	10-years' single center experience in percutaneous treatment of pulmonary artery stenosis in congenital heart disease: initial results, long-term outcomes and lessons learned	15
Chapter 3	Computational analysis of the pulmonary arteries in congenital heart disease – A review of the methods and results	37
Part II		
Chapter 4	Understanding stenotic pulmonary arteries, can Computational Fluid Dynamics help us out?	63
Chapter 5	Flow distribution and velocity measurements in transposition of the great arteries: a comparison between computational fluid dynamics and four-dimensional flow cardiac magnetic resonance	83
Part III		
Chapter 6	To treat or not to treat pulmonary arteries? Epinephrine provocation to unmask right ventricular load	103
Chapter 7	Pulmonary artery stenosis and valve insufficiency in Tetralogy of Fallot – A flow analysis pre and post treatment	123
Chapter 8	The Y-stenting technique for pulmonary artery bifurcation stenosis: Initial results and mid-term outcomes	143
Chapter 9	The hemodynamic impact of an oval versus cylindrical stent shape to prevent compression of adjacent structures in complex pulmonary artery stenting	161
Part IV		
Chapter 10	A 3D printed pulmonary mock loop for hemodynamic studies in congenital heart disease	179
Chapter 11	General discussion	197
Appendix	Nederlandse samenvatting	208
	List of publications	214
	Review committee	216
	Dankwoord	218
	Curriculum vitae	222



**GENERAL INTRODUCTION AND THESIS
OUTLINE.**

INTRODUCTION

Congenital heart disease (CHD) is the general term used for birth defects affecting the anatomy and function of the heart. With an incidence of 8 per 1000 live births, CHD is the most common birth defect.¹ Pulmonary artery (PA) stenosis is an abnormal narrowing in (one of) the pulmonary branches that occurs in 2-3% of all patients with CHD.² There is a large heterogeneity in causes, location and severity of PA stenosis. It may occur as a native lesion, either with or without additional cardiac abnormalities, but may also be a result of –multiple– surgical intervention(s) in the area of the pulmonary arteries. The stenosis may be on one, or on multiple locations over the PA tree.³ Severe PA stenosis with an increased right ventricular (RV) afterload causes elevation of the RV pressure with eventually RV hypertrophy and a diminished ventricular function. Symptoms of RV failure occur when the RV is seriously affected, either (sub)acute if lesions are caused by cardiac surgery or late in chronic lesions. In chronic lesions patients are often unaware of symptoms due to the slow decline in exercise tolerance and self-limitation. If left untreated, PA stenosis may result in lung underdevelopment, impaired exercise tolerance, arrhythmias and even sudden cardiac death.⁴

PA stenosis can be treated either surgically by arterioplasty, or percutaneously by balloon angioplasty and stent placement. Over the last decades, the interventional options for treatment of PA stenosis have greatly improved.⁵ Percutaneous treatment is minimal invasive, resulting in shorter hospital stays and easier recovery compared to open heart surgery. Surgical treatment of PA stenosis is therefore nowadays reserved for patients for whom there are no interventional options or for patients requiring surgery for additional cardiac lesions.^{2,5-7}

To optimize the timing and approach of treatment, a thorough evaluation of the anatomy and hemodynamic state of patients with PA stenosis is essential. Echocardiography is often the first step in the assessment of the pulmonary arteries. It provides information on the dimensions of the proximal arteries and on the function and pressure load of the RV. If necessary, Computed Tomography Angiography (CTA) and Cardiac Magnetic Resonance (CMR) provide additional information on the (3D) anatomy and volumes of the RV and PA branches. Based on the outcomes of the non-invasive evaluation, patients may be referred for cardiac catheterization with invasive assessment and treatment of the PA stenosis. Indications for treatment of PA stenosis include a gradient of >20 mmHg over a stenosis, a right to left ventricular pressure

ratio >0.6 and $<40\%$ flow to the affected branch.⁸ During cardiac catheterization, besides the invasive hemodynamic assessment of RV and arterial pressure, the anatomy can be visualized with 2D and 3-dimensional (3D) (rotational) angiography.

The use of (multi-modality) 3D imaging improves understanding of PA stenosis and the interaction between the pulmonary arteries and adjacent structures in the chest. What is happening with the flow of blood inside the arteries is less understood. The current imaging techniques are unable to provide in depth information on behavior of flow and the effect of a stenosis on hemodynamics. Studying flow patterns and hemodynamic parameters is essential to enhance our knowledge of causes of CHD and to improve diagnosis and treatment of PA stenosis. Over the last years, tools that are able to visualize and quantify blood flow are emerging. One of these is Computational Fluid Dynamics (CFD). CFD is an engineering tool for visualization and quantification of flow in complex geometries. With use of mathematics and physics, flow in a 3D reconstructed fluid domain is simulated. Nowadays, it is increasingly used for the evaluation of blood flow in congenital and acquired cardiac disease.^{9,10} CFD provides high resolution information on blood flow over the complete cardiac cycle with the possibility of simulating different treatment approaches and varying conditions of load, i.e. rest and exercise.

THESIS OUTLINE

This thesis studies hemodynamics of normal and obstructed pulmonary arteries. Part I, **chapter 2**, evaluates the initial outcomes and long-term results of interventional treatment of PA stenosis with an emphasis on (risk factors for) re-interventions. The chapter demonstrates the heterogeneity of PA stenosis and the additional value of 3D imaging in the catheterization room to prevent re-interventions. **Chapter 3** provides a general introduction on CFD methods for evaluation of flow in the pulmonary arteries. The available literature on this subject is reviewed, which shows the wide variety in applied CFD methods. In part II, the method for the CFD studies in this thesis is outlined. The outcomes of CFD simulations in pulmonary arteries with and without stenosis are compared to cardiac catheterization, CMR (**chapter 3**) and 4D flow CMR measurements (**chapter 4**). Part III describes interventional approaches for complex PA stenosis and the dilemmas in timing of treatment. In **chapter 5** a new approach for the invasive evaluation of RV load in PA stenosis is introduced. It demonstrates the use of epinephrine to counteract the hypotensive properties of general anesthetics

applied during cardiac catheterization. This prevents underestimation of pressure load and possible under treatment of PA stenosis. In **chapter 6** the clinical challenge of PA stenosis in combination with pulmonary valve regurgitation is computationally explored. The effect of stent placement on branch regurgitation and the additional hemodynamic impact of valve placement in these patients is evaluated. **Chapter 7** describes the Y-stenting technique for stenting of complex stenosis in the PA bifurcation. In **Chapter 8** the hemodynamic impact of the traditional cylindrical stent shape is compared to the novel oval stent shape with use of CFD. Oval stent implantation is beneficial in patients with PA stenosis in whom stenting the stenosis would lead to compression of adjacent structures as the bronchus or aorta. In part IV, **chapter 9**, our in house build mock loop is described and evaluated. This mock loop mimics the pulmonary circulation and enables future hemodynamic studies in a controllable environment without burden and risks for patients.

REFERENCES

1. Hoffman JJ, Kaplan S. The incidence of congenital heart disease. *J Am Coll Cardiol.* 2002;39(12):1890-1900.
2. Trivedi KR, Benson LN. Interventional strategies in the management of peripheral pulmonary artery stenosis. *J Interv Cardiol.* 2003;16(2):171-188.
3. Baum D, Khoury GH, Ongley PA, Swan HJ, Kincaid OW. Congenital stenosis of the pulmonary artery branches. *Circulation.* 1964;29:680-687.
4. Hiremath G, Qureshi AM, Prieto LR, et al. Balloon angioplasty and stenting for unilateral branch pulmonary artery stenosis improve exertional performance. *JACC: Cardiovascular Interventions.* 2019;12(3):289-297.
5. Patel AB, Ratnayaka K, Bergersen L. A review: Percutaneous pulmonary artery stenosis therapy: State-of-the-art and look to the future. *Cardiol Young.* 2019;29(2):93-99.
6. Hiremath G, Qureshi AM, Meadows J, Aggarwal V. Treatment approach to unilateral branch pulmonary artery stenosis. *Trends Cardiovasc Med.* 2021;31(3):179-184.
7. Zablah JE, Morgan GJ. Pulmonary artery stenting. *Interv Cardiol Clin.* 2019;8(1):33-46.
8. Feltes TF, Bacha E, Beekman RH, 3rd, et al. Indications for cardiac catheterization and intervention in pediatric cardiac disease: A scientific statement from the American Heart Association. *Circulation.* 2011;123(22):2607-2652.
9. DeCampi WM, Argueta-Morales IR, Divo E, Kassab AJ. Computational fluid dynamics in congenital heart disease. *Cardiol Young.* 2012;22(6):800-808.
10. Morris PD, Narracott A, von Tengg-Koblig H, et al. Computational fluid dynamics modelling in cardiovascular medicine. *Heart.* 2016;102(1):18-28.



PART I



**10-YEARS' SINGLE CENTER EXPERIENCE IN
PERCUTANEOUS TREATMENT OF PULMONARY
ARTERY STENOSIS IN CONGENITAL HEART
DISEASE: INITIAL RESULTS, LONG-TERM
OUTCOMES AND LESSONS LEARNED.**

Maartje Conijn
Martijn G. Slieker
Dorita H.P.M. Dekkers
Johannes M.P. Breur

Mirella M. Molenschot
Michiel Voskuil
Gregor J. Krings

Submitted

ABSTRACT

Background Pulmonary artery stenosis (PAS) is seen in 2-3% of all congenital heart disease (CHD) patients. In the recent era, most stenosis are treated by stent implantation or balloon angioplasty. Large reports on long-term outcomes of these procedures are limited. The aim of this study was to describe our institutional 10-years' experience in interventional treatment of PAS with an emphasis on re-interventions.

Methods For this retrospective study, all pulmonary artery interventions were included. Data on procedural details, complications, re-interventions and survival was collected and analyzed. A logistic regression was performed to identify risk factors for re-intervention.

Results 473 procedures were included (mean age 9.8 years (± 11.4)). A total of 499 stents were implanted, 312 balloon angioplasties and 84 percutaneous pulmonary valve implantations were performed. Over a five years period, 67% of the patients were free from re-intervention. Reason for re-intervention was somatic growth in 50% of the re-procedures. Intima proliferation was found in 4% of all cases. Independent risk factors for re-intervention were a low body surface area at intervention (OR 0.3 ($p < 0.001$)) and an underlying syndrome (OR 1.8 ($p = 0.026$)). The use of 3D rotational angiography (3DRA) significantly reduced the need for re-catheterization (OR no 3DRA 2.0 ($p = 0.018$)).

Conclusion Interventional treatment of PAS is associated with high rates of re-interventions. Somatic growth is the most seen reason for re-intervention. A low body surface area and an underlying syndrome are independent risk factors for re-intervention. The use of advanced imaging in the cathlab prevents the need for re-interventions.

1 INTRODUCTION

Stenosis of the pulmonary arteries is common in congenital heart disease (CHD). Of all CHD patients, 2-3% will sooner or later develop some degree of pulmonary artery stenosis (PAS).¹ PAS can be a native substrate or develop after corrective surgery. PAS is seen as an isolated lesion, but more often it is associated with other cardiac abnormalities, i.e. Tetralogy of Fallot (ToF) and pulmonary atresia (PA), Truncus Arteriosus Communis (TAC) and d-Transposition of the Great Arteries (TGA). A separate entity in PAS is the severe general hypoplasia of the pulmonary arteries.² This is often seen in patients with severe pulmonary atresia or underlying syndromes as Alagille, Williams and Noonan.³ The large variety in cause, appearance and severity makes PAS a highly heterogenic condition.

If left untreated, PAS induces pressure load on the right ventricle (RV) which may lead to impaired exercise tolerance, RV hypertrophy, RV failure and arrhythmia's. PAS can be treated either surgically or percutaneously. The surgical approach of PAS is often technically challenging and is associated with risk of early restenosis.⁴ Therefore, nowadays surgery is reserved for patients without percutaneous options or with coexisting defects requiring surgery. The percutaneous treatment of PAS is less invasive, resulting in shorter hospital stays and faster recovery. Due to the introduction of stents and balloons suitable for interventions in small children and the use of multimodality, three dimensional (3D) imaging, a wide variety of (complex) stenosis can now be treated percutaneously.⁵ However, in the –pediatric- CHD population the implantation of stents needs to be carefully considered in the face of possible follow-up surgeries. Also, due to somatic growth or restenosis patients may require multiple re-interventions.

Previous studies have reported on the success rates and outcomes of either stent placement or balloon angioplasty of unilateral or bilateral PAS.⁶⁻¹² Large reports on the initial and long-term outcomes of both balloon angioplasty and stent placement over the whole PAS spectrum are missing. The aim of this study is to describe our 10-year, single center experience in percutaneous treatment of PAS with an emphasis on long-term outcomes and need for re-interventions.

2 MATERIALS AND METHODS

2.1 Patient selection

The present study was a single center study with a retrospective, observational design. All cardiac catheterizations between January 2011 and June 2021 were screened. Interventional procedures with balloon angioplasty, stent placement or valve implantation in one of the pulmonary branches or the main pulmonary artery were included. Balloon angioplasty of the pulmonary valve in neonates with isolated pulmonary valve stenosis was excluded as well as interventions in aorta-pulmonary or Sano shunts and ductal stents.

Indication for treatment was primarily based on echocardiographic findings, if necessary complemented by Cardiac Magnetic Resonance (CMR) and Computer Tomography (CT) images. In our center, nowadays, CMR has replaced the ventilation-perfusion scintigraphy's to determine the right to left pulmonary artery perfusion. When an indication for treatment was present, the patient was referred to the cathlab after multidisciplinary deliberation. All procedures were performed under general anesthesia. Patients received Heparine (100 u/kg) with ACT measurements every 30 minutes (target ACT 180-220s). Antibiotics (Cefazolin) was routinely administered when stent implantation was performed. Post-intervention, patients received acetylsalicylic acid in case of a stent diameter <8mm. Additional Clopidogrel was prescribed in selected cases of neonates with severe PAS or patients with general hypoplasia of the pulmonary arteries. In univentricular patients a vitamin K antagonist was considered.

2.2 Ethical considerations

This study was approved by the Institutional Ethics Committee of our hospital. Due to the retrospective, observational and extensive design of this study, patient informed consent was waived.

2.3 Data collection

Data on three major areas was collected. First, baseline information was registered including age and weight at intervention, diagnosis, prior cardiac surgery and prior catheterization. Second, procedural details on location(s), pressure measurements and used materials were recorded. Finally, information on immediate outcomes including pressure reduction and complications and long-term outcomes including survival, re-interventions and surgeries was collected. Complications were subdivided in two groups: during intervention and post-intervention and further subdivided in major

and minor complications. Major complications were defined as an event requiring resuscitation, unplanned surgery, major bleeding including perforations treated with a covered stent, device embolization, embolic stroke, air embolus and an airway event requiring intubation. Minor complications included all other unplanned events for which no treatment or mild treatment was necessary including recurrent inguinal hemorrhage, vocal cord paresis and rhythm problems without the need for resuscitation. Re-intervention was defined as the first intervention in the follow-up in which the same location was treated as during the initial procedure. Re-surgery was defined as the first surgery in which the same location was treated as during the initial procedure.

2.4 Statistical analysis

Statistical analysis was performed using IBM SPSS Statistics (version 26.0.0.1). Unless stated otherwise all numbers are presented as mean (\pm Standard Deviation). Statistical differences between pre- and post-interventional pressures were calculated using a paired T-test. Logistic regression analysis was used to determine factors contributing to the probability for re-intervention. An univariate analysis was performed using a univariate logistic regression model. Statistic significant determinants ($p < 0.05$) were then included in a multivariate analysis using a forward logistic regression strategy. Only determinants with $>5\%$ missing values were included in the multivariate analysis.

As patients could be included more than once, cases or procedures are described instead of patients. Only survival outcomes are presented for individual patients. As in univentricular patients pressure gradients and RV pressure may not be representative for procedural outcomes, pressure results are shown for biventricular patients only.

3 RESULTS

3.1 Patient characteristics

A total of 473 eligible cases involving 288 unique patients were included (60% male). All baseline characteristics are displayed in table 1. Mean age of the patient population was 9.8 years (± 11.4). In about half of the procedures the patient was below 10 years of age. The most common diagnosis was PA (20.9%), followed by ToF (20.3%) and d-TGA (12.9%). Almost all patients had prior surgery (91.1%) and 71.7% of the patients had a cardiac catheterization in their medical history. 38.5% had a prior stent in one of the pulmonary arteries.

Table 1 - Baseline characteristics.

	% (N)
Gender (male)	60.0 (284)
Age	
• <1 month	3.4 (16)
• 1-12 months	12.1 (57)
• 1-5 years	26.0 (123)
• 5-10 years	19.7 (93)
• 10-16 years	18.6 (88)
• >16 years	20.3 (96)
Weight	
• 0-3 kg	1.3 (6)
• 3-10 kg	19.0 (90)
• 10-25 kg	36.8 (174)
• 25-50 kg	22.2 (105)
• >50 kg	20.7 (98)
Diagnosis	
• PA	20.9 (99)
• ToF	20.3 (96)
• d-TGA	12.9 (61)
• HLHS	8.9 (42)
• Native PPS	7.8 (37)
• Post-Ross	7.6 (36)
• TAC	5.9 (28)
• Valvar PS	4.9 (23)
• cc-TGA	2.7 (13)
• HLHC	1.7 (8)
• Other	6.3 (30)
Biventricular	80.5 (381)

Table 1 - (Continued)

	% (N)
Syndrome	19.0 (90)
• 22q11	4.4 (21)
• Alagille	4.0 (19)
• Trisomie 21	2.5 (12)
• Williams	1.9 (9)
• Noonan	0.8 (4)
Prior surgery (y)	91.1(431)
Prior catheterization (y)	71.7 (339)
Prior stent in pulmonary arteries (y)	38.5 (182)

PA: pulmonary atresia, ToF: Tetralogy of Fallot, d-TGA: dextro-Transposition of the Great Arteries, HLHS: hypoplastic left heart syndrome, PPS: peripheral pulmonary artery stenosis, TAC: truncus arteriosus communis, PS: pulmonary stenosis, cc-TGA: congenital corrected Transposition of the Great Arteries, HLHC: hypoplastic left heart complex, y: yes.

Most procedures were electively planned (97.5%), either based on findings during an outpatient clinic visit, or on findings during an admission to the (pediatric) cardiology ward. In 12.9% of the cases, the patient was already admitted to the hospital of which 47.5% at the (pediatric) intensive care unit ((P)ICU). Post-intervention, 17.5% of the patients were admitted to the (P)ICU. Most of these patients were below five years of age (75.9%) and <25 kg of weight (85.2%). 34.9% of these patients were already admitted to the (P)ICU and 19.3% was admitted to the ward prior to intervention. A quarter of the patients transported to the (P)ICU had PA (26.5%), followed by ToF (15.5%), HLHS (14.5%) and PPS (12.0%). When transported to the (P)ICU, patients were admitted there for 8.5 (\pm 16.9) days. All other patients (82.5%) were transported to the clinical ward. The length of post-procedural hospital stay for an elective procedure was 1.5 (\pm 1.8) days.

3.2 Procedures

In 75.3% of the procedures one or more stents were implanted. In 34.5% of the procedures one or more balloon angioplasties were performed and a total of 84 (17.8%) pulmonary valves were percutaneously implanted (PPVI). In 24.3% of the procedures more than one location was treated and in 27.5% of the procedures a combination of stent, balloon and/or PPVI treatment was performed. In 86.3% of the procedures a 3D rotational angiography (3DRA) was acquired and used

for treatment planning and overlay during intervention. The mean duration of an intervention was three hours and 28 minutes ($\pm 1:26$) from intubation to extubation. Overall, interventional treatment resulted in a RV pressure decrease from 63.1 (± 20) to 47.7 (± 48) mmHg ($p < 0.001$). The RV:LV pressure ratio dropped from 0.69 (± 0.22) to 0.49 (± 0.17) ($p < 0.001$) (figure 1).

3.3 Balloon angioplasty

A total of 312 balloon angioplasties were performed during 163 procedures (table 2). In 28.6% of these procedures a previous implanted stent was re-dilated. In 48.5% of the procedures, one balloon angioplasty was performed, while in 51.5%, two or more angioplasties were necessary. The target of balloon angioplasty was a LPA stenosis in 50.9% of the cases, followed by peripheral stenosis (29.4%) and RPA stenosis (27.6%). In 15 cases (3.2%) a prior implanted stent was ovally shaped by the double balloon technique.¹³ The most frequent used balloons were the Advance (Cook Medical, IN, USA) (24.0%), the CBV Balt (BARD, AZ, USA) (14.1%) and the Powerflex (Cordis Fremont, CA, USA) balloon (13.8%). Balloon angioplasty of the RPA resulted pressure gradient decrease of 15 (± 11) mmHg ($p < 0.001$). Relief of a LPA stenosis with balloon angioplasty lowered the pressure gradient with 13 (± 15) mmHg ($p = 0.004$) (figure 1).

3.4 Stent placement

A total of 499 stents were implanted during 356 procedures (table 3). In the majority of these procedures (68.8%), one stent was implanted while in 31.3% two or more stents were necessary. The most treated location was the LPA (48.6%) followed by the MPA (34.8%) and the RPA (24.4%). Only bare metal stents were implanted. The most used stent was the EV3 IntraStent Mega LD (Metronic, MN USA), of which 148 were used. Cook Formula stents 418 or 535 (Cook Medical, IN, USA) were implanted 142 times and the CP stent (NuMED, NY, USA) 76 times. 17.2% of the stents were covered. No self-expanding stents were implanted. The expanded stent diameter was below 8 mm in 25.9% of the procedures. In 10.6% of these procedures a coronary stent was implanted. In the other procedures, a 8 mm Cook Formula stent was down crimped on an Advance balloon with a smaller diameter.¹⁴ In 23 cases, the central or peripheral bifurcation was treated with the Y-stenting technique.¹⁵ Stent placement in the RPA decreased the gradient with 19 (± 14) mmHg ($p = 0.002$). Stent placement in the LPA resulted in a gradient decrease of 17 (± 13) mmHg ($p < 0.001$). Stent placement in the MPA lowered the gradient with 29 (± 18) mmHg ($p < 0.001$) (figure 1).

Table 2 - Balloon angioplasty procedures.

	% (N)
Total number of procedures with balloon angioplasty	34.5 (163)
Number of balloon angioplasty	
• 1	48.5 (79)
• 2	28.8 (47)
• ≥3	22.7 (37)
Dilatation of prior stent (y)	28.6 (90)
Location balloon angioplasty	
• Valve	11.0 (18)
• RVOT/MPA	6.1 (10)
• Bifurcation	3.7 (6)
• RPA	27.6 (45)
• LPA	50.9 (83)
• Peripheral	29.4 (48)
Used balloon	
• Advance (Cook Medical, IN, USA)	24.0 (75)
• CBV (Balt Extrusion, Montmorency, Fr.)	14.1 (44)
• Powerflex (Cordis Fremont, CA, USA)	13.8 (43)
• Coronary balloon (various)	13.8 (43)
• Atlas (Bard Peripheral Vascular inc, Tempe, USA)	11.9 (37)
• Drug eluting (Resonance GmbH, Aachen, Germ)	9.3 (29)
• Dorado (Bard Peripheral Vascular inc, Tempe, USA)	8.3 (26)
• Cutting balloon (various)	3.2 (10)
• Tyshak (NuMED Inc, NY, USA)	1.6 (5)

N: number of patients, y: yes, MPA: main pulmonary artery, RPA: right pulmonary artery, LPA: left pulmonary artery.

Table 3 - Stent procedures.

	% (N)
Total number of procedures with stent placement	75.3 (356)
Number of stents	
• 1	68.8 (245)
• 2	24.4 (87)
• ≥3	6.7 (24)
Location	
• RVOT/MPA	34.8 (124)
• Bifurcation	10.1 (36)
• RPA	24.4 (87)
• LPA	48.6 (173)
• Peripheral	12.1 (43)
Implanted stent	
• EV3 IntraStent Mega LD (Medtronic, MD, USA)	29.7 (148)
• Cook Medical Formula 418/535 (Cook Medical, IN, USA)	28.5 (142)
• CP Stent (NuMED Inc, NY, USA)	15.2 (76)
• EV3 Intrastent Max LD (Medtronic, MD, USA)	11.0 (55)
• AndraStent XXL (Andramed GmbH, Reutlingen, Germ)	5.4 (27)
• BeGraft (Bentley, Hechingen, Germ)	3.8 (19)
• Coronary stent (various)	2.6 (13)
• Cordis Palmaz Genesis (CardinalHealth, Dublin, Ireland)	2.2 (11)
• Atrium Advanta V12 (Getinge AB, Gotenborg, Sweden)	0.8 (4)
• Optimus XL (Andratec GmbH, Koblenz, Germ)	0.8 (4)
Covered (y)	17.2 (86)
Dm stent	
• ≤8 mm	25.9 (123)
• 9-16 mm	41.7 (198)
• 17-20 mm	17.5 (83)
• >20 mm	14.9 (71)
• UN	4.8 (24)
Pre-dilatation (y)	9.3 (33)
Post-dilatation (y)	55.3 (197)

RVOT: right ventricular outflow tract, MPA: main pulmonary artery, RPA: right pulmonary artery, LPA: left pulmonary artery, y: yes, UN: unknown.

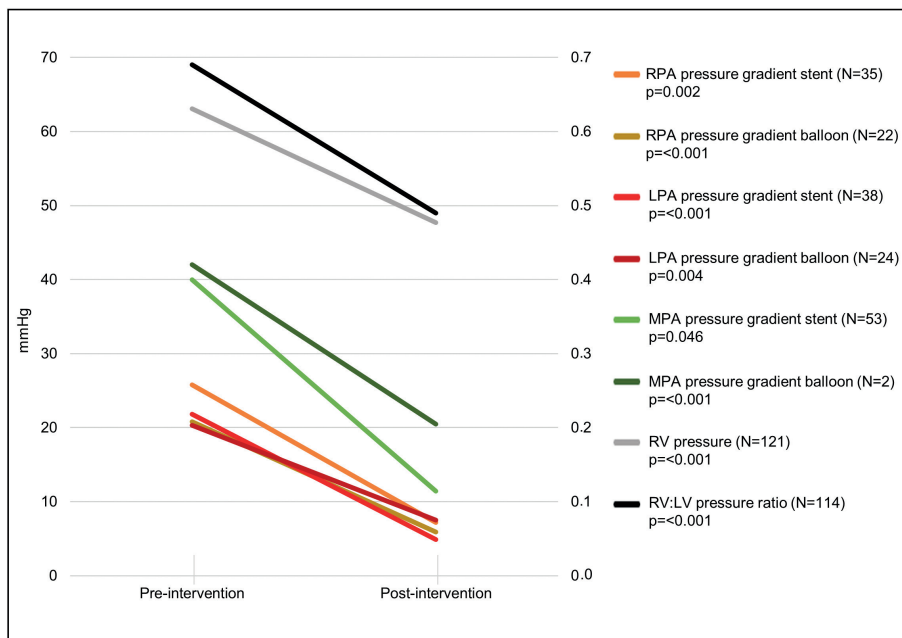


Figure 1 - Invasive measured pre- and post-interventional pressures for stent implantation and balloon angioplasty in the different locations. RPA: right pulmonary artery, LPA: left pulmonary artery, MPA: main pulmonary artery, RV: right ventricle, LV: left ventricle. The presented p-value represents the significance of the difference between the pre- and post-interventional pressure.

3.5 Complications

A total of 108 (22.8%) complications were registered. During the intervention, in 3.8% of the procedures a major complication and in 10.6% a minor complication was recorded. The major complications included nine (1.9%) lung bleedings with the necessity of post-ventilation on the (P)ICU and 11 (2.3%) resuscitation settings. Four (0.8%) of these were caused by a perforation, five (1.1%) by rhythm problems and two (0.4%) by thromboembolisms. Post-intervention a total of six (1.3%) major complications occurred. These included severe damage to the tricuspid valve with the need for surgery in one (0.2%) patient, three (0.6%) lung bleeds for which intubation and ventilation on the (P)ICU was necessary, one (0.2%) aortic-pulmonary (AP) window and one (0.2%) brain damage by a subdural hematoma developed during treatment of a thromboembolism in the LPA with anti-coagulation medication.

3.6 Follow-up

The mean follow-up was 46.7 (± 34.6) months with a minimum of 3 days and a maximum of 125 months.

3.7 Re-interventions

During follow-up, 120 (25.4%) re-interventions were performed. The time interval between the initial intervention and the first re-intervention was 29.3 (± 24.3) months. 34.1% of the re-interventions were performed within one year of the initial procedure, while over half of the re-interventions (51.7%) were performed more than two years after the initial procedure. Most re-interventions were performed in patients below 10 years of age (34.3%) and below 25 kg (35.6%). 47.8% of the patients with valvar PS had a re-intervention during follow-up, 37.8% of the patients with native PPS and 31.0% of the patients with HLHS. Patients with a syndrome needed a re-intervention more frequent compared to patients without a syndrome (37.8% and 22.5%, $p=0.003$). After 12 months, 90% of the patients was free from re-intervention (figure 2). At 5-years this was 67% and over a 10-years period, half of the patients was free from re-intervention (figure 2).

In almost half of the re-interventions (47.5%), the reason for re-treatment was relative restenosis caused by somatic growth. Intima proliferation was found in 4.4% of all cases. The majority of the patients (85.7%) with intima proliferation was below 25 kg of weight and below 10 years of age (90.5%). In 59.3% of these cases the stent diameter was less than 8mm. Intima proliferation was most frequent seen in patients with PA (28.6%) followed by patients with PPS (19.0%) and valvular PS (19.0%). In 12.8% of all Cook Medical Formula stents, intima proliferation occurred ($N_{total}=142$), in 9% of the Genesis stents ($N_{total}=11$), in 5.4% of all EV3 IntraStent Mega LD stents ($N_{total}=148$) and in 1.8% of the EV3 IntraStent Max LD stents ($N_{total}=55$). After balloon angioplasty, intima proliferation was only seen when a prior stent was dilated (23.8% of the cases with intima proliferation). Other reasons for re-intervention included a staged procedure in 3% of the cases (i.e. PPVI after pre-stenting) and severe hypoplasia of the pulmonary branches (in associated syndromes or severe PA) in 2.3%. Bronchus compression due to a LPA stent was reason for re-intervention in 1% of the cases. In most cases (56.1%) restenosis could be treated by balloon angioplasty. During 21.2% of the re-interventions an – additional- stent was implanted and a total of 20 PPVI's were performed during follow-up. After this first re-intervention, in 24 cases another procedure was necessary to re-treat the same location.

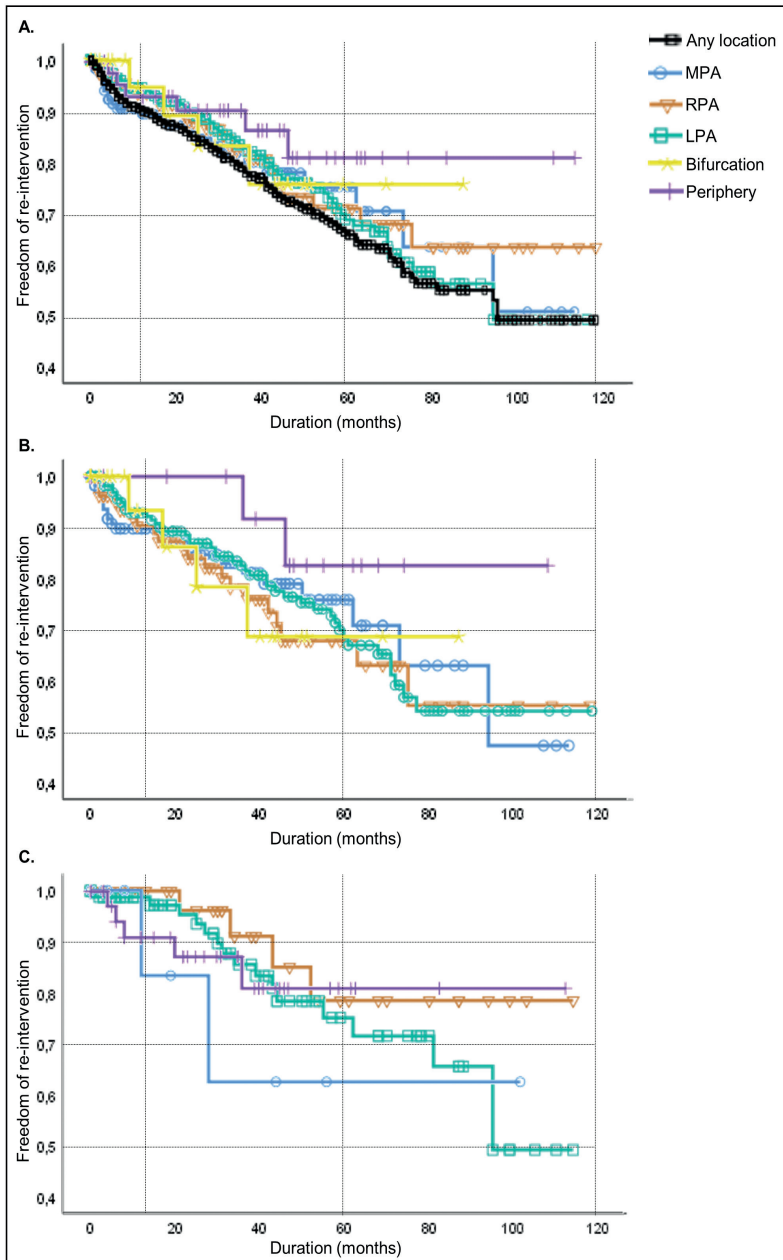


Figure 2. Kaplan-Meier curves representing the freedom of re-intervention for all interventions (A), stent implantation (B) and balloon angioplasty (C) for five locations in the pulmonary arteries. MPA: main pulmonary artery; RPA: right pulmonary artery, LPA: left pulmonary artery.

An univariate analysis identified eight determinants associated with an increased risk for re-intervention (table 4). These included three patient characteristics: younger age and lower BSA at intervention and a confirmed underlying syndrome. Procedural characteristics included the absence of the use of 3DRA. Hemodynamic factors included the RV:LV pressure ratio pre- and post-intervention and the pre-intervention RV pressure. In the multivariate analysis all these factors were included with exception of the hemodynamic factors as this information was missing for a significant portion of the procedures. The multivariate analysis identified three independent risk factors for re-intervention: lower BSA at intervention, a confirmed underlying syndrome and no use of 3DRA.

3.8 Re-surgery

During follow-up, re-surgery was performed in 25 (5.3%) cases. In half of these patients there was a preference for surgical treatment of one of the lesions identified during the initial intervention. In four (0.8%) cases the reason for surgery was an unsuccessful intervention. Other reasons for re-operation included endocarditis of the Melody valve, damage to the tricuspid valve and restenosis of a prior dilated lesion. In over half of the operated patients a homograft was electively implanted (54.3%), mostly in ToF and PA patients. In 10 cases a patch angioplasty was performed. 40% of these cases were PA patients. Other re-operations included pulmonary valve replacement, Bentall procedure and resection outflow obstruction. Mean time between intervention and re-surgery was 11.4 (\pm 13.3) months.

3.9 Survival

Of the 288 unique patients included in this study, 16 (5.6%) died during follow-up of which 13 due to a cardiac cause. Of the deceased patients, four had a univentricular heart. No periprocedural deaths were reported. Seven patients died within 30 days after the most recent procedure. In two (0.4%) patients the cause of death was directly linked to the procedure. One of them was a TGA patient after arterial switch operation who died 17 days after intervention due to an AP window which developed after complex bifurcation stenting. The second patient died of endocarditis of the Melody valve two years after PPVI implantation.

Table 4 - Univariate and multivariate analysis: risk factors for re-intervention.

	Univariate analysis		Multivariate analysis	
	OR (\pm SD)	P value	OR (\pm SD) [†]	P value
Age				
• 0-10 years	4.0 (\pm 0.4)	<0.001*		
• 10-16 years	1.0 (\pm 0.5)	0.9		
• >16 years	1.00			
BSA (m²)[#]				
	0.2 (\pm 0.3) [†]	<0.001*	0.3 (\pm 0.3) [†]	<0.001*
Syndrome diagnosis[#]				
	2.1 (\pm 0.3)	0.003*	1.8 (\pm 0.3)	0.026*
Univentricular anatomy				
	1.1 (\pm 0.3)	0.7		
Location intervention				
• Unilateral	1.0	0.2		
• Main	0.7 (\pm 0.3)	0.4		
• Bilateral	1.3 (\pm 0.3)	0.6		
• Bifurcation	0.8 (\pm 0.4)	0.9		
• Main + unilateral	0.9 (\pm 0.5)	0.2		
• Main + bilateral	2.3 (\pm 0.2)			
Number of locations treated				
	1.2 (\pm 0.1) [†]	0.2		
No 3D rotational angiography[#]				
	2.1 (\pm 0.3)	0.010*	2.0 (\pm 0.3)	0.018*
RV:LV pressure ratio				
• Pre-intervention ^{††}	4.9 (\pm 0.5) [†]	0.003*		
• Post-intervention ^{††}	24.0 (\pm 1.3) [†]	0.012*		
RV pressure (mmHg)				
• Pre-intervention ^{††}	1.0 (\pm 0.01) [†]	0.053		
• Post-intervention ^{††}	1.0 (\pm 0.01) [†]	0.021*		

OR: odds ratio, SD: standard deviation, BSA; body surface area, RV: right ventricle, LV: left ventricle. *p<0.05. [#]Variable included in multivariate logistic regression model. [†]OR represents increase of 1 in clinical value. ^{††}Not included in multivariate logistic regression model due to missing values: RV:LV pressure ratio pre-intervention N=356, post-intervention N=115, RV pressure pre-intervention N=407, post-intervention N=127. Re-intervention defined as first intervention after the initial intervention in which the same lesion is treated as during initial intervention. Categories with an OR of 1.00 represent the reference group for the other categories in the variable.

4 DISCUSSION

This study describes procedural details and long-term outcomes of a large cohort percutaneous treated patients with stenosis of the pulmonary arteries. To the best of our knowledge, this is the most extensive single center study describing both stent placement and balloon angioplasty for PAS. The four most relevant findings are: 1) PAS is a highly heterogeneous – not seldom complex- lesion in often young patients, requiring comprehensive interventions, 2) over 30% of the patients will need re-intervention(s) within five years after the initial procedure, 3) due to the young age of a large portion of the PAS population, somatic growth is an important reason for re-intervention, and 4) the use of advanced imaging in the cathlab prevents the need for re-interventions.

4.1 Patients with pulmonary artery stenosis

In retrospect, our cohort of patients with PAS in need for intervention, could be subdivided in five groups. First, the group of patients within the first year of life in whom intervention can prevent, or postpone, surgery. In example RV outflow tract stenting in ToF, PA and severe valvar PS. The second group consists of small infants who develop severe PAS with hemodynamic disruption shortly after corrective surgery. In the third group are patients with a single ventricle in stage two or three of palliation. In these patients, optimizing the pulmonary artery geometry allows the passive, breath dependent, blood flow to be the most efficient. The fourth group consists of patients with severe general pulmonary hypoplasia in combination with an underlying syndrome as Williams and Alagille. Intervention in the hypoplastic pulmonary arteries of these patients is often a strategy to support distal pulmonary artery growth rather than treatment of a single lesion. Lastly, there is the group of patients years after surgical correction, and/or previous interventions, requiring intervention due to (re)stenosis of one of the pulmonary arteries.

4.2 Re-interventions

The possible need for re-intervention after percutaneous pulmonary artery treatment is often topic for debate. Especially for the young CHD population, stent implantation needs to be carefully considered in the face of somatic growth. Previous reported rates of restenosis after percutaneous treatment of PAS vary between 25% and 68%.^{7,8,12,16,17} In our cohort, three quarters of the patients had a prior cardiac catheterization and 25% of the patients revisited the cathlab during follow-up. Survival analysis showed over half of the patients in need for re-intervention within

10 years. However, more information becomes available on the benefits of early treatment of PAS. Timely intervention promotes lung development, especially in pre-school children.¹⁸⁻²⁰ On top of that, treatment of PAS improves subjective and objective exercise tolerance, even in patients with no clinical complaints of impaired exercise tolerance.²¹ In our institution, a relative aggressive strategy for interventional treatment of PAS lesions is followed. This is reflected in the large portion of small patients in our cohort and somatic growth as the most common reason for re-intervention.

4.3 Intima proliferation

A not yet completely understood, but important reason for re-intervention is intima proliferation. The incidence of intima proliferation is previously described to be between 1.5% and 4%.^{7,22} This is consistent with the findings in our cohort in which intima proliferation was seen in 4% of all cases. Although every stent will be covered with a layer of intima within 6 months after implantation, in some patients excessive neo-intimal growth will lead to restenosis requiring re-intervention. Especially in vessels with small diameters, the formation of a small amount of intima can already cause significant stenosis.²³ This is also seen in our cohort. In almost 60% of the intima proliferation cases the stent diameter was below 8 mm. If a stent diameter above 8 mm cannot be reached due to the small size of the patient, Acetylsalicylic acid (3-5 mg/kg/day) is prescribed. Also, in patients prone for excessive neo-intimal growth, i.e. patients with Alagille or Williams, clopidogrel (0.25 mg/kg/day) is added. To monitor the possible development of intima proliferation in these patients, more frequent out-patient clinical evaluations are scheduled with non-invasive imaging. The platelet inhibitors are continued until the desired stent diameter of 8 mm or above is reached.

4.4 Stenting the small child

Due to our hands-on approach of PAS, our described cohort is relatively young in age and low in weight. This resulted in a steep learning curve in treatment of PAS in the young child. Considering the expected somatic growth of small children, our strategy is to avoid the implantation of coronary stents in the pulmonary arteries. Implanting stents with a limited final diameter would inevitably result in the need for unzipping or surgical removal of a stent in the future. Instead of coronary stents, we therefore prefer to implant 8 mm Cook Formula stents type 418 or 535 (Cook Medical, IN, USA). In our smallest patients, in which a diameter of 8 mm is unfeasible, we implant a 8 or 10 mm Cook Formula stent mounted on a smaller diameter Advance balloon.¹⁴ These

stents can be further dilated to a potential maximal diameter of 14 mm. This ensures the future possibility of re-dilatation to an adult size, without the associated risks of unzipping a stent. The frequent use of the Cook Formula stent in small patients, also explains the high incidence of intima proliferation in these stents found in our cohort.

4.5 Advanced imaging in the cathlab

One of the identified factors to prevent re-interventions was the use of 3DRA during the procedure. Previous research has described that the use of 3DRA is safe and reduces the total amount of radiation during cardiac catheterizations.^{24,25} This study now shows, that the use of 3DRA reduces the risk of re-intervention. When no 3DRA is acquired, patients have a two times higher change of re-intervention. We hypothesize that this is caused by better understanding of the pulmonary artery anatomy provided by 3DRA. With conventional 2D angiographies, lesions can be missed, or underestimated due to suboptimal angulations. 3DRA allows appreciation of the complete anatomy. Also, 3DRA is helpful for interventional guidance in complex procedures, allowing for better positioning of stents and balloons. In some cases, CT-images obtained before the procedure can be used to merge in the same way as 3DRA. However, in small children the chance for anatomic distortion is higher when a CT-scan is used for anatomic road mapping. Since radiation of 3DRA and a CT-scan is equal with 0.4-0.7 mSv, we prefer the acquisition of a 3DRA during the procedure for small and larger patients.

4.6 Limitations

The presented study has some limitations. Due to the retrospective design, the quality of the collected data was depended on the availability of follow-up information. I.e., post-procedural pressure outcomes were unavailable in a significant number of patients and details on indication for treatment could not always be recovered. However, follow-up data on re-interventions was complete in almost all patients. Due to the single center character of this study, the workflow, indication for treatment and choice of treatment is subject to local protocols and the learning curve and experience of the interventional cardiologists in our center (a total of four in 10 years). However, this is also an advantage as the presented data is not affected by differences between institutional protocols or operator preferences. The outcome of the multivariate analysis on the contribution of 3DRA imaging in the cathlab may be biased as patients in which a 3DRA was acquired or not acquired was not random. The leading interventionalist decides during the procedure whether a 3DRA is obtained or not. As it is our practice to acquire a 3DRA in all patients with complex

stenosis, one could argue that the actual positive contribution of 3DRA may be even higher. However, to further explore the influence of advanced imaging in the cathlab on re-interventions, randomized trials would be necessary.

5 CONCLUSION

This is the largest descriptive study of a single center cohort of interventional treated patients with pulmonary artery stenosis. The study shows the high heterogeneity of the PAS population and the large amount of –complex and comprehensive– interventions necessary to treat these patients. Over a quarter of all patients required re-intervention during follow-up. In our relatively young cohort, the most common reason for re-intervention was somatic growth. Intima proliferation was found in 4% of all cases. A lower BSA at intervention, a confirmed underlying syndrome were independent risk factors for re-intervention. The use of 3DRA for anatomical understanding and guidance during intervention significantly reduced the risk for re-intervention.

REFERENCES

1. Trivedi KR, Benson LN. Interventional strategies in the management of peripheral pulmonary artery stenosis. *J Interv Cardiol.* 2003;16(2):171-188.
2. Baum D, Khoury GH, Ongley PA, Swan HJ, Kincaid OW. Congenital stenosis of the pulmonary artery branches. *Circulation.* 1964;29:680-687.
3. Bacha EA, Kreutzer J. Comprehensive management of branch pulmonary artery stenosis. *J Interv Cardiol.* 2001;14(3):367-375.
4. Hiremath G, Qureshi AM, Meadows J, Aggarwal V. Treatment approach to unilateral branch pulmonary artery stenosis. *Trends Cardiovasc Med.* 2021;31(3):179-184.
5. Patel AB, Ratnayaka K, Bergersen L. A review: Percutaneous pulmonary artery stenosis therapy: State-of-the-art and look to the future. *Cardiol Young.* 2019;29(2):93-99.
6. Fujii T, Tomita H, Fujimoto K, et al. Morphological and hemodynamic effectiveness of stenting for pulmonary artery stenosis - subanalysis of JPIC stent survey. *Circ J.* 2016;80(8):1852-1856.
7. Gonzalez I, Kenny D, Slyder S, Hijazi ZM. Medium and long-term outcomes after bilateral pulmonary artery stenting in children and adults with congenital heart disease. *Pediatr Cardiol.* 2013;34(1):179-184.
8. Ing FF, Khan A, Kobayashi D, Hagler DJ, Forbes TJ. Pulmonary artery stents in the recent era: Immediate and intermediate follow-up. *Catheter Cardiovasc Interv.* 2014;84(7):1123-1130.
9. Kenny D, Amin Z, Slyder S, Hijazi ZM. Medium-term outcomes for peripheral pulmonary artery stenting in adults with congenital heart disease. *J Interv Cardiol.* 2011;24(4):373-377.
10. Lewis MJ, Kennedy KF, Ginns J, et al. Procedural success and adverse events in pulmonary artery stenting: Insights from the NCDR. *J Am Coll Cardiol.* 2016;67(11):1327-1335.
11. Ma I, El Arid JM, Neville P, et al. Long-term evolution of stents implanted in branch pulmonary arteries. *Arch Cardiovasc Dis.* 2021;114(1):33-40.
12. Patel ND, Sullivan PM, Takao CM, Badran S, Ing FF. Stent treatment of ostial branch pulmonary artery stenosis: Initial and medium-term outcomes and technical considerations to avoid and minimise stent malposition. *Cardiol Young.* 2020;30(2):256-262.
13. Krings GJ, van der Stelt F, Molenschot MMC, Breur JMPJ. Oval stenting in left pulmonary artery stenosis: A novel double balloon technique to prevent airway compression in single ventricle. *EuroIntervention.* 2020;15(13):1209-1215.
14. van Kalsbeek RJ, Krings GJ, Molenschot MMC, Breur JMPJ. Early and midterm outcomes of bare metal stenting in small children with recurrent aortic coarctation. *EuroIntervention.* 2021;16(15):e1281-e1287.
15. Conijn M, Breur H, Molenschot M, Voskuil M, Krings G. The Y-stenting technique for pulmonary artery bifurcation stenosis: Initial results and mid-term outcomes. *Int J Cardiol.* 2018;268:202-207.
16. Krisnanda C, Menahem S, Lane GK. Intravascular stent implantation for the management of pulmonary artery stenosis. *Heart Lung Circ.* 2013;22(1):56-70.

17. Stapleton GE, Hamzeh R, Mullins CE, et al. Simultaneous stent implantation to treat bifurcation stenoses in the pulmonary arteries: Initial results and long-term follow up. *Catheter Cardiovasc Interv.* 2009;73(4):557-563.
18. Takao CM, El Said H, Connolly D, Hamzeh RK, Ing FF. Impact of stent implantation on pulmonary artery growth. *Catheter Cardiovasc Interv.* 2013;82(3):445-452.
19. Bates ML, Anagnostopoulos PV, Nygard C, et al. Consequences of an early catheter-based intervention on pulmonary artery growth and right ventricular myocardial function in a pig model of pulmonary artery stenosis. *Catheter Cardiovasc Interv.* 2018;92(1):78-87.
20. Pewowaruk R, Hermsen J, Johnson C, et al. Pulmonary artery and lung parenchymal growth following early versus delayed stent interventions in a swine pulmonary artery stenosis model. *Catheter Cardiovasc Interv.* 2020;96(7):1454-1464.
21. Hiremath G, Qureshi AM, Prieto LR, et al. Balloon angioplasty and stenting for unilateral branch pulmonary artery stenosis improve exertional performance. *JACC Cardiovasc Interv.* 2019;12(3):289-297.
22. Shaffer KM, Mullins CE, Grifka RG, et al. Intravascular stents in congenital heart disease: Short- and long-term results from a large single-center experience. *J Am Coll Cardiol.* 1998;31(3):661-667.
23. Dussaillant GR, Mintz GS, Pichard AD, et al. Small stent size and intimal hyperplasia contribute to restenosis: A volumetric intravascular ultrasound analysis. *J Am Coll Cardiol.* 1995;26(3):720-724.
24. Minderhoud SCS, van der Stelt F, Molenschot MMC, Koster MS, Krings GJ, Breur JMPJ. Dramatic dose reduction in three-dimensional rotational angiography after implementation of a simple dose reduction protocol. *Pediatr Cardiol.* 2018;39(8):1635-1641.
25. Kang SL, Armstrong A, Krings G, Benson L. Three-dimensional rotational angiography in congenital heart disease: Present status and evolving future. *Congenit Heart Dis.* 2019;14(6):1046-1057.



COMPUTATIONAL ANALYSIS OF THE PULMONARY ARTERIES IN CONGENITAL HEART DISEASE – A REVIEW OF THE METHODS AND RESULTS.

Maartje Conijn

Gregor J. Krings

Computational and Mathematical Methods in Medicine
2021;2021:2618625

ABSTRACT

With the help of Computational Fluid Dynamics (CFD), hemodynamics of the pulmonary arteries (PA's) can be studied in detail and varying physiological circumstances and treatment options can be simulated. This offers the opportunity to improve the diagnostics and treatment of PA stenosis in biventricular congenital heart disease (CHD). The aim of this review was to evaluate the methods of computational studies for PA's in biventricular CHD and the level of validation of the numerical outcomes. A total of 34 original research papers was selected. The literature showed a great variety in the used methods for (re)construction of the geometry as well as definition of the boundary conditions and numerical set-up. There were 10 different methods identified to define inlet boundary conditions and 17 for outlet boundary conditions. A total of nine papers verified their CFD outcomes by comparing results to clinical data or by an experimental mock-loop. The diversity in used methods and the low level of validation of the outcomes results in uncertainties regarding the reliability of numerical studies. This limits the current clinical utility of CFD for the study of PA flow in CHD. Standardization and validation of the methods is therefore recommended.

1 INTRODUCTION

Stenosis of the pulmonary arteries (PA's) is commonly seen in patients with congenital heart disease (CHD). It can occur as a native substrate or after surgery.¹ Diagnosing patients with PA stenosis can be challenging as cardiac echography may be inconclusive. To confirm the diagnosis, often evaluation with multiple imaging modalities as CTA and CMR is necessary. The decision whether to treat the stenosis is primarily based on pressure gradients which need to be confirmed by cardiac catheterization.² However, pressure gradients might resolve under anesthesia resulting in possible under treatment of PA stenosis. In addition, restenosis and intima proliferation can occur after treatment. The mechanisms causing this are still not well understood but several flow characteristics – i.e., turbulence, wall shear stress (WSS), and the interaction of flow and (stent) geometry - are hypothesized to be of influence.³⁻⁵ Computational Fluid Dynamics (CFD) provides the opportunity to study these factors and enhance our knowledge of hemodynamics in the PA's. It allows for detailed flow visualization and simulation of exercise and treatment outcomes. However, it's clinical use is still limited as there is a great variety in used methods and validation of the numerical outcomes is often challenging.⁶⁻¹¹ The aim of this review was to analyze the available literature on numerical studies of the pulmonary arteries in biventricular CHD, focusing on the used methods and validation of the results.

2 METHODS

2.1 Search strategy

A Pubmed and Embase search was performed. The searched papers needed to include “pulmonary arteries” and “computational fluid dynamics” or a synonym in their title or abstract. The language for the search was restricted to English. All papers published before 1st of January 2021 were included.

2.2 Inclusion and exclusion criteria

All papers on numerical analysis of the PA's in biventricular hearts were included. Pediatric, adult as well as animal studies were considered. Papers with the focus on pulmonary hypertension were excluded as well as papers from before 2001, reviews and if no full text was available. All inclusion- and exclusion criteria are shown in figure 1.

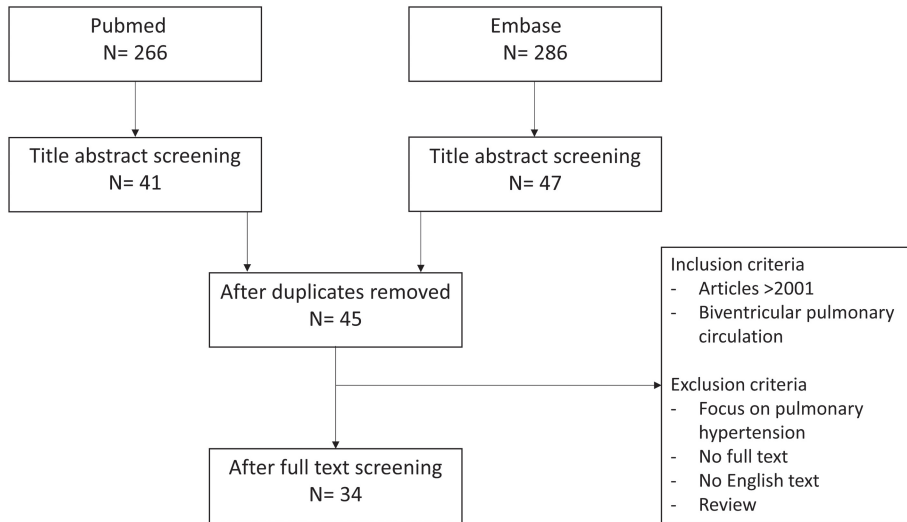


Figure 1 - Flowchart showing the outcomes of the literature search and in- and exclusion criteria. The terms used for the search were ‘pulmonary arteries’ and ‘computational fluid dynamics’ and their synonyms.

3 RESULTS

3.1 Study selection

The search in the Pubmed and Embase databases resulted in a total of, respectively, 266 and 286 papers. After undoubling and title abstract screening, 45 papers remained. The full text screening of these papers revealed exclusion criteria for 11 articles. This resulted in a total of 34 eligible papers for this review. The flowchart for the selection process is shown in figure 1.

3.2 Study overview

The 34 selected papers included four animal studies, and 25 papers presenting human cases. In one paper, both human and animal cases were described.¹² In six studies PA’s were represented by straight or curved tubes.¹³⁻¹⁸ Altogether the articles presented a total of 256 geometries based on 126 subjects (table 1).

Over half of the included papers focused on the surgical treatment of PA stenosis. These 19 studies described the use of CFD in surgical planning, for comparison of different shunt configurations or to study (post)-surgical complications.^{13-16,18-31} In two

papers numerical studies were used to evaluate interventional strategies.^{32,33} One of these described a CFD-assisted patient-specific stent design for PA interventions and the other studied a new device for percutaneous pulmonary valve replacement. Technical strategies for CFD analysis were the main subject in five papers.^{12,34-37} The focus was on improving or simplifying the process of numerical modeling of the PA's. The remaining eight papers described hemodynamics in the PA's for example, comparing rest and exercise conditions or describing the hemodynamic impact of abnormal anatomy.^{17,37-43}

Of the 34 studies, 13 were published in journals with a clinical orientation.^{13,16,18,20-22,25,27-30,37,43} Most of these papers - nine respectively - were published in cardiovascular surgical journals.^{13,21,22,25,27-30,43} The other 21 studies were published in technical journals, for example, focusing on biomedical engineering or numerical methods in medicine.^{12,14,15,17,19,23,26,31-42,44}

In the following sections, the various used methods for numerical analysis of the PA's will be compared. The sections are subdivided into the major steps necessary for solving a CFD case. First the anatomic reconstruction, then the meshing and setting the boundary conditions followed by the numerical set-up and finishing with postprocessing and validation of the results. Table 2 provides a summary of the different strategies used in the selected papers.

3.3 (Re)Construction of the geometry

Figure 2 shows the source for reconstruction of the geometry used in the selected papers. In 23 of the 34 papers, at least one patient-specific anatomy was reconstructed. The source for this reconstruction was a cardiac CT in 16 studies and CMR in six studies.^{18,20,21,23,25,26,30-32,35-37,42-45, 12,33,34,39-41} In the remaining two studies, multiple plane measurements on cardiac angiography were taken after which the anatomy was reconstructed.^{16,27} For surgical studies, often one patient-specific anatomy was created after which the anatomy was altered to mimic various surgical approaches.

Table 1: Characteristics of included papers.

Author + year	Journal	Article type	N geometries	N patients
Corno et al. 2006 ¹³	European Journal of Cardio-Thoracic Surgery	Surgical	7	-
Esmaily-Moghadam et al. 2015 ⁴	Journal of biomechanical engineering	Surgical	13	-
Lashkarinia et al. 2018 ¹⁹	Annals of Biomedical Engineering	Surgical	5	-
Matthews et al. 2011 ²⁰	The Journal of Heart Valve Disease	Surgical	1	1*
Migliavacca et al. 2002 ¹⁵	Computer Methods in Biomechanics & Biomedical Engineering	Surgical	1	-
Miyaji et al. 2019 ²¹	Interactive CardioVascular and Thoracic Surgery	Surgical	18	6
Mosbahi et al. 2014 ²²	Interactive CardioVascular and Thoracic Surgery	Surgical	1	5*
Piskin et al. 2017 (1) ²³	Journal of Biomechanics	Surgical	12	1
Piskin et al. 2017 (2) ²⁴	Cardiovascular Engineering and Technology	Surgical	6	-
Rao et al. 2015 ²⁵	Interactive CardioVascular and Thoracic Surgery	Surgical	6	2
Zhang et al. 2019 ²⁶	Computational and Mathematical Methods in Medicine	Surgical	6	2
Zhang et al. 2020 ⁴⁴	Computer methods and programs in biomedicine	Surgical	6	1
Ascutito et al. 2017 ²⁷	Interactive CardioVascular and Thoracic Surgery	Surgical	4	4 (3***)
Berdajs et al. 2015 (1) ²⁹	Journal of Surgical Research	Surgical	1	10*
Berdajs et al. 2015 (2) ²⁸	Interactive CardioVascular and Thoracic Surgery	Surgical	4	20*
Celestin et al. 2015 ¹⁶	Pediatric Cardiology	Surgical	8	2
Kato et al. 2018 ³⁰	Interactive CardioVascular and Thoracic Surgery	Surgical	6	6
Tomov et al. 2019 ¹⁸	Journal of the American Heart Association	Surgical	1	1
Liu et al. 2020 ³¹	Computational and mathematical methods in medicine	Surgical	35	1
Boumpouli et al. 2020 ¹⁷	Medical engineering and physics	Hemodynamics	9	-

Table 1: (Continued)

Author + year	Journal	Article type	N geometries	N patients
Chern et al. 2008 ³⁸	Journal of Biomechanics	Hemodynamics	3	10
Chern et al. 2012 ³⁹	Computational and Mathematical Methods in Medicine	Hemodynamics	4	4
Das et al. 2011 ⁴⁰	Tech Science Press	Hemodynamics	2	2
Tang et al. 2011 ⁴¹	Annals of Biomedical Engineering	Hemodynamics	6	6
Waniewski et al. 2005 ⁴²	Artificial Organs	Hemodynamics	5	1
Yang et al. 2017 ⁴⁵	Congenital Heart Disease	Hemodynamics	10	4
Zhang et al. 2016 ⁴³	Interactive CardioVascular and Thoracic Surgery	Hemodynamics	5	1
Guibert et al. 2014 ³⁴	Medical Image Analysis	Technical	17	17
Kong et al. 2017 ³⁵	International Journal for Numerical Methods in Biomedical Engineering	Technical	1	1
Kong et al. 2019 ³⁵	International Journal for Numerical Methods in Biomedical Engineering	Technical	1	1
Spilker et al. 2007 ¹²	Annals of Biomedical Engineering	Technical	4	2**
Yang et al. 2016 ³⁷	Biomechanics and Modeling in Mechanobiology	Technical	4	2
Caiazzo et al. 2015 ³³	Cardiovascular Engineering and Technology	Interventional	12	1
Gundelwein et al. 2018 ³²	Journal of Biomechanics	Interventional	32	16

* Animal cases, ** 1 animal case 1 human case, *** univentricular cases. N/A: not applicable, N:number



Table 2: Summary characteristics of included papers.

Author + year	Anatomy	Mesh test	N elements	Inlet BC	Outlet BC	Compliance	Fluid
Ascutto et al. 2017 ²⁷	Angiography	No	UN	Pressure	Pressure	No	Newtonian
Berdajs et al. 2015 (1) ²⁹	nps	No	365,000	Mass flow	Pressure	No	Newtonian
Berdajs et al. 2015 (2) ²⁸	nps	No	365,000	Mass flow	Pressure	No	Newtonian
Boumpouli et al. 2020 ¹⁷	nps	No	90,000-125,000	Velocity	Pressure, flow, lumped	No	Newtonian
Caiazzo et al. 2015 ³³	CMR	Yes	158,000-670,000	Pressure	Lumped	No	Newtonian
Celestin et al. 2015 ¹⁶	Angiography	Yes	1,000,000	Pressure	Pressure	No	Newtonian
Chern et al. 2008 ³⁸	nps	Yes	72,900	Velocity	UN	No	Newtonian
Chern et al. 2012 ³⁹	CMR	Yes	1,000,000	Velocity	Pressure	No	Newtonian
Corno et al. 2006 ¹³	nps	No	UN	Mass flow	UN	No	UN
Das et al. 2011 ⁴⁰	CMR	Yes	150,000-650,000	Womersley	Pressure/ Womersley	No	Non-newtonian
Esmaily-Moghadam et al. 2015 ¹⁴	nps	Yes	400,000	Lumped	Lumped	Yes	Newtonian
Guibert et al. 2014 ³⁴	CMR	No	UN	Mass flow	Lumped	No	UN
Gundelwein et al. 2018 ³²	CT	No	60,000	Mass flow	Lumped	Yes	Newtonian
Kato et al. 2018 ³⁰	CT	No	2,000,000	Mass flow	Pressure	No	Newtonian
Kong et al. 2017 ³⁶	CT	No	UN	Mass flow	No traction	No	Newtonian
Kong et al. 2019 ³⁵	CT	No	1,000,000	Velocity	No traction	Yes	Newtonian
Lashkarinia et al. 2018 ¹⁹	nps	Yes	UN	Velocity	Pressure	Yes	Newtonian
Liu et al. 2020 ³¹	CT	Yes	3,723,041	Mass flow	Resistance	No	Newtonian
Matthews et al. 2011 ²⁰	CT	No	1,000,000	Pressure	Pressure	Yes	N/A
Migliavacca et al. 2002 ¹⁵	nps	Yes	30,000-48,000	Mass flow	Pressure	Yes	Newtonian

Table 2: (Continued)

Author + year	Anatomy	Mesh test	N elements	Inlet BC	Outlet BC	Compliance	Fluid
Miyaji et al. 2019 ²¹	CT	No	1,000,000	Mass flow	Pressure	No	Newtonian
Mosbahi et al. 2014 ²²	nps	No	365,000	Mass flow	Pressure	No	Newtonian
Piskin et al. 2017 (1) ²³	CT	Yes	1,007,223	Velocity	Resistance	No	Newtonian
Piskin et al. 2017 (2) ²⁴	nps	Yes	1,135,156	Resistance	Resistance	No	Newtonian
Rao et al. 2015 ²⁵	CT	No	UN	Mass flow	Pressure	No	Newtonian
Spilker et al. 2007 ¹²	CMR	No	UN	Mass flow	Impedance	Yes	Newtonian
Tang et al. 2011 ⁴¹	CMR	Yes	1,500,000	Mass flow	Resistance	No	Newtonian
Tomov et al. 2019 ¹⁸	CT	Yes	>200,000	Velocity	No traction	No	Newtonian
Waniewski et al. 2005 ⁴²	CT	Yes	120,000–150,000	Velocity	Mass flow	No	Newtonian
Yang et al. 2016 ³⁷	CT	No	UN	Mass flow	Lumped	Yes	UN
Yang et al. 2017 ⁴⁵	CT	No	UN	Mass flow	Lumped	Yes	Newtonian
Zhang et al. 2016 ⁴³	CT	Yes	600,000	Mass flow	Pressure	No	Newtonian
Zhang et al. 2019 ²⁶	CT	No	UN	Lumped	Lumped	No	Newtonian
Zhang et al. 2020 ⁴⁴	CT	Yes	1,969,627	Mass flow	Resistance	No	Newtonian

BC: boundary condition, N: number, nps: not patient specific, CT: computed tomography, CMR: cardiac magnetic resonance, UN: unknown

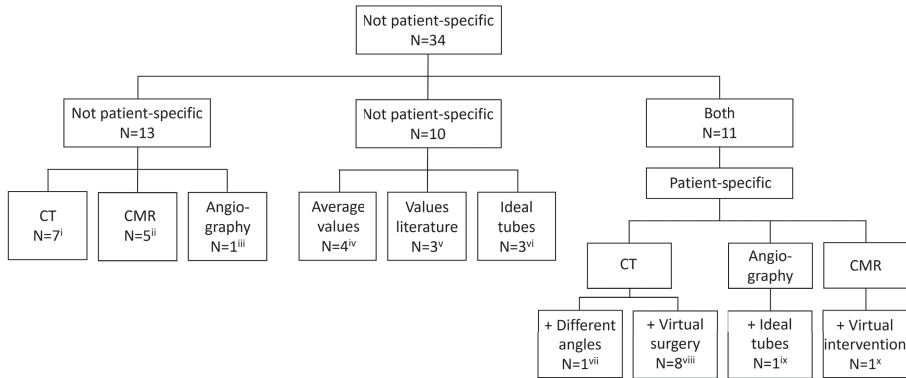


Figure 2 - The different sources for reconstruction of a PA anatomy used in the included papers. (i) Gundelwein et al. 2018³², Kato et al. 2018³⁰, Kong et al. 2017³⁶, Kong et al. 2019³⁵, Matthews et al. 2011²⁰, Waniewski et al. 2005⁴², Zhang et al. 2020⁴⁴, (ii) Chern et al. 2012³⁹, Das et al. 2011⁴⁰, Guibert et al. 2014³⁴, Spilker et al. 2007¹², Tang et al. 2011⁴¹, (iii) Ascuitto et al. 2017²⁷, (iv) Berdajs et al. 2015 (1)²⁹, Berdajs et al. 2015 (2)²⁸, Chern et al. 2008³⁸, Mosbahi et al. 2014²², (v) Lashkarinia et al. 2018¹⁹, Piskin et al. 2017 (2)²⁴, Boumpouli et al. 2020¹⁷, (vi) Corno et al. 2006¹³, Esmaily-Moghadam et al. 2015¹⁴, Migliavacca et al. 2002¹⁵, (vii) Zhang et al. 2016⁴³, (viii) Miyaji et al. 2019²¹, Piskin et al. 2017 (1)²³, Rao et al. 2015²⁵, Yang et al. 2016³⁷, Yang et al. 2017⁴⁵, Zhang et al. 2019²⁶, Tomov et al. 2019¹⁸, Liu et al. 2020³¹, (ix) Celestin et al. 2015¹⁶. (x) Caiazza et al. 2015³³. CT: computed tomography, CMR: cardiac magnetic resonance.

Most groups (re)constructed a geometry consisting of the main PA bifurcation and the right- and left pulmonary artery.^{17,18,21,22,28,29,32-34,38-40} All these models had one inlet and two outlets. Shunt anatomy was mostly represented by one aortic or shunt inlet and two or three outlets representing the RPA, LPA and/or the descending aorta.^{14-16,23,25-27,31,42,44} In three studies, the flow in the main PA was computed using a model with one inlet and one outlet.^{13,19,20} Kong et al. analyzed a model with one inlet and 274 outlets, making it the biggest PA anatomy studied.³⁶ In seven other studies the pulmonary circulation was reconstructed up to the peripheral arteries. Here, imaging resolution was always the limiting factor for reconstruction.^{12,30,35,37,41,43,45} The number of outlets in these studies varied between 8 and 100 outlets per model.

An artificial geometry was used in ten studies.^{13-15,17,19,24,28,38} A geometry was constructed based on general values obtained by literature or measurements in multiple patients in seven papers.^{17,19,22,24,28,29,38} The other three studies analyzed arteries represented by ideal (curved) tubes.¹³⁻¹⁵

After geometry reconstruction, inlet and outlet extensions were added in four of the 34 studies.^{19,21,30,40} The extension of the inlet varied between five and 20 times the diameter of the inlet. The outlet region was extended 20 times the diameter of the outlet. In the other 30 studies the inlet and outlet regions were not extended.

A variety of software was used for segmentation of the patient-specific anatomies. The most mentioned open-source software package was Simvascular (simvascular.org). For commercial software this was MIMICS (Materialise, Leuven, Belgium). Other software for segmentation included ITK-SNAP (open-source, itk-snap.org), Osirix (commercial, Pixmeo SARL, Geneva, Swizerland) and CardioViz3D (open-source, Asclepios Research Project, Inria Sophia Antipolis, Greece).

3.4 Meshing

The meshing process was – partly – described in 27 of the 34 papers, while in seven this information was completely missing. A nonstructured meshing strategy with tetrahedral elements was used in 20 of the 27 studies.^{12,14,16,17,19,21,23,24,30-33,35,36,39-44} A structured mesh was applied by six groups.^{15,20,22,28,29,38} Boundary layers were described by 16 authors, but the majority of the studies did not mention any boundary layer use. Of the 27 articles specifying their meshing process, 20 reported the program they used.^{14,15,17-24,28-30,32,33,36,39-41,43} In most cases this was ANSYS software (ANSYS Inc, Canonsburg PA, USA).

A mesh independence test to evaluate mesh quality was performed in 16 of the 34 papers.^{14-16,18,19,23,24,31,33,38-44} In 12 of these, information on the criteria for mesh independency was provided.^{14,18,19,23,24,31,33,38-41,44} These criteria included velocity profiles on different locations and a difference of <5% in calculations of pressure, velocity or WSS. In 18 of the 34 papers a mesh independence test was not performed or at least not mentioned. Three studies applied an element size determined by a mesh independence test performed on a different geometry.^{17,21,30} The number of elements for the final mesh varied between 30.000 and 4 million.

3.5 Boundary conditions

3.5.1 Inlet

Table 3 shows all the used inlet- and outlet boundary conditions in the included papers. The inlet boundary conditions were pulsatile in 23 and constant in 11 papers. The most common inlet boundary condition was flow rate (l/min) followed by velocity

and pressure in 18, 10 and four studies respectively. In two studies an electrical system was applied at the inlet.^{14,26} The inlet conditions were patient-specific in seven papers.^{12,16,27,39-41,43} In these studies the stroke volume as well as the waveform were patient-specific. These conditions were mostly obtained by MRI or invasive measurements during cardiac catheterization. In five studies a patient-specific stroke volume was implemented but with a general waveform.^{25,30,32,37,45} This waveform was scaled to a cardiac index suitable for the analyzed geometry. In the other 23 studies a general inlet boundary condition was used.

In 13 papers the applied velocity profile was specified. This was a flat or plug flow velocity profile in six and a parabolic profile in three studies.^{16,19,22-24,28, 12,17,34} Three articles implemented a Womersley flow at the inlet and one study used a patient-specific velocity profile obtained by phase-contrast MRI.^{32,40,41, 39} However, most studies did not mention the kind of velocity profile they used on their inlet.

3.5.2 Outlet

The most applied outlet boundary condition was a constant pressure outlet. 14 studies used a variation of this condition, i.e. atmospheric pressure, zero pressure or the mean PA or aortic pressure obtained by cardiac catheterization.^{15,16,18-22,25,27-30,39,43} In one study a pulsatile pressure on the LPA outlet was implemented while a Womersley velocity profile was set on the RPA outlet.⁴⁰ In another study the outflow boundary condition was defined by the LPA:RPA flowsplit.⁴² In five papers, the three-element Windkessel model was imposed to the outlet.^{32-34,37,45} The pure resistance strategy was used in five studies.^{23,24,31,41,44} Spilker et al. described a method for the impedance boundary condition in which they reconstructed an one-dimensional (1D) anatomy and calculated the impedance value for the pulmonary anatomy.¹² One study applied multiple outlet boundary conditions and compared results. These included zero pressure, constant pressure, prescribed flow split and a lumped parameter model.¹⁷ In two papers the outlet boundary conditions were not specified.^{13,38}

Patient-specific information was used to calculate resistance and windkessel values in four papers.^{16,27,31,32,37,40,41,45} For this i.e. the flow split derived from flow perfusion scans, pressure from catheterization and cardiac output from catheterization or echocardiography were taken. The other authors estimated values based on more general information.

Table 3 - Used boundary conditions in the included articles.

Author + year	Inlet	Pulsatile	Patient specific?	Outlet	Patient specific?
Berdajs et al. 2015 (1) ²⁸	Mass flow	Yes	-	Atmospheric pressure	-
Berdajs et al. 2015 (2) ²⁹	Mass flow	-	-	Atmospheric pressure	-
Mosbahi et al. 2014 ²²	Mass flow	-	-	Atmospheric pressure	-
Yang et al. 2016 ³⁷	Mass flow	Yes	In volume	3-element Windkessel	Yes
Yang et al. 2017 ⁴⁵	Mass flow	Yes	In volume	3-element Windkessel	Yes
Guibert et al. 2014 ³⁴	Mass flow	Yes	-	3-element Windkessel	-
Gundelwein et al. 2018 ³²	Mass flow	Yes	In volume	3-element Windkessel	Yes
Kato et al. 2018 ³⁰	Mass flow	Yes	In volume	Pressure	-
Zhang et al. 2016 ⁴³	Mass flow	Yes	Yes	Pressure	-
Zhang et al. 2020 ⁴⁴	Mass flow	-	-	Resistance	-
Rao et al. 2015 ²⁵	Mass flow	-	In volume	Pressure	-
Migliavacca et al. 2002 ¹⁵	Mass flow	-	-	Pressure	-
Miyaji et al. 2019 ²¹	Mass flow	-	-	Pressure	-
Spilker et al. 2007 ¹²	Mass flow	Yes	For one case	Impedance	For one case
Tang et al. 2011 ⁴¹	Mass flow	Yes	Yes	Resistance	Yes
Liu et al. 2020 ³¹	Mass flow	-	-	Resistance	Yes
Kong et al. 2017 ³⁶	Mass flow	Yes	-	No traction	-
Corno et al. 2006 ¹³	Mass flow	Yes	-	UN	UN
Piskin et al. 2017 (1) ²³	Velocity	-	-	Resistance	-
Boumpouli et al. 2020 ¹⁷	Velocity	Yes	-	Pressure, flow split, lumped	-
Chern et al. 2012 ³⁹	Velocity	Yes	Yes	Atmospheric pressure	-



Table 3 - (Continued)

Author + year	Inlet	Pulsatile	Patient specific?	Outlet	Patient specific?
Lashkarinia et al. 2018 ¹⁹	Velocity	-	-	Pressure	-
Kong et al. 2019 ³⁵	Velocity	Yes	-	No traction	-
Tomov et al. 2019 ¹⁸	Velocity	Yes	-	Pressure	-
Waniewski et al. 2005 ⁴²	Velocity	Yes	-	Mass flow	-
Chern et al. 2008 ³⁸	Velocity	Yes	-	UN	UN
Ascuitto et al. 2017 ²⁷	Pressure	Yes	Yes	Pressure	Yes
Celestin et al. 2015 ¹⁶	Pressure	-	Yes	Pressure	Yes
Caiazzo et al. 2015 ³³	Pressure	Yes	-	3-element Windkessel	-
Matthews et al. 2011 ²⁰	Pressure	Yes	-	Pressure	-
Piskin et al. 2017 (2) ²⁴	Resistance	-	-	Resistance	-
Das et al. 2011 ⁴⁰	Womersley profile	Yes	Yes	Pressure/Womersley profile	Yes
Zhang et al. 2019 ²⁶	Electrical system	-	-	Electrical system	-
Esmaily-Moghadam et al. 2015 ¹⁴	0-D model	Yes	-	0-D model	-

UN: unknown

3.5.3 Vessel wall compliance

In nine of the included papers FSI was used to simulate deformation of the vessel wall during the cardiac cycle.^{12,14,15,19,20,32,35,37,45} One of these groups applied case-specific compliance.²⁰ Here the mesh was subdivided in five regions. The Young's modulus for each region was obtained by stretch testing the tissue of freshly harvested porcine pulmonary roots. These values were then imposed to the *in silico* geometry of the porcine pulmonary roots. No studies were available using patient-specific compliance in human cases. The eight other groups assumed a global and constant value for the compliance of the artery wall. The highest Young's modulus was 5×10^7 Pa and the lowest 2.6×10^5 .^{19,32} One group implemented a Young's modulus varying between 2.6 - 4.2×10^5 Pa.³⁷ They tuned the value until the computed outcomes matched the desired patient-specific outcomes. The wall thickness was assumed to be between 0.5-1.5 mm. In one article a variable thickness of 10% of the diameter of the vessel was applied.¹⁴ Four articles specified the Poisson's ratio used. These were respectively 0.42, 0.45, 0.49 and 0.5.^{14,19,35,37}

3.6 Numerical set up

The program most used for solving the numerical cases was ANSYS Fluent (ANSYS Inc, Canonsburg PA, USA). This software package utilized by 12 groups included in this review.^{16,18,19,21,23-25,27,30,40,42,44} Other mentioned software included CFD-ACE + (ESI group, Paris, France) and Simvascular (simvascular.org) and ABAQUS (Simuleon, 's-Hertogenbosch, The Netherlands). Four groups calculated their solution with special build-in-house software^{12,14,35,36}. In nine papers the software was not specified.^{13,26,31,33,34,37,41,43,45}

3.6.1 Fluid characteristics

In 29 of the 34 included papers blood was assumed to behave as a Newtonian fluid while in one paper it was assumed to be a Non-Newtonian fluid.⁴⁰ Three papers did not specify the assumption they made.^{13,34,37} In most studies the blood density was set to be 1060 kg/m³. Only three studies assigned a different density of 1050 kg/m³ and 1000 kg/m³ respectively.^{33,35,40} In nine papers the used density was not described. Viscosity was mostly assumed to be 0.004 kg/ms.^{12,14,15,17,21,22,28-30,33,39,41,42,45} Other imposed values were 0.0035 kg/ms, 0.003 kg/ms and 0.00371 kg/ms.^{25,26,35,38,43,44} Four authors applied a varying viscosity number.^{16,18,36,40} One of them varied the viscosity of blood between 0.003 and 0.008 kg/ms depending on hematocrits levels varying between 30-55%.¹⁶ Two authors used the Carreau model

to capture the varying viscosity of blood depending on the shear rate.^{18,40} The last one analyzed the stability of their algorithm with varying viscosity numbers.³⁶

3.6.2 Number of cardiac cycles simulated

As 10 studies were performed with a constant inlet flow, the number of simulated cardiac cycles here is irrelevant. In 11 of the other 24 papers the number of simulated cycles was specified.^{12,14,17,18,32,35,36,38-41} In the majority of these studies four cardiac cycles were calculated.^{12,32,38,39,41} The minimal and maximal number of simulated cycles was respectively one and five.^{14,17}

3.6.3 Time step size

Information on time step size for the simulation was provided in 13 papers.^{12,14,18,30,32,33,35,36,38-42} The value varied between 0.0001 and 0.015 seconds per step. In three papers only the total number of time steps was specified. This varied between 256 and 16000 time steps for four cardiac cycles.^{12,38,41} A time-step independence test was performed in one study.⁴⁰

3.6.4 Convergence criteria

The used convergence criteria were specified in 13 papers.^{14,15,17,19,23,24,30,35,36,38,39,42,44} In most of these studies convergence criteria were set at $10e-4$.^{14,35,36,38,39} The used convergence criteria varied between 10^{-3} and 10^{-7} .^{15,42}

3.7 Computational time

The computational time for the cases was described in six papers. The reported time per case varied between a couple of hours up to 1-2 months.^{21,23,35,38,39,41} In one paper the difference in computational time for the same case with a different number of cores was shown. With the use of 'supercomputers' computational time was reduced to a couple of hours for highly complex cases.³⁵

3.8 Results and validation

The results presented in the included papers varied according to the research question proposed. In most papers two or three numerical outcomes were presented. I.e. pressure and WSS or streamlines and flow rates. In the majority of the papers figures showed the results of the peak systolic and one or two diastolic time steps. Velocity and WSS were the results most reported followed by respectively pressure, streamlines and flow rates. Pressure outcomes were either presented by the peak

systolic numbers, energy loss over a stenosis or as the time-pressure curve over the cardiac cycle.

In nine papers clinical data of the included patients was used to validate the CFD results (Table 4).^{12,19,27,32,33,37,39,40,45} In seven of these papers one hemodynamic outcome was validated.^{12,19,27,32,33,37,39,45} These were flow results in four, pressure in two papers and regurgitation fraction in one paper. One paper verified pressure as well as flow rate results.⁴⁰ In all the papers validating computational pressure outcomes cardiac catheterization data was used as the golden standard. In three papers the absolute numbers of diastolic and systolic pressure outcomes were presented and validated.^{12,27,32} The invasively measured pressure curve was compared to the computational pressure curve in one study.⁴⁰ Other sources for validation were cardiac MRI or lung perfusion scans. With data from these sources flow rate, flow split and regurgitation fraction outcomes were validated. In one paper the source of validation of the flow rates was not specified.³³ One paper verified wall deformation results of a non-patient-specific case using an experimental mock-loop set-up.¹⁹ In the 26 other papers there was no comparison between CFD outcomes and clinical data.

Table 4 - Validation.

Author + year	Validation of	Source validation
Ascutto et al. 2017²⁷	Flow rates	Cardiac catheterization, continuous wave Doppler
Caiazzo et al. 2015³³	Flow rates	UN
Yang et al. 2016³⁷	Flow split	Lung perfusion scan
Yang et al. 2017⁴⁵	Flow split	Lung perfusion scan
Das et al. 2011⁴⁰	Pressure and flow rates	Cardiac catheterization, CMR
Gundelwein et al. 2018³²	Pressure	Cardiac catheterization
Spilker et al. 2007¹²	Pressure	Cardiac catheterization
Chern et al. 2012³⁹	Regurgitation fraction	CMR
Lashkarinia et al. 2018¹⁹	Wall deformation	Experimental set-up

UN: unknown, CMR: cardiac magnetic resonance

4 DISCUSSION

The use of advanced imaging modalities to describe the hemodynamic impact of PA stenosis is increasing. CFD is one of these techniques providing detailed visualization of patient-specific hemodynamics. The aim of this paper was to review the numerical methods and – clinical - validation of CFD for evaluation of PA's in biventricular CHD. All of the papers included in this review emphasize the importance of hemodynamic evaluation of the PA's in biventricular CHD. They show the use and feasibility of CFD for this purpose and the wide variety of applications of the technique i.e. for surgical or interventional treatment planning, research on complications and exercise simulation. However, this review also shows limitations of the current available literature.

The literature reveals a large diversity in the setup for the numerical analysis of PA stenosis. This heterogeneity is important as variations in the numerical case set-up significantly influence the outcomes. Results of patient-specific analysis are highly dependable on the source and quality of the anatomic reconstruction. In addition, small differences in the applied inlet- or outlet boundary conditions can have a major impact. Outcomes of WSS and velocity can differ up to 30% with different boundary conditions.⁴⁶⁻⁴⁹ In the included papers for this review 10 different sources for anatomic reconstruction were used and 10 different methods were identified for the definition of the inlet boundary conditions. The largest variety however is seen in the definition of outlet boundary conditions. The 34 papers described 17 different approaches to assign outlet boundary conditions with very limited use of complete patient-specific boundary conditions. In the majority of cases assumptions or generalizations defined inlet- and or outlet boundary conditions. In several papers key methodological information was missing. This included missing information on mesh size (23/34), number of cardiac cycles simulated (15/34) and convergence criteria (21/34).

The heterogeneity, assumptions and generalizations in the computational set-up result in uncertainties regarding the outcomes. The validation of methods and results is therefore of major importance. It provides direct feedback on the used methods and increases confidence in the reliability of the technique. This review shows that the level of validation of the CFD outcomes is very low. Studies with the main aim to validate CFD outcomes were completely missing and only nine of the 31 papers compared their outcomes to clinical data. This lowers the translational value of the studies.

Another important limitation for the clinical utility of CFD is the computational time. This was reported to be as long as several days to even months per case. However, more and more progress is made in speeding up the computational process. By use of 'super computers', improved algorithms and cloud-based environments the simulation time can be significantly reduced. Great examples of these efforts are shown by the two papers of Kong et al. included in this review. They show how the use of multiple cores and adjustment of algorithms can decrease computational time with several hours.^{35,36} This can be expected to further decrease in the coming years.

5 CONCLUSION

The aim of this review was to evaluate the available literature on numerical analysis of the PA's in biventricular CHD. The focus was on the used methods and the rate of – clinical – validation of the outcomes. To the best of our knowledge this is the first review evaluating the different strategies for numerical studies of the PA's. The included literature shows the wide variety of applications of CFD and emphasizes the added value of numerical studies for hemodynamic assessment of the PA's. However, this review also shows the large heterogeneity in used methods in all parts of the numerical set-up and little validation of the results. This limits the current clinical utility of CFD. To increase the translation towards clinical use standardization of the methodologies is desirable. Future research should therefore be pointed towards validation of methods of numerical studies.

REFERENCES

1. Hoffman JI, Kaplan S. The incidence of congenital heart disease. *Journal of the American College of Cardiology JID* - 8301365.
2. Krisnanda C, Menahem S FAU - Lane, Geoffrey,K., Lane GK. Intravascular stent implantation for the management of pulmonary artery stenosis. *Heart, lung & circulation JID* - 100963739.
3. Gonzalez I, Kenny DF, Slyder S FAU - Hijazi, Ziyad,M., Hijazi ZM. Medium and long-term outcomes after bilateral pulmonary artery stenting in children and adults with congenital heart disease. *Pediatric cardiology JID* - 8003849.
4. Hallbergson A, Lock JE, Marshall AC. Frequency and risk of in-stent stenosis following pulmonary artery stenting. *The American journal of cardiology JID* - 0207277.
5. Stapleton GE, Hamzeh R FAU - Mullins, Charles,E., FAU MC, et al. Simultaneous stent implantation to treat bifurcation stenoses in the pulmonary arteries: Initial results and long-term follow up. *Catheterization and cardiovascular interventions : official journal of the Society for Cardiac Angiography & Interventions JID* - 100884139. (1522-726).
6. DeCampi WM, Argueta-Morales IF, Divo E FAU - Kassab, Alain,J., Kassab AJ. Computational fluid dynamics in congenital heart disease. *Cardiology in the young JID* - 9200019.
7. Morris PD, Narracott A, von Tengg-Kobligh H, et al. Computational fluid dynamics modelling in cardiovascular medicine. *Heart*. 2016;102(1):18-28.
8. Pennati G, Corsini C, Hsia T, Migliavacca F. Modeling of Congenital HA. Computational fluid dynamics models and congenital heart diseases. *Frontiers in pediatrics*. 2013;1:4-4.
9. Pittaccio S, Migliavacca FF, Dubini GF, Kocyildirim E FAU - de Leval, Marc,R., de Leval MR. On the use of computational models for the quantitative assessment of surgery in congenital heart disease. *The Anatolian journal of cardiology JID* - 101095069.
10. Slesnick TC. Role of computational modelling in planning and executing interventional procedures for congenital heart disease. *The Canadian journal of cardiology JID* - 8510280. (0828-282).
11. Sun Z, Xu L. Computational fluid dynamics in coronary artery disease. *Computerized medical imaging and graphics : the official journal of the Computerized Medical Imaging Society JID* - 8806104.
12. Spilker RL, Feinstein JA, Parker DW, Reddy VM, Taylor CA. Morphometry-based impedance boundary conditions for patient-specific modeling of blood flow in pulmonary arteries. *Ann Biomed Eng*. 2007;35(4):546-559.
13. Corno A.F., Prosi M., Fridez P., Zunino P., Quarteroni A., Von SL. The non-circular shape of FloWatch®-PAB prevents the need for pulmonary artery reconstruction after banding. computational fluid dynamics and clinical correlations. *Eur J Cardio-thorac Surg*. 2006;29(1):93-99.
14. Esmaily-Moghadam M, Murtuza B, Hsia TY, Marsden A. Simulations reveal adverse hemodynamics in patients with multiple systemic to pulmonary shunts. *J Biomech Eng*. 2015;137(3):10.1115/1.4029429. Epub 2015 Jan 29.
15. Migliavacca F., Pennati G., Di ME, Dubini G., Pietrabissa R. Pressure drops in a distensible model of end-to-side anastomosis in systemic-to-pulmonary shunts. *Comput Methods Biomech Biomed Engin*. 2002;5(3):243-248.

16. Celestin C, Guillot M, Ross-Ascuitto N, Ascuitto R. Computational fluid dynamics characterization of blood flow in central aorta to pulmonary artery connections: Importance of shunt angulation as a determinant of shear stress-induced thrombosis. *Pediatr Cardiol.* 2015;36(3):600-615.
17. Boumpouli M, Danton MHD, Gourlay T, Kazakidi A. Blood flow simulations in the pulmonary bifurcation in relation to adult patients with repaired tetralogy of fallot. *Med Eng Phys.* 2020;85:123-138.
18. Tomov ML, Cetnar A, Do K, Bauser-Heaton H, Serpooshan V. Patient-specific 3-dimensional-bioprinted model for in vitro analysis and treatment planning of pulmonary artery atresia in tetralogy of fallot and major aortopulmonary collateral arteries. *J Am Heart Assoc.* 2019;8(24):e014490.
19. Lashkarinia S.S., Piskin S., Bozkaya T.A., Salihoglu E., Yerebakan C., Pekkan K. Computational pre-surgical planning of arterial patch reconstruction: Parametric limits and in vitro validation. *Ann Biomed Eng.* 2018;46(9):1292-1308.
20. Matthews P.B., Jhun C.-S., Young S., et al. Finite element modeling of the pulmonary autograft at systemic pressure before remodeling. *J Heart Valve Dis.* 2011;20(1):45-52.
21. Miyaji K., Miyazaki S., Itatani K., Oka N., Kitamura T., Horai T. Novel surgical strategy for complicated pulmonary stenosis using haemodynamic analysis based on a virtual operation with numerical flow analysis. *Interact Cardiovasc Thorac Surg.* 2019;28(5):775-782.
22. Mosbahi S., Mickailly-Huber E., Charbonnier D., et al. Computational fluid dynamics of the right ventricular outflow tract and of the pulmonary artery: A bench model of flow dynamics. *Interact Cardiovasc Thorac Surg.* 2014;19(4):611-616.
23. Piskin S, Altin HF, Yildiz O, Bakir I, Pekkan K. Hemodynamics of patient-specific aorta-pulmonary shunt configurations. *J Biomech.* 2017;50:166-171.
24. Piskin S, Unal G, Arnaz A, Sarioglu T, Pekkan K. Tetralogy of fallot surgical repair: Shunt configurations, ductus arteriosus and the circle of willis. *Cardiovasc Eng Technol.* 2017;8(2):107-119.
25. Rao AS, Menon PG. Presurgical planning using image-based in silico anatomical and functional characterization of tetralogy of fallot with associated anomalies. *Interact Cardiovasc Thorac Surg.* 2015;20(2):149-156.
26. Zhang N., Yuan H., Chen X., et al. Computational fluid dynamics characterization of two patient-specific systemic-to-pulmonary shunts before and after operation. *Comp Math Methods Med.* 2019:2019.
27. Ascuitto R, Ross-Ascuitto N, Guillot M, Celestin C. Computational fluid dynamics characterization of pulsatile flow in central and sano shunts connected to the pulmonary arteries: Importance of graft angulation on shear stress-induced, platelet-mediated thrombosis. *Interact Cardiovasc Thorac Surg.* 2017;25(3):414-421.
28. Berdajs D., Mosbahi S., Vos J., Charbonnier D., Hullin R., Von SL. Fluid dynamics simulation of right ventricular outflow tract oversizing. *Interact Cardiovasc Thorac Surg.* 2015;21(2):176-182.
29. Berdajs D.A., Mosbahi S., Charbonnier D., Hullin R., Von SL. Analysis of flow dynamics in right ventricular outflow tract. *J Surg Res.* 2015;197(1):50-57.
30. Kato N, Yamagishi M, Itatani K, et al. Effects of blood flow dynamics on autologous pericardial degeneration in reconstructed pulmonary arteries. *Interact Cardiovasc Thorac Surg.* 2018;26(2):293-300.

31. Liu J, Yuan H, Zhang N, et al. 3D simulation analysis of central shunt in patient-specific hemodynamics: Effects of varying degree of pulmonary artery stenosis and shunt diameters. *Comput Math Methods Med.* 2020;2020:4720908.
32. Gundelwein L, Miro J, Gonzalez Barlatay F, Lapierre C, Rohr K, Duong L. Personalized stent design for congenital heart defects using pulsatile blood flow simulations. *J Biomech.* 2018;81:68-75.
33. Caiazzo A., Guibert R., Boudjemline Y., Vignon-Clementel I.E. Blood flow simulations for the design of stented valve reducer in enlarged ventricular outflow tracts. *Cardiovasc Eng Technol.* 2015;6(4):485-500.
34. Guibert R., McLeod K., Caiazzo A., et al. Group-wise construction of reduced models for understanding and characterization of pulmonary blood flows from medical images. *Med Image Anal.* 2014;18(1):63-82
35. Kong F., Kheyfets V., Finol E., Cai X.-C. Simulation of unsteady blood flows in a patient-specific compliant pulmonary artery with a highly parallel monolithically coupled fluid-structure interaction algorithm. *Int J Numer Method Biomed Eng.* 2019;35(7):e3208.
36. Kong F, Kheyfets V, Finol E, Cai XC. An efficient parallel simulation of unsteady blood flows in patient-specific pulmonary artery. *Int J Numer Method Biomed Eng.* 2018;34(4):e2952.
37. Yang W., Feinstein J.A., Vignon-Clementel I.E. Adaptive outflow boundary conditions improve post-operative predictions after repair of peripheral pulmonary artery stenosis. *Biomech Model Mechanobiology.* 2016;15(5):1345-1353.
38. Chern M.-J., Wu M.-T., Wang H.-L. Numerical investigation of regurgitation phenomena in pulmonary arteries of tetralogy of fallot patients after repair. *J Biomech.* 2008;41(14):3002-3009.
39. Chern M.-J., Wu M.-T., Her S.-W. Numerical study for blood flow in pulmonary arteries after repair of tetralogy of fallot. *Comp Math Methods Med.* 2012;2012.
40. Das A., Gottliebson W.M., Karve M., Banerjee R. Comparison of hemodynamic endpoints between normal subject and tetralogy patient using womersley velocity profile and MR based flow measurements. *Mol Cell Biomech.* 2011;8(1):21-42.
41. Tang B.T., Fonte T.A., Chan F.P., Tsao P.S., Feinstein J.A., Taylor C.A. Three-dimensional hemodynamics in the human pulmonary arteries under resting and exercise conditions. *Ann Biomed Eng.* 2011;39(1):347-358.
42. Waniewski J, Kurowska W, Mizerski JK, et al. The effects of graft geometry on the patency of a systemic-to-pulmonary shunt: A computational fluid dynamics study. *Artif Organs.* 2005;29(8):642-650. doi: AOR29102 [pii].
43. Zhang W., Liu J., Yan Q., Liu J., Hong H., Mao L. Computational haemodynamic analysis of left pulmonary artery angulation effects on pulmonary blood flow. *Interact Cardiovasc Thorac Surg.* 2016;23(4):519-525.
44. Zhang N, Yuan H, Chen X, et al. Hemodynamic of the patent ductus arteriosus in neonates with modified blalock-taussig shunts. *Comput Methods Programs Biomed.* 2020;186:105223.
45. Yang W., Hanley F.L., Chan F.P., Marsden A.L., Vignon-Clementel I.E., Feinstein J.A. Computational simulation of postoperative pulmonary flow distribution in alagille patients with peripheral pulmonary artery stenosis. *Congenit Heart Dis.* 2018;13(2):241-250.
46. Madhavan SA, Kemmerling EMC. The effect of inlet and outlet boundary conditions in image-based CFD modeling of aortic flow. *Biomedical engineering online JID -* 101147518. (1475-925; 1475-925).

47. Boccadifuoco A, Mariotti A, Celi S, Martini N, Salvetti MV. Impact of uncertainties in outflow boundary conditions on the predictions of hemodynamic simulations of ascending thoracic aortic aneurysms. *Comput Fluids*. 2018;165:96-115.
48. Liu BF, Zheng JF, Bach RF, Tang D. Influence of model boundary conditions on blood flow patterns in a patient specific stenotic right coronary artery. *Biomedical engineering online JID - 101147518*. (1475-925; 1475-925).
49. Campbell IC, Ries J FAU - Dhawan, Saurabh,S., FAU DS, FAU QA, FAU TW, Oshinski JN. Effect of inlet velocity profiles on patient-specific computational fluid dynamics simulations of the carotid bifurcation. *Journal of biomechanical engineering JID - 7909584*.



PART II



UNDERSTANDING STENOTIC PULMONARY ARTERIES: CAN COMPUTATIONAL FLUID DYNAMICS HELP US OUT?

Maartje Conijn

Gregor J. Krings

Progress in Pediatric Cardiology
2021, 101452

ABSTRACT

Background Although pulmonary artery stenosis is common in congenital heart disease, not much is known about the hemodynamic impact. The effect of stenosis on flow, pressure and wall shear stress can be visualised with computational fluid dynamics.

Objectives The aim of this study was to evaluate whether computational fluid dynamics is able to predict flow distribution and pressure gradients in normal and stenotic pulmonary arteries.

Methods Three cases were selected. The cases included one normal anatomy and two geometries representing common patterns in pulmonary artery stenosis. The pulmonary bifurcation was reconstructed using 3D rotational angiography. On the inlet a patient-specific transient mass flow curve was applied. Full patient-specific outlet boundary conditions were calculated and applied on the outlets of the models. Pressure and flow distribution outcomes were compared to cardiac catheterization and cardiovascular magnetic resonance imaging data respectively.

Results In all three cases the computationally calculated flow distribution was equal to the values measured by magnetic resonance imaging. In one case the pressure in the main pulmonary artery was slightly overestimated by computational fluid dynamics with 7 mmHg. All other pressure outcomes were in complete agreement with the invasive pressure measurements.

Conclusions Pressure and flow distribution can be reliably predicted by computational fluid dynamics for normal and stenotic pulmonary arteries. The calculated values of pressure and flow distribution were in excellent agreement with the clinical values. This demonstrates the feasibility and reliability of this method for flow analysis in patients with stenotic pulmonary arteries.

1 INTRODUCTION

Although pulmonary artery stenosis is common in congenital heart disease little is known about the hemodynamic impact of these obstructions.¹ The effects of unilateral, bilateral and bifurcation stenosis on right ventricular pressure load in different physiological circumstances – i.e. rest and exercise - remains unclear. On top of that, the long-term prognosis and the effect of pulmonary artery stenosis on lung development are still not well understood and guidelines on the best approach and timing of treatment are based on low evidence. This makes the decision whether to treat and when to treat pulmonary artery stenosis challenging.²

Studying blood flow with engineering tools as computational fluid dynamics is helpful in increasing the knowledge of causes and consequences of pathological anatomies.^{3,4} With computational fluid dynamics different conditions of load as well as different treatment options can be simulated in high resolution.⁵ Nowadays computational fluid dynamics is emerging as a clinical tool in structural heart disease i.e. assisting in the diagnosis of coronary disease and treatment planning for transcatheter aortic valve implantation procedures.^{6,7} Computational fluid dynamics has also been used for treatment planning and understanding of several congenital heart disease including ventricular and atrial septal defects and coarctation of the aorta.⁸⁻¹² For the pulmonary circulation, numerical studies have added in the knowledge of pulmonary hypertension and the univentricular circulation.^{13,14} Pulmonary artery flow in biventricular congenital heart disease is described in several papers. These include studies on the best approach for interventional or surgical treatment and the effect of pulmonary regurgitation.¹⁵⁻¹⁹ However, in most of these studies non-patient specific anatomies or boundary conditions are used with a rigid wall assumption and validation of the used methods is limited or completely lacking. The use of a compliant artery wall in combination with patient-specific anatomies and boundary conditions is limited.^{20,21} The aim of this study is to evaluate the feasibility of patient-specific numerical studies of compliant pulmonary artery anatomies by comparing the numerical outcomes to clinical data of the two most important determinants for clinical decision making: pressure gradients and flow separation between the right- and left pulmonary artery.

2 MATERIAL AND METHODS

2.1 Case selection

Three cases were selected. One patient with normal pulmonary arteries and two patients with stenosis in one or both of the pulmonary arteries. These stenosis needed to represent one of the following common patterns seen in patients with congenital heart disease; pulmonary artery stenosis after correction for Transposition of the Great arteries and an isolated stenosis of the left pulmonary artery either native or after ductal closure. To select these patients, all right-sided cardiac catheterization procedures performed in our institution over the last year were screened. First, patients were considered based on the presence of a 3D rotational angiography for anatomic reconstruction and invasive pressure measurements in both the main, right and left pulmonary artery. Next, the availability of other imaging modalities such as cardiovascular magnetic resonance imaging, and echocardiography was evaluated. Lastly, in case of equal suitability the case with the highest quality imaging for anatomic reconstruction was selected. This study was approved by the ethical committee of the University Medical Center Utrecht. Informed consent was waived.

2.2 Anatomic reconstruction

The anatomic reconstruction of the pulmonary arteries was based on the dicom files obtained by the 3D rotational angiography. For segmentation ITK-SNAP software was used.²² The pulmonary arteries were segmented from the pulmonary valve up to the first branches of the right- and left pulmonary artery. The 3D-model was then manually smoothed with a non-shrinking method using Meshmixer software (Autodesk Inc, San Rafael, USA). CRIMSON software (Cardiovascular Integrated Modelling and Simulation (CRIMSON), Available at: <http://www.crimson.software/> accessed 10.6.2020) was used to mesh the resulting geometry with a non-structured mesh consisting of tetrahedral elements. A total of 5 boundary layers was created to accurately capture near-wall flow behaviour.

2.3 Boundary conditions

The cardiovascular magnetic resonance imaging data were used to define patient-specific inlet boundary conditions. The inlet flow curve measured just above the pulmonary valve was applied at the inlet of the reconstructed model with the same frequency as the heart rate during cardiovascular magnetic resonance imaging. Since no cardiovascular magnetic resonance imaging was performed in the normal case, physiological inflow patterns were adjusted to fit the body surface area of

this patient. A plug flow inlet velocity profile was applied in all cases. At the outlets of the models a 3-element windkessel was applied consisting of a proximal- and distal resistor and a capacitor (R_{prox} , R_{dist} and C). Calculations for these values were based on previously published work of other authors on boundary conditions for the aorta and carotid arteries.²³⁻²⁵ The values for the three elements were calculated as described below for the right pulmonary artery. Calculations for the left pulmonary artery outlets were performed similarly. All values were calculated separately for the right- and left branch.

The percentage of flow going to the right pulmonary artery ($Q_{\%RPA}$) was calculated by equation (1). In this equation A_{RPA} is the smallest cross sectional area of the branch right after the bifurcation and A_{total} is the total cross sectional area of both the right- and left pulmonary artery. The flow split values determined by this equation were then used to calculate maximal and mean flows in the branches in the subsequent equations.

$$Q_{\%RPA} = A_{RPA} * 100 / A_{total} \quad (1)$$

First, the total resistance (R_{TRPA}) was calculated by equation (2), in which $P_{meanRPA}$ is the mean pressure in the right pulmonary artery over the whole cardiac cycle calculated by (3) and $Q_{meanRPA}$ is the mean flow through the right pulmonary artery.

$$R_{TRPA} = P_{meanRPA} / Q_{meanRPA} \quad (2)$$

$$P_{meanRPA} = P_{diastolic} + \frac{1}{3}(P_{systolic} - P_{diastolic}) \quad (3)$$

In equation (3) $P_{diastolic}$ is the diastolic pressure and $P_{systolic}$ is the systolic pressure in the right pulmonary artery obtained by cardiac catheterization.

The total resistance was divided into a proximal ($R_{proxRPA}$) and a distal ($R_{distRPA}$) part. The $R_{proxRPA}$ was assumed to depend on the density (ρ_{blood}), the wave speed (V_{wave}) and the area of the cross-section of the artery (A_{RPA}) as described by equation (4) and (5).

$$R_{\text{proxRPA}} = \rho_{\text{blood}} * V_{\text{wave}} / A_{\text{RPA}} \quad (4)$$

$$V_{\text{wave}} = 13.3 / (2 * \varnothing_{\text{RPA}})^{0.3} \quad (5)$$

In equation (5) the \varnothing_{RPA} is the radius of the outlet. The R_{distRPA} was then calculated by equation (6).

$$R_{\text{distRPA}} = R_{\text{TRPA}} - R_{\text{proxRPA}} \quad (6)$$

To assign a proximal and distal resistance to the individual outlets the total distal and proximal resistance were distributed over the outlets according to their areas (equation (7) and (8)). In which $A_{\text{alloutletsRPA}}$ is the sum of the areas of all outlets of the RPA and $A_{\text{outlet1RPA}}$ is the area of the defined outlet of the RPA.

$$R_{\text{distoutlet1RPA}} = R_{\text{distRPA}} * (A_{\text{alloutletsRPA}} / A_{\text{outlet1RPA}}) \quad (7)$$

$$R_{\text{proxoutlet1RPA}} = R_{\text{proxRPA}} * (A_{\text{alloutletsRPA}} / A_{\text{outlet1RPA}}) \quad (8)$$

The total capacitor values for the right pulmonary artery (C_{TRPA}) depended on the cardiac output, heart frequency and the expected pressures distal in the arteries as described in equation 9. In this equation Q_{max} is the maximum flow over the right pulmonary artery, PP_{RPA} is the pulse pressure in the right pulmonary artery and T_{max} is the time difference between the start and peak of the systole.

$$C_{\text{TRPA}} = (Q_{\text{max-RPA}} / PP_{\text{RPA}}) * T_{\text{max}} \quad (9)$$

$$PP_{\text{RPA}} = P_{\text{systolic}} - P_{\text{diastolic}} \quad (10)$$

This C_{T} was then subdivided over the outlets by equation (11) resulting in C_{outlet1} for the first outlet of the right pulmonary artery (outlet1RPA).

$$C_{\text{outlet1}} = C_{\text{TRPA}} * (A_{\text{outlet1RPA}} / A_{\text{alloutletsRPA}}) \quad (11)$$

The wall was assigned an overall compliance with a Young's modulus of 260.000 and a poisson ratio of 0.5.²⁶ The wall thickness was set to be 0.5mm. Blood was modelled as a Newtonian fluid with a blood density of 1060 kg/m³ and a viscosity of 0.004 kg/ms.

2.4 Mesh independence test

A mesh independence test was performed to ensure a grid independent solution. To obtain this the element size was decreased until the numerical results showed a difference of <1 mmHg in pressure outcomes and <1 ml for flow split outcomes. The final simulation was performed with a mesh of respectively 745.000, 866.000 and 825.000 elements for case 1, 2 and 3. A total of 4 cardiac cycles was simulated until cycle to cycle periodicity was reached with a time step size of 0.001s. Residuals needed to drop below 10^{-4} for convergence of the solution. CRIMSON software was used to perform the numerical studies.

2.5 Post-processing results

Results were post-processed and visualized in Paraview software. The evaluated results included velocity streamlines, systolic peak pressures and flow distribution values. The flow ratios were calculated as the percentage of main pulmonary artery flow going through the right or left pulmonary artery over the whole cardiac cycle. The distensibility of the arterial wall was measured at three locations, respectively the main-, right- and left pulmonary artery. The diastolic and systolic cross sectional areas in these locations were measured to evaluate the amount of expansion of the vessel wall.

2.6 Validation

The results were compared to clinical data to validate the numerical outcomes. The numerical systolic and diastolic pressures were compared to the invasive pressure measurements. The flow distribution as calculated by the computational fluid dynamics analysis were compared to cardiovascular magnetic resonance imaging data. Available measurements from cardiovascular magnetic resonance imaging or echocardiography of velocities in the main-, right- or left pulmonary artery were collated to the outcomes of the numerical solutions.

3 RESULTS

3.1 Cases

The three selected cases involved one normal and two pathological pulmonary artery anatomy's (Table 1). The normal case (case 1) was of a 1 year old girl undergoing cardiac catheterization due to a mild coarctation of the aorta. During catheterization the pressures in the pulmonary arteries were routinely measured. No cardiovascular magnetic resonance imaging was available for this case. During the selection process no case could be found with normal pulmonary arteries, complete invasive pressure measurements, high quality imaging for anatomic reconstruction and cardiovascular magnetic resonance imaging measurements. As flow split values for normal pulmonary arteries are well known in the literature high quality imaging was preferred above cardiovascular magnetic resonance imaging flow data. Case 2 was a 4 year old boy with a dextro-transposition of the great arteries corrected by arterial switch procedure with LeCompte manoeuvre. Echocardiography showed elevated right ventricular pressures for which he was assessed both with cardiovascular magnetic resonance imaging and cardiac catheterization. During catheterization a stent was placed to treat the right pulmonary artery stenosis. The second pathological case (case 3) is of a 17 year old girl treated as a newborn for a persistent ductus arteriosus. She now presented with complaints of exercise intolerance caused by a left pulmonary artery coarctation confirmed by cardiovascular magnetic resonance imaging. During cardiac catheterization a stent was placed in the left pulmonary artery to relieve the obstruction. Figure 1 shows the segmented geometries and the inflow conditions for the cases.

Table 1 - Patient characteristics.

	Case 1	Case 2	Case 3
Diagnosis	Normal PA's (mild CoA)	TGA	LPA coarctation
Age	1.2 y	4 y	17 y
BSA	0.38	0.66	1.43

BSA: body surface area (m^2), PA's: pulmonary arteries, CoA: coarctation of the aorta, TGA: Transposition of the Great Arteries, LPA: left pulmonary artery, PDA: patent ductus arteriosus, y: years.

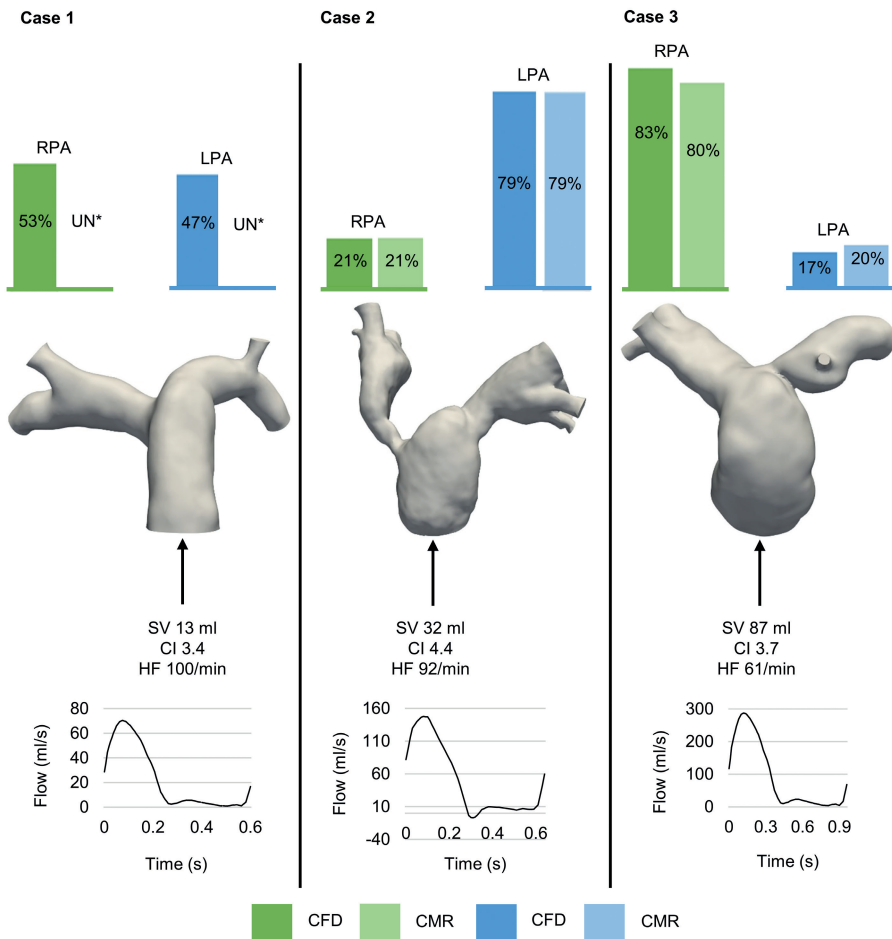


Figure 1 - The segmented anatomy for case 1-3 is displayed in grey with the used inlet boundary conditions (SV; Stroke Volume, CI; Cardiac Index, HF; Heart Frequency). The bars show the percentage of total flow through the right pulmonary artery (RPA, green) and left pulmonary artery (LPA, blue) calculated by the numerical analysis (CFD) and the cardiovascular magnetic resonance imaging (CMR). *UN: unknown.

3.2 Velocity streamlines

Figure 2 shows the velocity and streamlines for all cases during top systole and during a time step just before top systole. In case 1 the streamlines represent a laminar flow with flow acceleration in the branches. The maximal flow velocity was 1.1 m/s in the right pulmonary artery and 0.8 m/s in both the main- and left

pulmonary artery. The streamlines in case 2 reveal a more complex flow especially in the post-stenotic area in the right pulmonary artery but also in the less stenotic but still aberrant left pulmonary artery. The peak velocity was 3 m/s in the right pulmonary artery and 2.8 m/s in the left pulmonary artery. In case 3 the streamlines from the main pulmonary artery to the right pulmonary artery show a normal laminar flow. Vortices are seen in the area of the left pulmonary artery where a post-stenotic dilatation has developed. In the stenotic area velocity reaches a maximum of 2 m/s whereas in the right pulmonary artery the maximum velocity is 1 m/s.

For both case 2 and 3 during cardiovascular magnetic resonance imaging only volume assessments were performed and thus no velocity data was available. Echocardiographic measurements of velocity in the pulmonary arteries were only available for case 3. In this case the maximal measured velocity in the left pulmonary artery was 2.5 m/s. For the other cases no echocardiographic information was available. Either visualization during echography was not possible (case 2) or the pulmonary arteries were not screened (case 1).

3.3 Flow distribution

In Figure 1 the outcomes for flow distribution are shown. In case 1 the right- and left pulmonary artery received respectively 53% and 47% of the inlet flow. The stenotic right pulmonary artery in case 2 was under perfused with 21% of the flow, while the left pulmonary artery received 79%. The exact same flow distribution was found on the cardiovascular magnetic resonance imaging. In case 3 the flow distribution was in favour of the right pulmonary artery with 83% over 17% for the left pulmonary artery. These outcomes were similar to the cardiovascular magnetic resonance imaging findings with a flow distribution of 80%:20% for respectively the right- and left pulmonary artery.

3.4 Pressure outcomes

In the normal anatomy of case 1 there was no gradient over the pulmonary artery bifurcation. Pressures were equally distributed over the whole geometry. Computational fluid dynamics outcomes were similar to the invasive measured pressures. In case 2 there was a gradient over both the right- and left pulmonary artery. The gradient over the right pulmonary artery was 14 mmHg while over the left pulmonary artery the gradient was almost 30 mmHg. The measured pressure in the main pulmonary artery was 6 mmHg higher in the numerical solution as compared to the invasive measured pressure. Case 3 shows a gradient over the stenosis in the

left pulmonary artery of 7 mmHg. There was no energy loss over the right pulmonary artery in this case. Invasive and numerical measured pressures were similar. The pressure distribution outcomes of the computational fluid dynamics analysis and the comparison with the invasive pressures is shown in Figure 3.

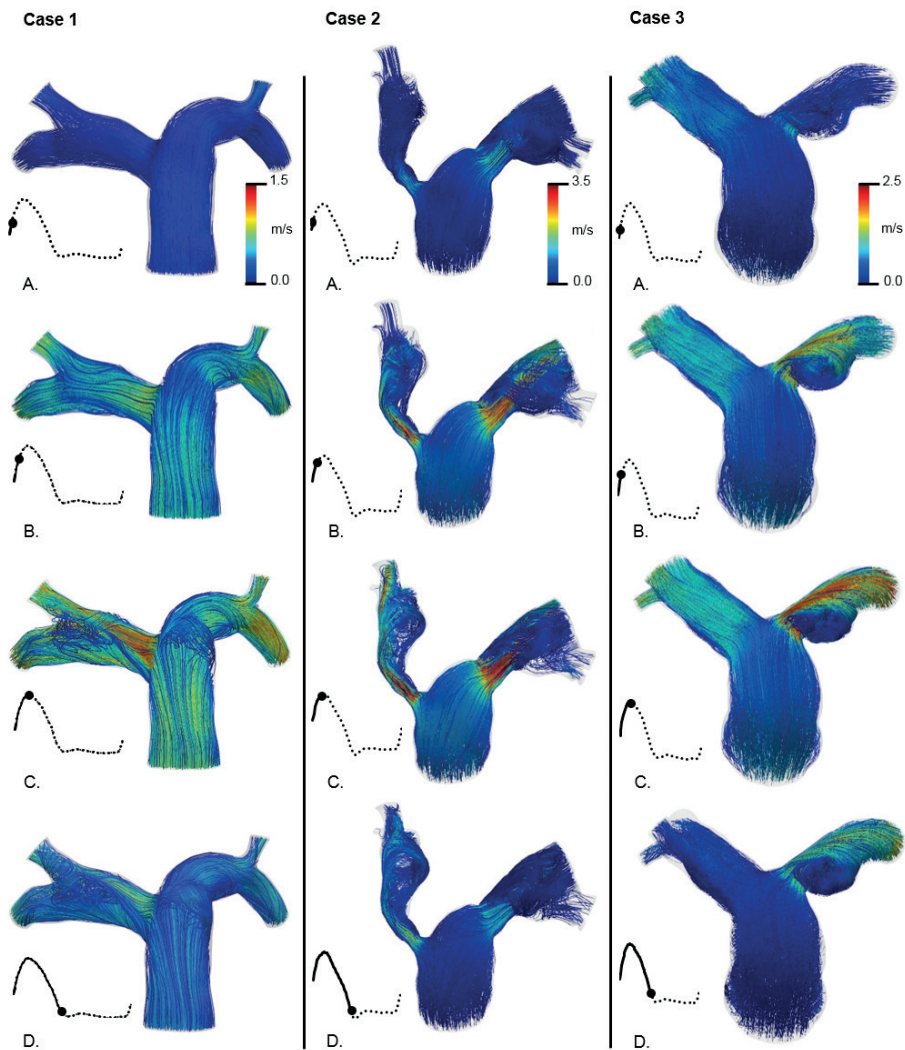


Figure 2 - Velocity streamlines for case 1-3. A-D for each case represent the velocity (m/s) on the moment in the cardiac cycle represented by the point on the inflow waveform.

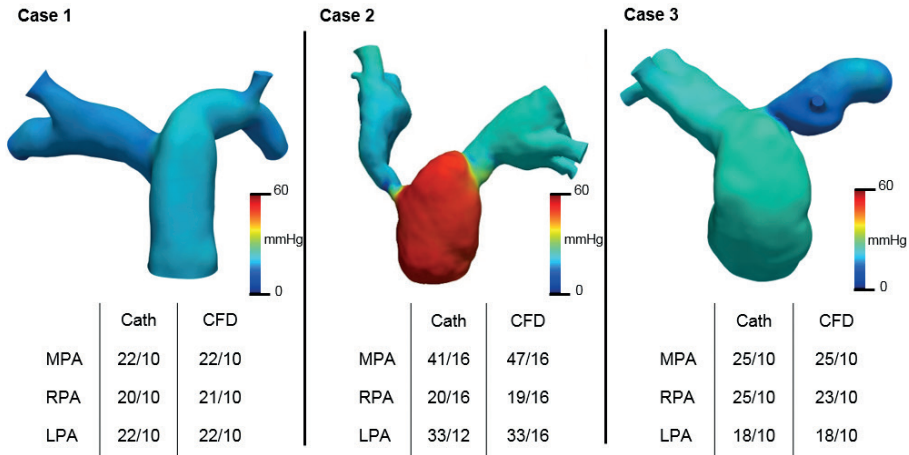


Figure 3 - The distribution of pressure in mmHg for case 1-3 during top systole. Invasive pressure measurements and computational pressure outcomes are compared for top systole and diastole (systole/diastole). Cath: invasive pressure measurements, CFD: computational fluid dynamics, MPA: main pulmonary artery, RPA: right pulmonary artery, LPA: left pulmonary artery.

3.5 Arterial wall movement

Figure 4 shows the cross sectional area of the arteries during systole and diastole showing the expansion of the artery wall over the cardiac cycle. In the normal anatomy (case 1) the area of the main pulmonary artery increased with 5.5% from 104 mm² in diastole to 110 mm² in systole. The areas of both the right- and left pulmonary artery increased approximately the same amount (5.3% and 4.1% respectively). The case with the stenosis in the right pulmonary artery (case 2) shows the largest increase in cross sectional area in the main-, right- and left pulmonary artery. The main pulmonary artery increases with 53.4% and the right- and left pulmonary artery with 27.7% and 26.2% respectively. In the case with left pulmonary artery stenosis (case 3) the diastolic area of the main pulmonary artery increases up to 22.8% during top systole. The systolic area of the right pulmonary artery is 22.0% larger than in diastole and the left pulmonary artery increases with 12.9%.

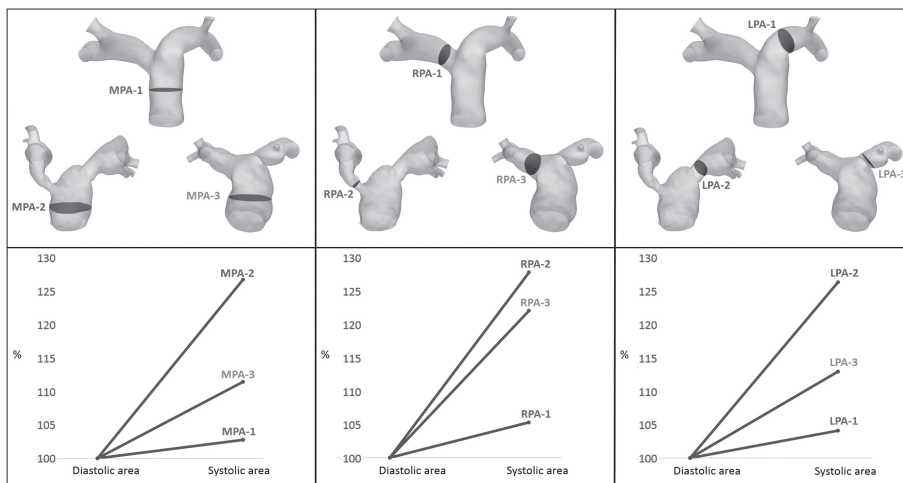


Figure 4 - The dilatation of the arterial wall during systole for case 1-3 on three locations. The cross sectional areas where the expansion is measured are shown as grey slices in the anatomy. The dilatation is displayed as the percentage increase in area from diastole (100%) to systole. MPA: main pulmonary artery, RPA: right pulmonary artery, LPA: left pulmonary artery.

4 DISCUSSION

The aim of this study was to evaluate whether computational fluid dynamics is able to predict flow distribution and pressure gradients in normal and stenotic pulmonary arteries. Patient-specific inlet- and outlet boundary conditions were applied on the in- and outlets of the 3D models reconstructed from 3D rotational angiography. Outcomes of the numerical studies were compared to cardiac catheterization and cardiovascular magnetic resonance imaging data. The results showed almost complete agreement between the numerical outcomes and the clinical data. This demonstrates that the computational method in this study is reliable in predicting pressure and flow distribution for normal and more complex pulmonary artery anatomies. The cases visualize the laminar flow in a normal pulmonary bifurcation and the complex flow patterns when an aberrant anatomy with a stenosis is present. Especially the areas with post-stenotic vortices are interesting as they are hypothesized to be of influence on the development of post-stenotic dilatation.²⁷⁻²⁹ The cases also show the unfavourable flow distribution between the right- and left pulmonary artery when a stenosis is present. Although the flow distribution is similar for case 2 and 3 the left pulmonary artery stenosis shows to be of less influence on

the main pulmonary artery pressure. This is consistent with the clinical experience that a left pulmonary artery stenosis has to be more severe before causing elevated right ventricular pressure as compared to a right pulmonary artery stenosis.

In most numerical studies analyzing stenotic pulmonary arteries the arterial wall is assumed to be rigid. As the pulmonary circulation represents a low pressure environment it is assumed that compliance is of little importance on numerical outcomes. However, in stenotic pulmonary arteries, with high afterload, compliance is of major importance to assist the right ventricle in maintaining a sufficient cardiac output.^{30,31} In these cases a rigid wall assumption will result in an overestimation of pressure and wall shear stress results.^{32,33} This is also seen when comparing the normal case and the stenotic case. In the normal case the distensibility of the pulmonary arteries is minimal with a maximal increase of 5.5% in cross sectional area of the main pulmonary artery during systole. In case 3 with a left pulmonary artery stenosis and relatively low pressure gradients the main pulmonary artery expanded to 22.9% of its original size. Case 2, the most severe stenosis with the highest pressure in the main pulmonary artery shows an increase of 53.4% in cross sectional area of the main pulmonary artery. Although the mechanical properties of the artery wall were equal in all cases the expansion of the artery wall is significantly different. This larger expansion of the artery when the pressure is higher is consistent with the windkessel function of the great arteries.³⁴

In case 2 the numerical main pulmonary artery pressure was higher than the invasive measured pressure (41 versus 47 mmHg). This could be explained by the effects of anaesthesia during intervention and the cardiac output used for the numerical study. The patient had a relatively high cardiac output during cardiovascular magnetic resonance imaging acquisition as compared to the other cases (Cardiac Index respectively 3.4, 3.7 for case 1 and 3 and 4.4 for case 2). Under anaesthesia the cardiac output is generally lower explaining a lower main pulmonary artery pressure during the procedure. However, the difference in pressure gradient over the stenosis is clinically irrelevant as it would not change the choice for interventional treatment in this case. For case 1 no cardiovascular magnetic resonance imaging was available for flow distribution validation but the flow distribution of 53% to the right pulmonary artery and 47% to the left pulmonary artery is within the expected values for normal pulmonary arteries. The validation of the numerical velocity outcomes was limited as information on velocities was available for one case only. For this case (3) maximal velocities in the left pulmonary artery were determined by echocardiography.

However, the focus of this study was validation of the numerical pressure and flow outcomes as clinical decision making is primarily based on these two variables.

Computational studies of the pulmonary arteries can improve our understanding of the interaction between the different factors resulting in the pulmonary circulation and may provide some clue's for improving diagnostics and treatment of pulmonary artery stenosis. Comparing the outcomes of these analysis to clinical data is essential to gain confidence in the reliability of computational fluid dynamics. It is therefore an important step towards the increase of the clinical utility. The outcomes of this study adds to the crack in the door for clinical applications of computational fluid dynamics in the evaluation of stenotic pulmonary arteries. Currently diagnosis and timing of treatment of pulmonary artery stenosis is primarily based on pressure gradients and to a lesser extent on flow distribution. The results of clinical evaluations are however, often inconclusive and provide only a snapshot of reality. Echocardiography is often indecisive and cardiovascular magnetic resonance imaging measurements are impossible with a stent in situ. During cardiac catheterization gradients are often underestimated due to the hypotensive properties of anaesthetics. On top of that all these diagnostic modalities lack the option of evaluation under different conditions of load. This makes determination of the hemodynamic impact of the obstruction incomplete. Exercise testing in small children is impossible and interpretation of these test in older children and adults can be challenging. In these cases computational fluid dynamics can be of added value. By simulating different conditions of load it can be used in complicated cases in which other diagnostic modalities are inconclusive or not feasible. When the indication for treatment is set computational fluid dynamics provides the opportunity to simulate post-intervention or post-surgical outcomes enabling comparison of different treatment options and thereby offering real patient-specific treatment planning.²⁰

The presented study has some limitations. First, this is a retrospective study and thereby the selection of cases was limited by the availability of measured data. The cardiovascular magnetic resonance imaging and the cardiac catheterization used for validation of the results were not acquired at the same moment and under different conditions. This may limit the hemodynamic comparability of the data. However, with the results being in good agreement this has been of little effect on the numerical results. Second, a general inlet velocity profile was applied at the inlet of the models. It is known that the appliance of a patient-specific inflow is of greater influence on the results than a patient-specific velocity profile.³⁵ A patient-specific velocity profile

can expected to be important in cases with abnormal valves. All patients selected for this study had normal pulmonary valves. To study the influence of different velocity profiles in the future it would be interesting to compare the numerical streamlines and wall shear stress outcomes to 4D flow cardiovascular magnetic resonance imaging data.

5 CONCLUSION

Studying the complex phenomenon of flow in the pulmonary circulation is important to increase the understanding and improve treatment of pulmonary artery stenosis in congenital heart disease. This study shows the use of computational analysis to evaluate blood flow in one normal and two stenotic pulmonary arteries. The aim was to evaluate the feasibility of these numerical studies and to compare the outcomes to clinical data. The results of the numerical studies were in excellent agreement with the available clinical data. These kind of studies are important to increase the confidence in the clinical utility of computational fluid dynamics for flow evaluation in congenital heart disease. In the future, larger studies are necessary to validate used methods and evaluate the added clinical value.

REFERENCES

1. Hoffman JI, Kaplan S. The incidence of congenital heart disease. *Journal of the American College of Cardiology JID* - 8301365.
2. Bacha EA, Kreutzer J. Comprehensive management of branch pulmonary artery stenosis. *J Interv Cardiol*. 2001;14(3):367-375.
3. Tawhai MH, Clark AR, Burrowes KS. Computational models of the pulmonary circulation: Insights and the move towards clinically directed studies. *Pulm Circ*. 2011;1(2):224-238.
4. DeCampi WM, Argueta-Morales IF, Divo E FAU - Kassab, Alain,J., Kassab AJ. Computational fluid dynamics in congenital heart disease. *Cardiology in the young JID* - 9200019.
5. Tang BT, Fonte TA, Chan FP, Tsao PS, Feinstein JA, Taylor CA. Three-dimensional hemodynamics in the human pulmonary arteries under resting and exercise conditions. *Ann Biomed Eng*. 2011;39(1):347-358.
6. Morris PD, van de Vosse FN, Lawford PV, Hose DR, Gunn JP. "Virtual" (computed) fractional flow reserve: Current challenges and limitations. *JACC Cardiovasc Interv*. 2015;8(8):1009-1017.
7. Bianchi M, Marom G, Ghosh RP, et al. Patient-specific simulation of transcatheter aortic valve replacement: Impact of deployment options on paravalvular leakage. *Biomech Model Mechanobiol*. 2019;18(2):435-451.
8. Morris PD, Narracott A, von Tengg-Kobligk H, et al. Computational fluid dynamics modelling in cardiovascular medicine. *Heart*. 2016;102(1):18-28.
9. DeCampi WM, Argueta-Morales IR, Divo E, Kassab AJ. Computational fluid dynamics in congenital heart disease. *Cardiol Young*. 2012;22(6):800-808.
10. Pennati G, Corsini C, Hsia TY, Migliavacca F, Modeling of Congenital Hearts Alliance (MOCHA) Investigators. Computational fluid dynamics models and congenital heart diseases. *Front Pediatr*. 2013;1:4.
11. Pittaccio S, Migliavacca F, Dubini G, Koçyıldırım E, de Leval MR. On the use of computational models for the quantitative assessment of surgery in congenital heart disease. *Anadolu Kardiyol Derg*. 2005;5(3):202-209.
12. Slesnick TC. Role of computational modelling in planning and executing interventional procedures for congenital heart disease. *The Canadian journal of cardiology JID* - 8510280. (0828-282).
13. Hunter KS, Feinstein JA, Ivy DD, Shandas R. Computational simulation of the pulmonary arteries and its role in the study of pediatric pulmonary hypertension. *Prog Pediatr Cardiol*. 2010;30(1-2):63-69.
14. Trusty PM, Slesnick TC, Wei ZA, et al. Fontan surgical planning: Previous accomplishments, current challenges, and future directions. *J Cardiovasc Transl Res*. 2018;11(2):133-144.
15. Miyaji K., Miyazaki S., Itatani K., Oka N., Kitamura T., Horai T. Novel surgical strategy for complicated pulmonary stenosis using haemodynamic analysis based on a virtual operation with numerical flow analysis. *Interact Cardiovasc Thorac Surg*. 2019;28(5):775-782.
16. Mosbahi S., Mickaily-Huber E., Charbonnier D., et al. Computational fluid dynamics of the right ventricular outflow tract and of the pulmonary artery: A bench model of flow dynamics. *Interact Cardiovasc Thorac Surg*. 2014;19(4):611-616.

17. Rao AS, Menon PG. Presurgical planning using image-based in silico anatomical and functional characterization of tetralogy of fallot with associated anomalies. *Interact Cardiovasc Thorac Surg.* 2015;20(2):149-156.
18. Chern M.-J., Wu M.-T., Wang H.-L. Numerical investigation of regurgitation phenomena in pulmonary arteries of tetralogy of fallot patients after repair. *J Biomech.* 2008;41(14):3002-3009.
19. Piskin S, Unal G, Arnaz A, Sarioglu T, Pekkan K. Tetralogy of fallot surgical repair: Shunt configurations, ductus arteriosus and the circle of willis. *Cardiovasc Eng Technol.* 2017;8(2):107-119.
20. Gundelwein L, Miro J, Gonzalez Barlatay F, Lapierre C, Rohr K, Duong L. Personalized stent design for congenital heart defects using pulsatile blood flow simulations. *J Biomech.* 2018;81:68-75.
21. Yang W., Hanley F.L., Chan F.P., Marsden A.L., Vignon-Clementel I.E., Feinstein J.A. Computational simulation of postoperative pulmonary flow distribution in alagille patients with peripheral pulmonary artery stenosis. *Congenit Heart Dis.* 2018;13(2):241-250.
22. Yushkevich PA, Piven J, Hazlett HC, et al. User-guided 3D active contour segmentation of anatomical structures: Significantly improved efficiency and reliability. *Neuroimage.* 2006;31(3):1116-1128.
23. Pirola S, Cheng Z, Jarral OA, et al. On the choice of outlet boundary conditions for patient-specific analysis of aortic flow using computational fluid dynamics. *J Biomech.* 2017;60:15-21.
24. Xiao N, Alastruey J, Alberto Figueroa C. A systematic comparison between 1-D and 3-D hemodynamics in compliant arterial models. *Int J Numer Method Biomed Eng.* 2014;30(2):204-231.
25. Boccadifuoco A, Mariotti A, Celi S, Martini N, Salvetti MV. Impact of uncertainties in outflow boundary conditions on the predictions of hemodynamic simulations of ascending thoracic aortic aneurysms. *Comput Fluids.* 2018;165:96-115.
26. Huang W, Yen RT. Zero-stress states of human pulmonary arteries and veins. *J Appl Physiol* (1985). 1998;85(3):867-873.
27. Baratchi S, Khoshmanesh K, Woodman OL, Potocnik S, Peter K, McIntyre P. Molecular sensors of blood flow in endothelial cells. *Trends Mol Med.* 2017;23(9):850-868.
28. Andersson M, Ebbers T, Karlsson M. Characterization and estimation of turbulence-related wall shear stress in patient-specific pulsatile blood flow. *J Biomech.* 2019;85:108-117.
29. McCormick SM, Seil JT, Smith DS, Tan F, Loth F. Transitional flow in a cylindrical flow chamber for studies at the cellular level. *Cardiovasc Eng Technol.* 2012;3(4):439-449.
30. Thenappan T, Prins KW, Pritzker MR, Scandurra J, Volmers K, Weir EK. The critical role of pulmonary arterial compliance in pulmonary hypertension. *Ann Am Thorac Soc.* 2016;13(2):276-284.
31. Ghio S, Schirinzi S, Pica S. Pulmonary arterial compliance: How and why should we measure it? *Glob Cardiol Sci Pract.* 2015;2015(4):58.
32. Reymond P, Crosetto P, Deparis S, Quarteroni A, Stergiopoulos N. Physiological simulation of blood flow in the aorta: Comparison of hemodynamic indices as predicted by 3-D FSI, 3-D rigid wall and 1-D models. *Med Eng Phys.* 2013;35(6):784-791.
33. He F, Hua L, Gao L. Effects of wall condition on flow distributions in arterial modeling: Comparison of rigid, dynamic, and compliant walls. *Journal of Mechanical Science and Technology.* 2016;30:1471-1475.

Understanding stenotic pulmonary arteries, can Computational Fluid Dynamics help us out?

34. Westerhof N, Lankhaar JW, Westerhof BE. The arterial windkessel. *Med Biol Eng Comput.* 2009;47(2):131-141.
35. Campbell IC, Ries J FAU - Dhawan, Saurabh,S., Fau DS, Fau QA, Fau TW, Oshinski JN. Effect of inlet velocity profiles on patient-specific computational fluid dynamics simulations of the carotid bifurcation. *Journal of biomechanical engineering JID* - 7909584.



FLOW DISTRIBUTION AND VELOCITY MEASUREMENTS IN TRANSPOSITION OF THE GREAT ARTERIES: A COMPARISON BETWEEN COMPUTATIONAL FLUID DYNAMICS AND FOUR-DIMENSIONAL FLOW CARDIAC MAGNETIC RESONANCE.

Maartje Conijn*

Evangeline G. Warmerdam*

Jos J.M. Westenberg

Felix Haas

Tim Leiner

Julio Sotelo

Sergio Uribe

Arno A.W. Roest

Friso M. Rijnberg

Hildo J. Lamb

Michiel Voskuil

Gregor J. Krings**

Heynric B. Grotenhuis**

* This authors contributed equally

** This authors contributed equally

Submitted

ABSTRACT

Background In this study Computational fluid dynamics (CFD) and 4D flow cardiac magnetic resonance (CMR) were compared for hemodynamic evaluation of the pulmonary arteries (PAs) of patients with Transposition of the Great Arteries (TGA).

Methods Four cases were included: 3 TGA patients and 1 control. A 3D non-contrast and a 4D flow CMR scan were acquired. For CFD, the anatomy was reconstructed using the 3D scan. A mass flow inlet was applied with 3-element windkessels on the outlets and a compliant wall. The anatomical reconstruction, flow distribution and velocities were compared between CFD and 4D flow CMR.

Results There was a mean difference of 61.6 mm² in cross sectional areas between the CFD and 4D flow CMR anatomy. The largest discrepancies were observed in the main branches (mean 126.1 mm²). Flow distribution over the right and left branch differed 1-10% between both modalities. High velocities with comparable maximal values were observed in stenotic areas in both techniques.

Discussion The comparability of CFD and 4D flow CMR for hemodynamic assessment of the PAs in TGA patients is depending on the accuracy of the reconstructed anatomy. This explains the reported differences between both modalities on velocity and flow distribution outcomes.

1 INTRODUCTION

Transposition of the Great Arteries (TGA) is seen in 0.2 of 1000 live births and comprises 20% of all cyanotic congenital heart diseases.¹ The Arterial Switch Operation (ASO) is the most common procedure for correction of this heart defect. The outcomes of this approach have greatly improved over the last decades. Nowadays, the majority of the TGA patients will survive into adulthood.² This increased survival goes hand in hand with higher long-term morbidity. One of the common effects of the ASO is stenosis of the pulmonary arteries (PAs). Up to 80% of the patients develops some degree of PA stenosis and many TGA patients will require (repeat) intervention at some point in life.^{1,2} All TGA patients will therefore require lifelong follow-up with evaluation of the PAs.

During follow-up, the cardiovascular status of TGA patients is evaluated non-invasively with several imaging modalities, including echocardiography, cardiac magnetic resonance (CMR), computed tomography (CT) and ventilation-perfusion scans. In-depth evaluation of flow patterns with visualization and quantification of PA blood flow is not routinely applied in the clinical assessment. However, previous studies have shown that abnormal blood flow patterns within the pulmonary vascular bed may contribute to a decline in cardiovascular functioning.³ Imaging techniques that provide visualization and quantification of blood flow could improve our understanding of the often complex hemodynamics in TGA patients and potentially guide the timing and nature of interventions. Two advanced diagnostic modalities provide a comprehensive assessment of blood flow: computational fluid dynamics (CFD) and 4D flow cardiac magnetic resonance (4D flow CMR). Both modalities allow for flow visualization and assessment of a broad range of parameters for flow quantification.

CFD is a specialized area of mathematics and a branch of fluid mechanics, which can be used to evaluate blood flow in the cardiovascular system of patients in a reconstructed 3D model of the patient's anatomy. CFD has several advantages: the high spatial and temporal resolution, the potential to perform virtual surgery or stent implantation, and the ability to simulate different loading conditions i.e. rest and exercise. However, CFD outcomes are always an approximation of reality and highly depend on the quality of the reconstructed anatomy images and the applied boundary conditions.^{4,5} Furthermore, processing time can be extensive, ranging between hours up to several days, depending on the complexity of the case. 4D

flow CMR is the term used for time-resolved phase-contrast CMR with velocity-encoding in all three spatial directions.^{6,7} Using 4D flow CMR, qualitative analysis and quantification of flow over an entire volume can be obtained. This technique has been available for several decades now. However, only in the last years acquisition time has reached acceptable levels for clinical application.⁸ Despite limitations such as limited spatial and temporal resolution, 4D flow CMR is currently the only non-invasive imaging technique available to visualize blood flow in vivo.

In this study, CFD studies and 4D flow CMR measurements of the PAs of post-ASO TGA patients with and without stenosis are compared. The aim of this study was to compare the clinical relevant measurements of flow distribution and velocities between both modalities to explore their potential of hemodynamic evaluation in TGA patients.

2 MATERIALS AND METHODS

2.1 Patients

For this study four cases were selected: three post-ASO TGA patients and one control. The control case (case 1) involved a patient with normal PAs but a history of coarctation of the aorta. The three TGA patients included 1 patient with bilateral PA stenosis (case 2), one with unilateral PA stenosis (case 3) and one without PA stenosis (case 4) (table 1). All study participants underwent CMR as part of routine follow-up care. In the same session 4D flow CMR was performed for study purposes. Both the regular CMR and 4D flow CMR were used for this study. Approval from the local Medical Ethical Committee was granted for this study (number 16-197 and 18-200, respectively). Written informed consent was obtained from all patient and, if applicable, their guardians.

Table 1. Patient characteristics.

Case	Condition	Age (y)	Sex	BSA (m ²)	PAS	Heart rate (beats/min)
1	Control (CoA)	7	Female	1.04	None	73
2	TGA	18	Male	1.99	Bilateral	52
3	TGA	17	Male	2.1	Unilateral	75
4	TGA	11	Male	1.05	None	67

BSA: body surface area, PAS: pulmonary artery stenosis, CoA: coarctation of the aorta, TGA: transposition of the great arteries. y: years, ml: milliliters, min: minutes.

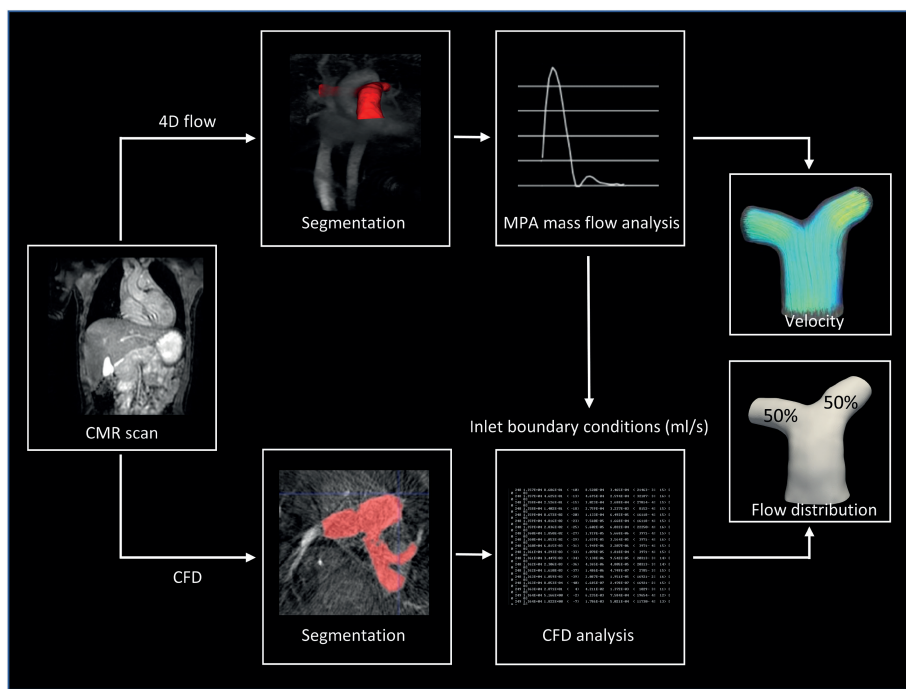


Figure 1 - Used methods For both modalities, segmentation of the vessel of interest is the first step. Subsequently, flow waveform and volumes in the main pulmonary artery just above the pulmonary valve are measured using 4D flow CMR, which will be used as inlet boundary condition for the CFD analysis. For both modalities, peak velocities and flow volumes are measured in the main, right and left pulmonary artery.

2.2 CMR acquisition

A visual summary of the study methods can be found in Figure 1. CMR imaging was performed on a 3.0 T magnetic resonance scanner (Ingenia R5.6.1, Philips Healthcare, Best, The Netherlands). A 3D non-contrast end-diastolic scan, in axial orientation, with prospective ECG-triggering and respiratory navigator-gating was performed to visualize cardiovascular anatomy, with specific focus on the PAs. Imaging parameters for the 3D non-contrast scan were as follows: spatial resolution = $0.92 \times 0.92 \text{ mm}^2$, FOV = 294 mm^2 , slice thickness = 1.5 - 3 mm, echo time: 1.31 ms, repetition time: 3.7 - 4.1 ms, flip angle = 10° . Scan times were typically 10 minutes per scan. The 4D flow CMR was a respiratory navigator-gated scan with retrospective ECG-gating, in a sagittal orientation, scan parameters were as follows: spatial resolution = $2.5 \times 2.5 \times 2.5 \text{ mm}^3$, field of view = 300 mm^2 , temporal resolution = 32.8 - 46.1 ms, echo time = 2.1 - 2.4 ms, repetition time: 3.9 - 4.2 ms, flip angle = 8° , velocity encoding

speed = 200–380 cm/s based on 2D CMR results. The acquired volume covered the entire PAs. Concomitant gradient correction was performed from standard available scanner software. Acquisition times were typically 8–12 minutes per scan.

2.3 CMR post-processing

The 4D flow CMR images were processed using an in-house MATLAB toolbox (The MathWorks, Natick, MA, USA)⁹ which included the segmentation of the PAs and the generation of the tetrahedral finite element mesh as detailed in previous reports.^{10,11} The angiographic image was segmented at peak systole using thresholding, labeling, and manual separation of the vessels, based on the angiographic image generated by the velocities field.¹² The tetrahedral finite element mesh was created using the iso2mesh MATLAB toolbox.¹³ Once the mesh was constructed, we transferred the velocity values to each node of the mesh from the 4D flow CMR using a cubic interpolation.

2.4 CFD method

For the CFD analysis, the end-diastolic 3D non-contrast CMR scan was used to construct a 3D model of the PAs. Segmentation was performed with ITK-SNAP software (<http://itksnap.org>). The Surface Tessellation Language (STL) mesh was manually smoothed in Meshmixer software (Autodesk Inc, San Rafael, USA). A tetrahedral mesh with a total of five boundary layers was created using CRIMSON software (Cardiovascular Integrated Modelling and Simulation (CRIMSON; available at <http://www.crimson.software/> accessed 10.6.2020). To ensure numerical outcomes independent of mesh size, a grid independence test was performed. The solution was considered mesh independent in case of <1 mmHg difference in pressure outcomes, <0.5 mmHg in wall shear stress and <1 ml in flow split outcomes. The final simulation was performed with a mesh of respectively 884.536, 1.010.000, 1.004.000 and 1.000.000 elements for case A, B, C and D.

In order to be able to compare both modalities during an identical physiological state, the 2D measured mass flow waveform and cardiac frequency obtained by the 4D flow CMR scan were used to define the inlet boundary conditions for the CFD analysis. A general parabolic velocity profile was applied. A three-element windkessel was coupled to each outlet consisting of a proximal- and distal resistor and a capacitor. The windkessel parameters were calculated as previously described.¹⁴ CRIMSON software was used to perform the numerical studies. Several conditions were set as follows: the wall was assigned an overall compliance with a Young's modulus of

0.26 MPa and a Poisson ratio of 0.5 [15]. The wall thickness was set to be 0.5mm. Blood was assumed to behave as a Newtonian fluid with a blood density of 1060 kg/m³ and a viscosity of 0.004 kg/m·s. Four cardiac cycles with a time step size of 0.001s were simulated. The last simulated cardiac cycle was used for analysis. The solution was considered converged when residuals dropped below 10⁻⁴.

2.5 Comparison of CMR and CFD

For the visualization and quantification of the flow, Paraview software was used.¹⁵ Due to the compliant wall applied at the boundaries of the CFD model, the diastolic segmented anatomy changed over the cardiac cycle. In order to compare the accuracy of this anatomical reconstruction we measured the cross-sectional area of the main pulmonary artery (MPA), the right pulmonary artery (RPA) and the left pulmonary artery (LPA) at the locations displayed in figure 2. In the presence of a stenosis, the smallest cross-sectional area was measured. In all other cases the area was measured just distal to the bifurcation. At the same locations as these measurements, the anatomy was sliced. Flow (ml/s) over the whole area of this slice and over the complete cardiac cycle was obtained to calculate stroke volumes and visualize flow curves over time. The stroke volumes were then used to calculate the flow distribution between the LPA and RPA. The point on the slice with the highest velocity over the cardiac cycle was extracted. For this point a velocity-time graph was constructed. Streamlines with velocity color were obtained and visually compared at the peak systolic phase.

3 RESULTS

3.1 Anatomy

In table 1 the characteristics of the included patients are displayed. The difference in artery cross-sectional area between both reconstructions are shown in table 2. The mean difference between the measurements was 61.6 mm². The largest discrepancies between the CFD and 4D flow anatomies were seen in the reconstructed main branches with a mean difference of 126.1 mm². The reconstructed branches differed mean 49.4 mm² and 9.4 mm² for the right and left branch respectively. In four of the 12 measurements, the cross-sectional area of the CFD anatomy was smaller compared to the 4D flow segmented anatomy, while the CFD cross-sectional area was larger in eight measurements. The maximal difference was 327.0 mm² in the MPA of case 3 and the minimal difference was 0.4 mm² in both branches of case 2.

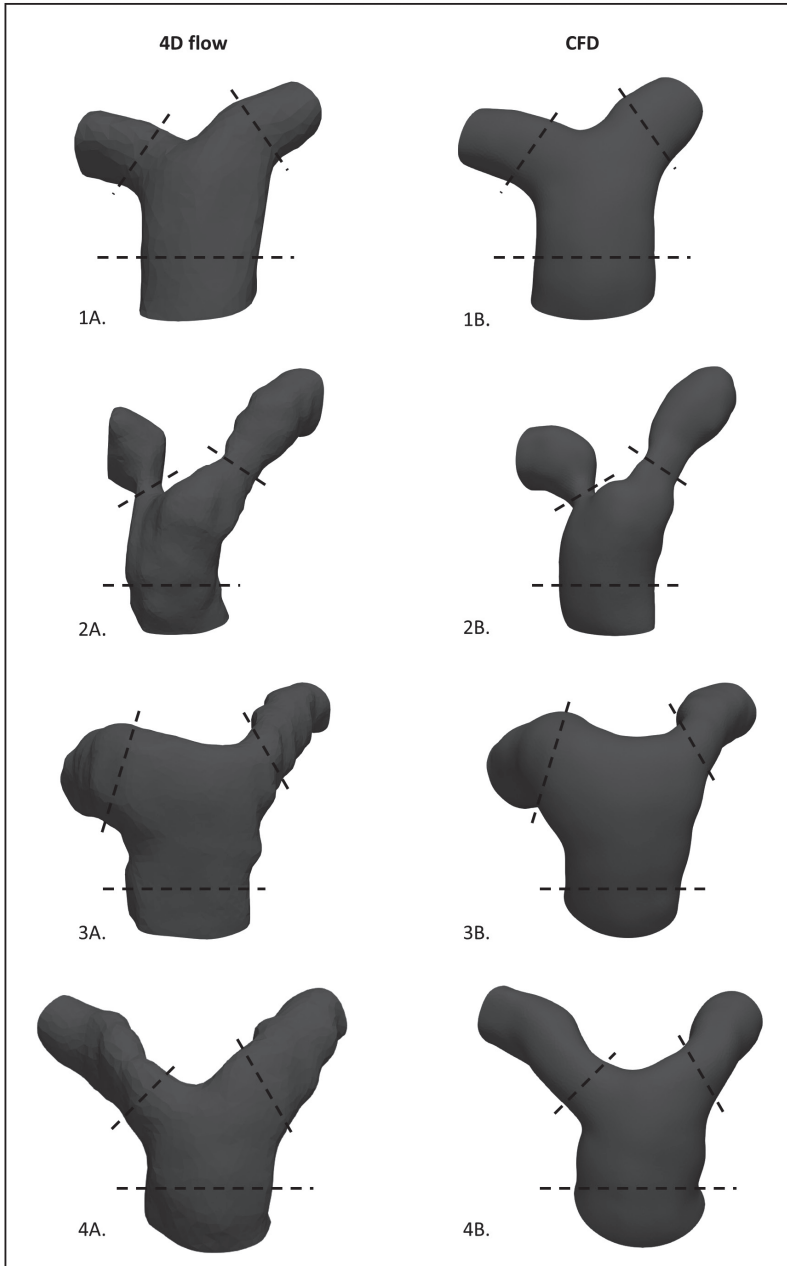


Figure 2 - 3D anatomy and planes for analysis The 4 cases are displayed with the reconstructed anatomy for 4D flow CMR analysis (Case 1a-4a) and CFD analysis (Case 1b-4b). The lines through the main, right and left pulmonary artery show the location for diameter measurements and slices for velocity and flow analysis.

3.2 Flow pattern and peak velocity

Figure 3 shows the velocity streamlines for all 4 cases. By visual comparison, 4D flow CMR and CFD are in agreement on the areas of increased flow velocity. In the bilateral stenotic branches of case 2, a clear increase in flow velocity is seen. However, this color encoding shows a more abrupt and higher increase in the CFD case compared to the 4D flow CMR measurements. Case 3 shows an increase in velocity over the unilateral stenosis of the LPA which seems more distinct in the 4D flow CMR measurements. A small area of higher velocity is seen on the right side of the MPA, also more distinct in the 4D flow CMR measurements. Case 4 shows an increase in velocity in both the RPA and LPA with comparable color encoding. In the control case (case 1), 4D flow CMR measured a lower velocity over the whole fluid domain compared to CFD. The course of the colored streamlines is comparable in all case with CFD and 4D flow CMR in good agreement on the origin of recirculation. Examples of these recirculation areas can be seen in the RPA of case 2 where a post-stenotic recirculation area develops and in case 3 where an enlarged RPA results in recirculation in the ostia.

In figure 4, the time-velocity graphs over the complete cardiac cycle are displayed. In table 2, the maximal velocity in the slices is numerically compared between CFD and 4D flow CMR. In case 1, 4D flow CMR measured lower velocities as compared to CFD. In the MPA, the CFD velocity is two times higher compared to 4D flow CMR (1.4 m/s and 0.7 m/s respectively). In the other three cases, differences between CFD and 4D flow measurements vary between 0.0 and 0.5 m/s. The curve forms with timing of the peak velocity are equal for 4D flow CMR and CFD.

3.3 Flow distribution

Flow distribution comparison between CFD and 4D flow CMR is shown in Table 2. In two cases, the difference in RPA flow between CFD and 4D flow CMR was 1%. In case 3, the CFD measurements showed 68% flow towards the RPA while 4D flow measured 61%. In case 2 the largest difference in flow distribution was observed. In this case, 4D flow CMR measured an equal flow distribution while CFD calculated an increased flow to the LPA compared to the RPA. Flow-time curves for all cases are displayed in Figure 4. In the three TGA cases, the sum of forward LPA and RPA flow was higher than the total volume of flow measured in the MPA by 4D flow CMR. Differences were 10.5%, 5.2% and 21.0%, respectively, for cases 2, 3 and 4. In case 1, the MPA stroke volume was 27.2% higher compared to the sum of the measured forward RPA and LPA flow. The difference in MPA stroke volume and the sum of RPA and LPA flow in the CFD calculations was 0.6%, 3.3%, 0.6% and 0.2% for case 1, 2, 3 and 4 respectively.

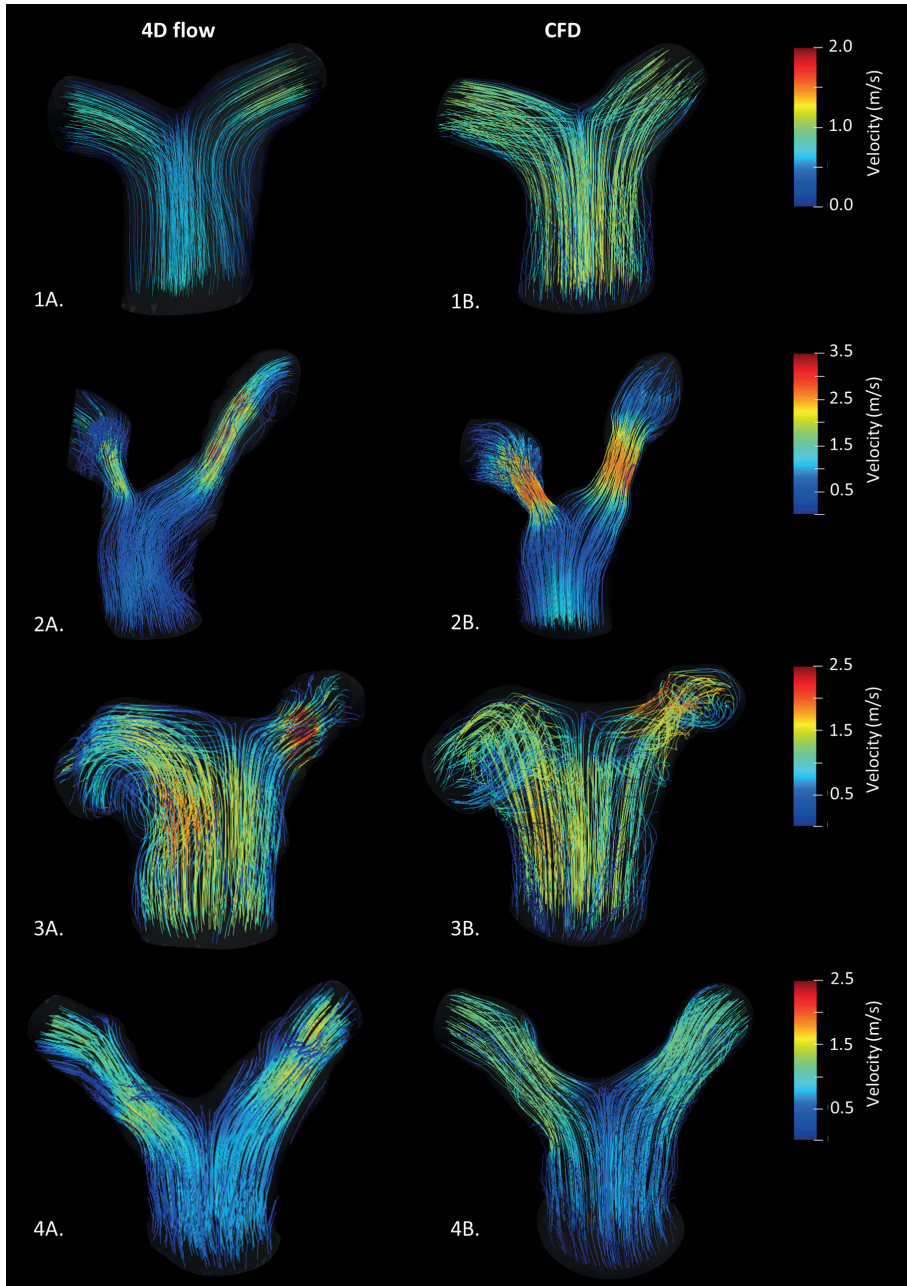


Figure 3 - Velocity streamlines Visual assessment of flow patterns and flow velocities using color-coded streamlines of the 4D flow CMR cases (1a-4a) and the CFD cases (1b-4b).

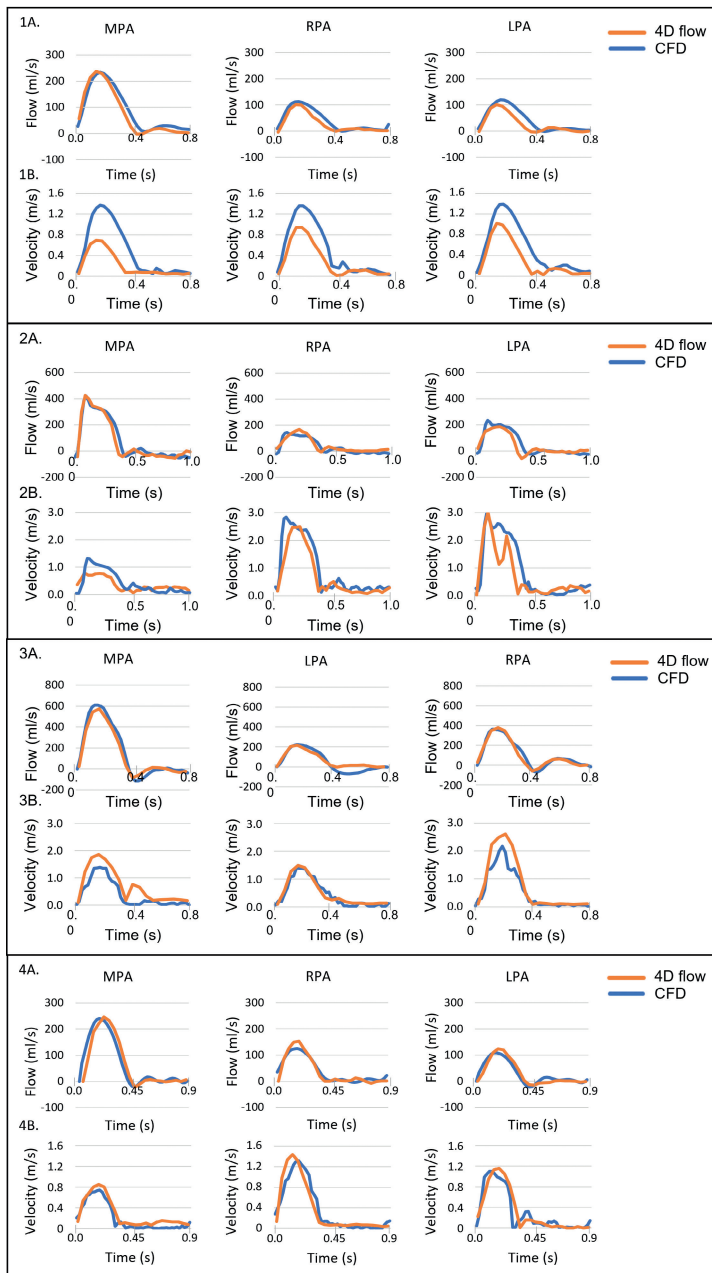


Figure 4. Velocity and flow graphs The flow-time graphs (1a-4a) show the flow curve in the area of the slice as presented in figure 2. The velocity-graphs (1b-4b) show the velocity on the point with the maximal velocity in the slice as presented in figure 2. MPA; main pulmonary artery, RPA; right pulmonary artery, LPA; left pulmonary artery, 4D flow: 4D flow CMR.

Table 2 - Comparison 4D flow and CFD outcomes.

	4D flow	CFD	Difference
Case 1			
Anatomy			
• MPA area	316.8 mm ²	311.5 mm ²	-5.3 mm ²
• RPA area	157.9 mm ²	152.7 mm ²	-5.2 mm ²
• LPA area	151.3 mm ²	155.3 mm ²	+4.0 mm ²
Maximal velocity			
• MPA	0.7 m/s	1.4 m/s	+0.7 m/s
• RPA	0.9 m/s	1.4 m/s	+0.5 m/s
• LPA	1.0 m/s	1.4 m/s	+0.4 m/s
Flow distribution			
• MPA	50.4 ml	50.8 ml	+ 0.4 ml
• RPA	18.8 ml	25.5 ml	+ 6.7 ml
• LPA	17.9 ml	25.6 ml	+ 7.7 ml
• RPA + LPA	36.7 ml	51.1 ml	+ 14.4 ml
• RPA	50 %	51 %	+1 %
• LPA	50 %	49 %	-1 %
Case 2			
Anatomy			
• MPA area	755.3 mm ²	762.5 mm ²	+7.2 mm ²
• RPA area	106.7 mm ²	107.1 mm ²	+0.4 mm ²
• LPA area	132.4 mm ²	132.0 mm ²	-0.4 mm ²
Maximal velocity			
• MPA	0.8 m/s	1.3 m/s	+0.5 m/s
• RPA	2.5 m/s	2.8 m/s	+0.3 m/s
• LPA	3.0 m/s	3.0 m/s	+/-0.0 m/s
Flow distribution			
• MPA	92.6 ml	93.5 ml	+ 0.9 ml
• RPA	50.9 ml	38.5 ml	- 12.4 ml
• LPA	51.4 ml	58.1 ml	+ 6.7 ml
• RPA + LPA	102.3 ml	96.6 ml	-5.7 ml
• RPA	50 %	40 %	-10 %
• LPA	50 %	60 %	+10 %

Table 2 - (Continued)

	4D flow	CFD	Difference
Case 3			
Anatomy			
• MPA area	416.4 mm ²	743.6 mm ²	+327.0 mm ²
• RPA area	402.8 mm ²	569.9 mm ²	+167.1 mm ²
• LPA area	158.1 mm ²	187.1 mm ²	+29.0 mm ²
Maximal velocity			
• MPA	1.5 m/s	1.4 m/s	-0.1 m/s
• RPA	1.9 m/s	1.4 m/s	-0.5 m/s
• LPA	2.6 m/s	2.2 m/s	-0.4 m/s
Flow distribution			
• MPA	122.5 ml	125.6 ml	+3.1 ml
• RPA	91.1 ml	85.4 ml	-5.7 ml
• LPA	57.1 ml	39.5 ml	-17.6 ml
• RPA + LPA	148.2 ml	124.9 ml	-23.3 ml
• RPA	61 %	68 %	+7.0 %
• LPA	39 %	32 %	-7.0 %
Case 4			
Anatomy			
• MPA area	371.0 mm ²	535.9 mm ²	+164.9 mm ²
• RPA area	115.1 mm ²	139.9 mm ²	+24.8 mm ²
• LPA area	144.3 mm ²	140.3 mm ²	-4.0 mm ²
Maximal velocity			
• MPA	0.9 m/s	0.8 m/s	-0.1 m/s
• RPA	1.4 m/s	1.3 m/s	-0.1 m/s
• LPA	1.2 m/s	1.1 m/s	-0.1 m/s
Flow distribution			
• MPA	59.4 ml	60.9 ml	+1.5 ml
• RPA	36.1 ml	34.9 ml	-1.2 ml
• LPA	26.4 ml	26.1 ml	-0.3 ml
• RPA + LPA	62.5 ml	61.0 ml	-1.5 ml
• RPA	58 %	57 %	-1 %
• LPA	42 %	43 %	+1 %

MPA: main pulmonary artery, RPA: right pulmonary artery, LPA: left pulmonary artery.

4 DISCUSSION

CFD and 4D flow CMR are emerging imaging modalities for hemodynamic evaluation of patients with congenital heart defects. To the best of our knowledge, this is the first study comparing results of PA flow analysis by CFD and 4D flow CMR in TGA patients after ASO. The cases of this study show three major findings:

1. CFD and 4D flow were good agreement on flow distribution between the RPA and LPA with a maximum difference of 10%. 4D flow CMR shows large differences in measured total MPA flow and the sum of the branch flow.
2. Velocity-time graphs were comparable in form. Absolute maximal velocity values were similar in areas with high velocity, while in areas with low flow velocity larger differences were observed.
3. Segmentation resulted in uncertainties regarding the accuracy of the reconstructed anatomies with large differences in cross sectional areas especially in the main branches of the cases.

Peak velocities and flow distribution are of great importance in the clinical evaluation of PA stenosis. A high peak velocity in one of the pulmonary branches on echocardiography is often one of the first indications for intervention. The distribution of flow between the RPA and LPA and thus the perfusion mismatch between the right and left lung is an important measure for the degree of stenosis. A reduction of ipsilateral lung perfusion above 35% is considered a rationale for intervention of the stenosed PA branch.¹⁶ In clinical practice, peak velocities are obtained using Doppler echocardiography or 2D phase-contrast CMR. Both modalities use a single plane for measurements in the region of interest and thus may not provide an accurate peak velocity measurement. Furthermore, the limited acoustic window in older or obese children and adults can make visualization and thus velocity measurements of the branch PAs a challenge or even impossible. Previous research has clearly shown that 2D phase-contrast CMR often underestimates peak velocities and individual flow to the affected branches TGA patients, thereby underestimating the number of TGA patients suitable for intervention.¹⁷ This is also seen in our study in which 4D flow CMR measured differences between MPA stroke volume and the sum of RPA and LPA flow were between 5% and 27%. On top of that, when a stent is implanted in one of the PAs, stent flow and velocity measurements are unfeasible. Ventilation-perfusion scans can then be used to determine the flow distribution but require a

high dose of radiation, which is undesirable in the young TGA population in need for life-long, frequent follow-up.

The results of patient-specific CFD analysis are highly dependable on the quality of the 3D reconstruction of the patient anatomy. It therefore always depends on the spatial and temporal resolution of the available imaging and the quality of the performed segmentation. Even small differences in geometry used for the CFD analysis can greatly impact the numerical outcomes. In this study, the PAs were segmented using the 3D non-contrast CMR (spatial resolution $0.92 \times 0.92 \times 2$ mm) rather than the 4D flow CMR (spatial resolution $2.5 \times 2.5 \times 2.5$ mm). By using the higher spatial resolution source for the anatomic reconstruction, the accuracy of the numerical outcomes was improved. However, because of this, the 3D non-contrast CMR represented the end-diastolic anatomy given the timing of acquisition, and the 4D flow CMR the peak-systolic anatomy. To overcome this, a compliant arterial wall was applied. This compliant wall ensured enlargement of the diastolic anatomy over the cardiac cycle, expanding with the increase of flow in the fluid domain.¹⁸ However, as this was not a patient-specific compliance, the entire domain had the same mechanical properties. It does not take into account the possible increased stiffness of arteries i.e. after surgery. This may explain the visible and measured differences between the systolic CFD and 4D flow CMR anatomy.

The measurements of velocities in the fluid domain of the reconstructed anatomies were comparable for all cases. The largest differences were found in velocities in areas with low flow velocity. Here the underestimation of velocity by CMR is shown, i.e. in case 1. In the more stenotic areas and areas with higher velocities, measurements of CFD and 4D flow CMR were comparable. In one of the cases, the difference in flow distribution between CFD and 4D flow CMR would cause uncertainties about the indication for intervention. In case 3, CFD showed a RPA perfusion of 32% which would be amenable for intervention with, whereas 4D flow CMR demonstrated a RPA perfusion of 39% which would not indicate treatment. In the future it would be interesting to further explore the influence of small variations in segmented anatomy on computational outcomes of clinically relevant parameters and the impact on clinical decision making.

4.1 Limitations

There are several limitations that need to be taken into account for this study. First, only four cases were evaluated, which is insufficient for statistical comparison. Second, no

interobserver comparison was performed, segmentations were performed by only one experienced observer (MC: CFD, EW: 4D flow CMR). Segmentation and analysis by multiple observers could have made the results more robust. The difference of timing of segmentation (CFD: diastolic scan, 4D flow: systolic scan) limits the ability of comparison of the segmented anatomy. Also, although patient-specific mass flow, waveform and heart frequency were used as inlet boundary conditions, generic values were used for the inlet velocity profile (parabolic profile) and compliance of the vessel. Since all of the presented cases had normal functioning valves with only mild valve regurgitation, this probably did not influence our results. However, in case of valvular regurgitation or an anatomically abnormal valve, thus abnormal inlet velocity profiles, patient-specific velocity profiles will likely be necessary to achieve comparable results. Last, no analysis was performed on downsampled CFD data to detect whether the reported differences are caused by the low spatial resolution of the 4D flow CMR.

5 CONCLUSION

In the presented study flow distribution and peak velocities measured by CFD and 4D flow CMR were compared in 3 TGA patients and 1 control case. The difference in measured flow distribution by CFD and 4D flow CMR was clinically relevant in 1 case. Areas with high velocity were equally detected with similar absolute velocity values. In areas with low flow velocity 4D flow CMR underestimated the flow velocity. Further research is warranted in larger patient groups to identify the influence of difference in segmentation and the clinical application of both techniques.

REFERENCES

1. Moe TG, Bardo DME. Long-term outcomes of the arterial switch operation for d-transposition of the great arteries. *Prog Cardiovasc Dis.* 2018;61(3-4):360-364.
2. Santens B, Van De Bruaene A, De Meester P, et al. Outcome of arterial switch operation for transposition of the great arteries. A 35-year follow-up study. *Int J Cardiol.* 2020;316:94-100.
3. Vanderlaan RD, Caldarone CA, Backx PH. Heart failure in congenital heart disease: The role of genes and hemodynamics. *Pflugers Arch.* 2014;466(6):1025-1035.
4. Boccadifuoco A, Mariotti A, Celi S, Martini N, Salvetti MV. Impact of uncertainties in outflow boundary conditions on the predictions of hemodynamic simulations of ascending thoracic aortic aneurysms. *Comput Fluids.* 2018;165:96-115.
5. DeCampi WM, Argueta-Morales IR, Divo E, Kassab AJ. Computational fluid dynamics in congenital heart disease. *Cardiol Young.* 2012;22(6):800-808.
6. Markl M, Harloff A, Bley TA, et al. Time-resolved 3D MR velocity mapping at 3T: Improved navigator-gated assessment of vascular anatomy and blood flow. *J Magn Reson Imaging.* 2007;25(4):824-831.
7. Uribe S, Beerbaum P, Sørensen TS, Rasmusson A, Razavi R, Schaeffter T. Four-dimensional (4D) flow of the whole heart and great vessels using real-time respiratory self-gating. *Magn Reson Med.* 2009;62(4):984-992.
8. Sierra-Galan LM, François CJ. Clinical applications of MRA 4D-flow. *Curr Treat Options Cardiovasc Med.* 2019;21(10):58.
9. Sotelo J, Mura J, Hurtado D, Uribe S. A novel matlab toolbox for processing 4d flow mri data. ; 2019.
10. Sotelo J, Urbina J, Valverde I, et al. 3D quantification of wall shear stress and oscillatory shear index using a finite-element method in 3D CINE PC-MRI data of the thoracic aorta. *IEEE Trans Med Imaging.* 2016;35(6):1475-1487.
11. Sotelo J, Urbina J, Valverde I, et al. Three-dimensional quantification of vorticity and helicity from 3D cine PC-MRI using finite-element interpolations. *Magn Reson Med.* 2018;79(1):541-553.
12. Bock J, Frydrychowicz A, Stalder AF, et al. 4D phase contrast MRI at 3 T: Effect of standard and blood-pool contrast agents on SNR, PC-MRA, and blood flow visualization. *Magn Reson Med.* 2010;63(2):330-338.
13. Fang Q, Boas D. Tetrahedral mesh generation from volumetric binary and grayscale images. ; 2009:1142-1145.
14. Conijn M, Krings GJ. Understanding stenotic pulmonary arteries: Can computational fluid dynamics help us out? *Prog Pediatr Cardiol.* 2021:101452.
15. Ahrens J, Geveci B, Law C. *ParaView: An end-user tool for large data visualization, visualization handbook.* Elsevier; 2005.
16. Feltes TF, Bacha E, Beekman RH, 3rd, et al. Indications for cardiac catheterization and intervention in pediatric cardiac disease: A scientific statement from the american heart association. *Circulation.* 2011;123(22):2607-2652.
17. Jarvis K, Vonder M, Barker AJ, et al. Hemodynamic evaluation in patients with transposition of the great arteries after the arterial switch operation: 4D flow and 2D phase contrast cardiovascular magnetic resonance compared with doppler echocardiography. *J Cardiovasc Magn Reson.* 2016;18(1):59-016-0276-8.
18. Figueroa C, Vignon-Clementel I, Jansen K, Hughes T, Taylor C. A coupled momentum method for modeling blood flow in three-dimensional deformable arteries. *Comput Methods Appl Mech Eng.* 2006;195:5685-5706.



PART III



TO TREAT OR NOT TO TREAT PULMONARY ARTERIES: EPINEPHRINE PROVOCATION TO UNMASK RIGHT VENTRICULAR LOAD.

Maartje Conijn

Dorita H.P.M. Dekkers

Mirella M. Molenschot

Johannes M.P. Breur

Martijn G. Sliker

Felix Haas

Gregor J. Krings

International Journal of Cardiology Congenital Heart Disease

Volume 7;2022;100306

ABSTRACT

Background Pulmonary artery stenosis (PAS) is common in congenital heart disease (CHD). The indication for treatment of PAS is primarily based on invasively measured pressure gradients. Anesthetics used during cardiac catheterization cause systemic and pulmonary hypotension. We hypothesize that this leads to underestimation of right ventricular (RV) pressure load and under treatment of PAS. The aim of this study is to describe the use of epinephrine to unmask RV pressure load in patients with PAS.

Methods All cardiac catheterizations in which epinephrine was administered to evaluate RV load were included. There was an indication for treatment in case of a right to left ventricular (RV:LV) pressure ratio >0.6 . The indication for treatment before and after epinephrine was evaluated to determine its role in clinical decision making.

Results A total of 74 procedures were included. In all procedures the invasively measured LV pressure was below the awake blood pressure. At baseline, 33 patients had a RV:LV ratio >0.6 . In 41 patients the baseline RV:LV ratio was <0.6 . After epinephrine bolus, the LV pressure was raised up to the awake blood pressure. In 19 of the 41 patients without baseline indication, this resulted in a RV:LV ratio >0.6 thereby revealing the indication for treatment. No epinephrine related complications were registered.

Conclusion The hypotensive properties of anesthetics during cardiac catheterization may lead to underestimation of RV pressure load. Invasive pressure measurements should be performed under conditions similar to awake conditions. Epinephrine provocation prevented under treatment in 25% of our patients.

1 INTRODUCTION

Pulmonary artery branch stenosis (PAS) occurs in 2-3% of all congenital heart disease (CHD).¹ As a native substrate it is often seen in patients with Tetralogy of Fallot (ToF), Pulmonary Atresia with Ventricular Septal Defect (PA-VSD) and in genetic syndromes such as Alagille, Williams and Noonan.² It is a common lesion after corrective surgery for several CHD, including Transposition of the Great Arteries (TGA), ToF, PA-VSD and Aortic valve surgery (Ross procedure). Depending on the degree of stenosis, patients may be asymptomatic or complain of exercise intolerance. If left untreated PAS may result in pulmonary artery hypoplasia, right ventricular (RV) dysfunction, aneurysm formation and even sudden cardiac death.^{3,4}

The decision whether to treat PAS is primarily based on pressure gradients. However, quantifying gradients and RV systolic pressure (RVSP) with echocardiography can be challenging.^{4,5} Branch pulmonary arteries are often difficult to visualize and the estimation of RVSP depends on the quality and quantity of the tricuspid regurgitation (TR) signal. On top of that, objectifying clinical complaints of exercise intolerance is often impossible in small children. CMR and/or CTA are often used to determine the severity of PAS. The resulting measurements define whether there is an indication for invasive treatment.

Cardiac catheterization in the pediatric population is regularly performed under general anesthesia. The anesthetics used during these procedures affect the cardiovascular stability, resulting in systemic and pulmonary hypotension.⁶ This may lead to false low pressure gradients over the stenosis. Invasive measured pressure gradients are therefore often in disagreement with other imaging modalities.⁷ The indication for intervention seems resolved which may result in underestimation of the obstruction and possible under treatment of the stenosis.

Several anti-hypotensive drugs are used to counteract the hypotensive properties of anesthetics. During cardiac catheterization catecholamines such as epinephrine, nor-adrenalin or dobutamin are applied for stress testing of the left ventricle (LV) and the assessment of aortic pathology.⁷ No publications are available on the use of catecholamines for the evaluation of PAS and RV pressure load. The aim of this paper is to describe our experience with epinephrine provocation as a tool to unmask RV load in patients with – suspicion of - PAS under general anesthesia. In

the discussion a new approach for the invasive assessment of these patients will be proposed.

2 MATERIALS AND METHODS

2.1 Study design

All right sided cardiac catheterizations performed between January of 2011 and June 2020 in the Wilhelmina Children's Hospital were retrospectively screened. Procedures were included if epinephrine was used to evaluate the RV load in patients with –suspicion of- PAS. All procedures needed to be performed under general anesthesia. Procedures in patients with single ventricle morphology were excluded. All patients had undergone evaluation of their pulmonary arteries through non-invasive image modalities including echocardiography and/or CT- or MR-scans. In case of abnormalities, outcomes of these examinations were discussed in a multidisciplinary team consisting of cardiac surgeons and pediatric cardiologists. In case of definite suspicion of significant PAS the patient was referred to the cathlab for further invasive evaluation. This study was approved by the Medical Research Ethics Committee of the University Medical Center Utrecht. Informed consent was waived.

2.2 Indication for intervention

In all cases a baseline invasive pressure measurement was performed. RV, LV pressure and gradients over the PV, main PA (MPA), right and left PA (RPA and LPA) were determined. An epinephrine bolus was administered when the baseline invasive arterial blood pressure (IBP) was substantially below the awake non-invasive arterial blood pressure (NIBP). Other indications for epinephrine testing were a relatively low pressure gradient over a morphological severe stenosis and/or a RV:LV pressure ratio <0.6 .

Indications for intervention included a RV:LV pressure ratio in rest and/or with epinephrine of ≥ 0.6 , a pressure gradient of ≥ 20 mmHg over a PAS or ≥ 30 mmHg over the PV. In cases with an absent PV, lower thresholds for intervention were considered depending on the amount of RV dilation. The indications for intervention based on epinephrine testing and the dosage of epinephrine will be further explored in the discussion section.

2.3 Data collection and statistical analysis

Clinical data was collected including diagnosis, surgical and interventional history. The most recent echocardiography was screened to obtain data on RV function, PV regurgitation and RVSP. Periprocedural data included invasively measured pressures, indication for epinephrine testing, complications and, if applicable, the type of intervention. Statistical analysis was performed using SPSS version 25. Presented numbers in the results section are given in mean unless stated otherwise. Pre- and post-interventional pressures and ratios were compared using a paired sample T-test. The correlation between non-invasive and invasive pressure measurements was determined by linear regression.

The awake LV pressure was defined as the systolic NIBP measured prior to the catheterization. The awake RV pressure was defined by the measured RV pressure on cardiac echography or calculated using the velocity of the TR signal by equation (1).

$$\text{RV pressure} = (4(\text{TR}_{\text{preak}})^2) + 10 \text{ mmHg} \quad (1)$$

3 RESULTS

3.1 Patient characteristics

A total of 74 procedures was included involving 69 unique patients. In the majority of the procedures the patient was <16 years (61.9%) and <50 kg (56.7%). The most common cardiac diagnosis was ToF followed by TGA and PA-VSD. An underlying syndrome with known cardiac involvement was confirmed in 8 patients. All but 4 patients had undergone surgery to correct their CHD. In most cases (64.9%) a balloon angioplasty or stent implantation was performed during previous interventions. In 33.3% of these cases the current intervention was due to suspicion of stenosis at the same location. Echocardiographic RV function was quantified as normal in 64.9% of the cases. None of the patients had a poor RV function. In most cases (78.4%) there was some degree of PV regurgitation on cardiac echography. This PV regurgitation was mild in the majority (43.8%) of these cases while 33.3% had severe PV regurgitation. All baseline characteristics are displayed in table 1.

Table 1 - Baseline characteristics.

	N (%)
Gender	
• Male	41 (55.4)
• Female	33 (44.6)
Age	
• 0-1 y	6 (8.1)
• 1-5 y	9 (12.2)
• 5-10 y	15 (20.3)
• 10-16 y	16 (21.6)
• >16 y	28 (37.8)
Weight	
• 0-10 kg	4 (5.4)
• 10-25 kg	18 (24.3)
• 25-50 kg	20 (27.0)
• >50 kg	32 (43.2)
Diagnosis	
• ToF	20 (27)
• TGA	16 (21.6)
• PA + VSD	12 (16.2)
• Post-Ross	8 (10.8)
• TAC	4 (5.4)
• Valvular PS	4 (5.4)
• PPS	4 (5.5)
• Other	6 (8.1)
Syndrome	
• Yes	10 (13.5)
Associated with cardiac abnormalities	8 (80)
Not associated with cardiac abnormalities	2 (20)
Previous surgery	
• Yes	70 (94.6)
Intervention during previous catheterization	
• Yes	48 (64.9)
Same substrate	16 (33.3)

Table 1 - (Continued)

	N (%)
RV function on echocardiography	
• Normal	48 (64.9)
• Mildly decreased	18 (24.3)
• Moderately decreased	8 (10.8)
• Poor	0 (0)

PA+VSD: pulmonary atresia with ventricular septal defect, PPS: peripheral pulmonary stenosis, RV: right ventricle, ToF: Tetralogy of Fallot, TGA: Transposition of the Great Arteries, TAC: truncus arteriosus communis, Valvular PS: valvular pulmonary stenosis, y: years.

3.2 Interventional characteristics

In 45 of the 74 procedures an intervention was performed. In 15 cases there was no indication for intervention. In 14 patients the indication was confirmed but the actual treatment was performed in a follow-up procedure, after re-evaluation of the case in a multidisciplinary team with surgeons and cardiologist. In 18 cases one or more stents were placed. In 11 cases the stenosis was treated with balloon angioplasty and in 16 cases a percutaneous pulmonary valve implantation was performed. In the following sections the patients undergoing a staged procedure, for whom the indication was set in the first procedure, are considered to be part of the 'intervention' group. All interventional characteristics are displayed in table 2.

Table 2 - Procedural characteristics.

	N (%)
Intervention	
• Yes	45 (60.8)
• No	15 (20.3)
• Staged	14 (18.9)
Type intervention	
• Stent	18 (24.3)
• PPVI	16 (21.6)
• Staged	14 (20.3)
• Balloon angioplasty	11 (14.9)
• N/A	15 (18.9)

Table 2 - (Continued)

	N (%)
Location intervention	
• RPA	2 (2.7)
• LPA	2 (2.7)
• MPA	12 (16.2)
• Bilateral	12 (16.2)
• PV	17 (23.0)
Complications during cath	
• Yes	8 (10.8)
Major	0 (0.0)
Minor	8 (10.8)
• No	66 (89.2)
Complications <24h after procedure	
• Yes	5 (6.8)
Major	0 (0.0)
Minor	5 (6.8)
• No	69 (93.2)
Epinephrine related complications	
• Yes	0 (0)
• No	74 (100)
Re-interventions follow-up	
• Yes	6 (8.1)
Somatic growth	2
PPVI	4
• No	53 (71.6)
• N/A	15 (20.3)
Re-surgery follow-up	
• Yes	2 (2.7)
Homograft replacement	2
• No	57 (77)
• N/A	15 (20.3)

LPA: left pulmonary artery, MPA: main pulmonary artery, N/A: not applicable, PPVI: percutaneous pulmonary valve implantation, PV: pulmonary valve, RPA: right pulmonary artery.

3.3 Decision making

Figure 1 shows the decision making process for all procedures. The RV:LV pressure ratio during baseline testing was <0.6 in 41 and ≥ 0.6 in 33 cases. Of the 33 cases with a high baseline ratio, 30 had a high ratio during epinephrine testing as well (grey box). In the other 3 cases this ratio was <0.6 with epinephrine (yellow box). Of the 41 cases with a low baseline ratio the ratio remained <0.6 in 22 cases. 15 of them were not treated for PAS (green box). The other 7 cases were treated based on high pressure gradients over the PA or PV (pink box). Of the cases with a baseline ratio <0.6 , 19 had a ratio of ≥ 0.6 after epinephrine. In these 19 cases (blue box) epinephrine was the decisive reason for intervention.

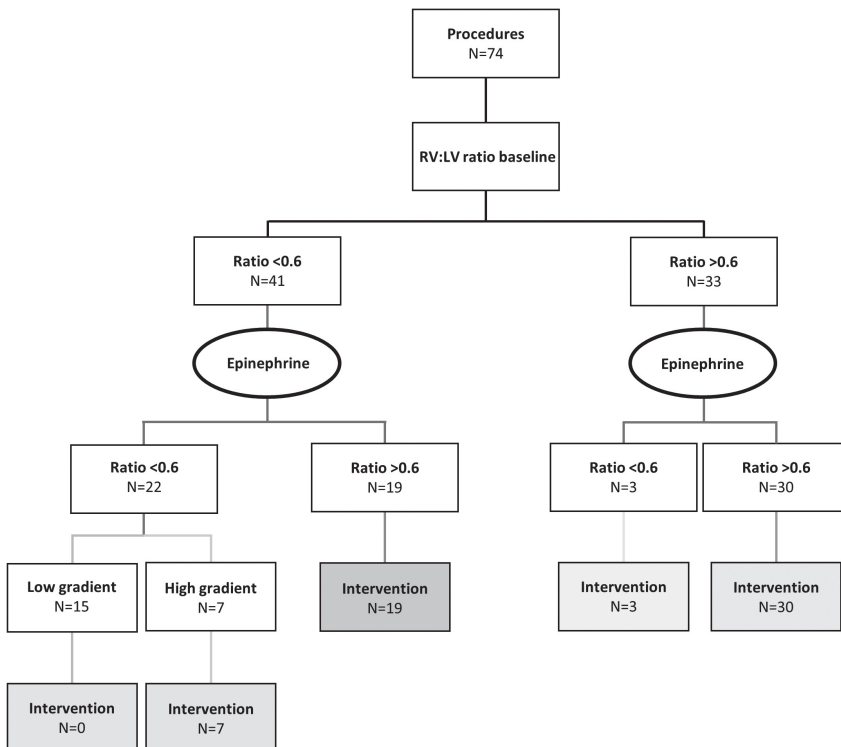


Figure 1 - Flowchart. The decision process in the 74 included procedures.

3.4 Awake versus baseline measurements

In all but one patient the baseline IBP was below the NIBP (figure 2A). Under anesthetics the baseline IBP was on average 22 mmHg below the NIBP ($p < 0.001$, 95% CI [19, 25]). For 66 of the 74 cases an awake RV pressure measured with echocardiography was available (figure 2B). In most cases ($N=42$) the pressure estimated with echocardiography was above the invasive baseline RV pressure, in 24 cases the awake RV pressure was below the invasive baseline RV pressure. On average the difference between the awake and the invasive RV pressure was 4 mmHg ($p=0.015$, 95% CI [1, 7]).

3.5 Baseline versus epinephrine measurements

In order to evaluate the behavior of the RV and to compare baseline and epinephrine pressures the cases were subdivided in 3 groups. Group 1 contains the patients with a low RV:LV ratio both at baseline and under epinephrine who did not undergo intervention ('No intervention' $N=15$, green box figure 1). Group 2 includes patients with a high baseline ratio and a high epinephrine ratio ('Intervention' $N=30$, grey box figure 1). Group 3 involves patients with a low baseline ratio and a high epinephrine ratio ('Epinephrine indication' $N=19$, blue box figure 1). For this analysis patients were excluded if the indication for intervention was based on high gradients over a stenosis ($N=7$, pink box figure 1) and if the baseline ratio was ≥ 0.6 with the epinephrine ratio < 0.6 ($N=3$, yellow box figure 1).

Figure 3 shows all pressure measurements for the 3 groups. In group 1 ('No intervention') the LV pressure increased from 106 to 172 mmHg after the epinephrine bolus. The RV pressure rose with 25 mmHg to 67 mmHg coming from 43 mmHg. The ratio RV:LV pressure was similar during the awake, baseline and epinephrine measurements (0.36, 0.4 and 0.39 respectively with $p=0.23$ and $p=0.89$). In the second group ('Intervention') the RV:LV ratio was high during the baseline measurements (0.68). The ratio increased to 0.76 after epinephrine ($p < 0.001$). The RV pressure rose with 40 mmHg, from 58 to 98 mmHg respectively, while the LV pressure increased with 20 mmHg from 110 to 130 mmHg. The rise in RV pressure was highest in the patients of group 3 ('Epinephrine indication'). In this group the RV pressure went up from 49 mmHg at baseline to 103 with epinephrine. The LV pressure rose from 97 to 139 mmHg. This caused an elevation of the RV:LV ratio from 0.49 to 0.75 ($p < 0.001$).

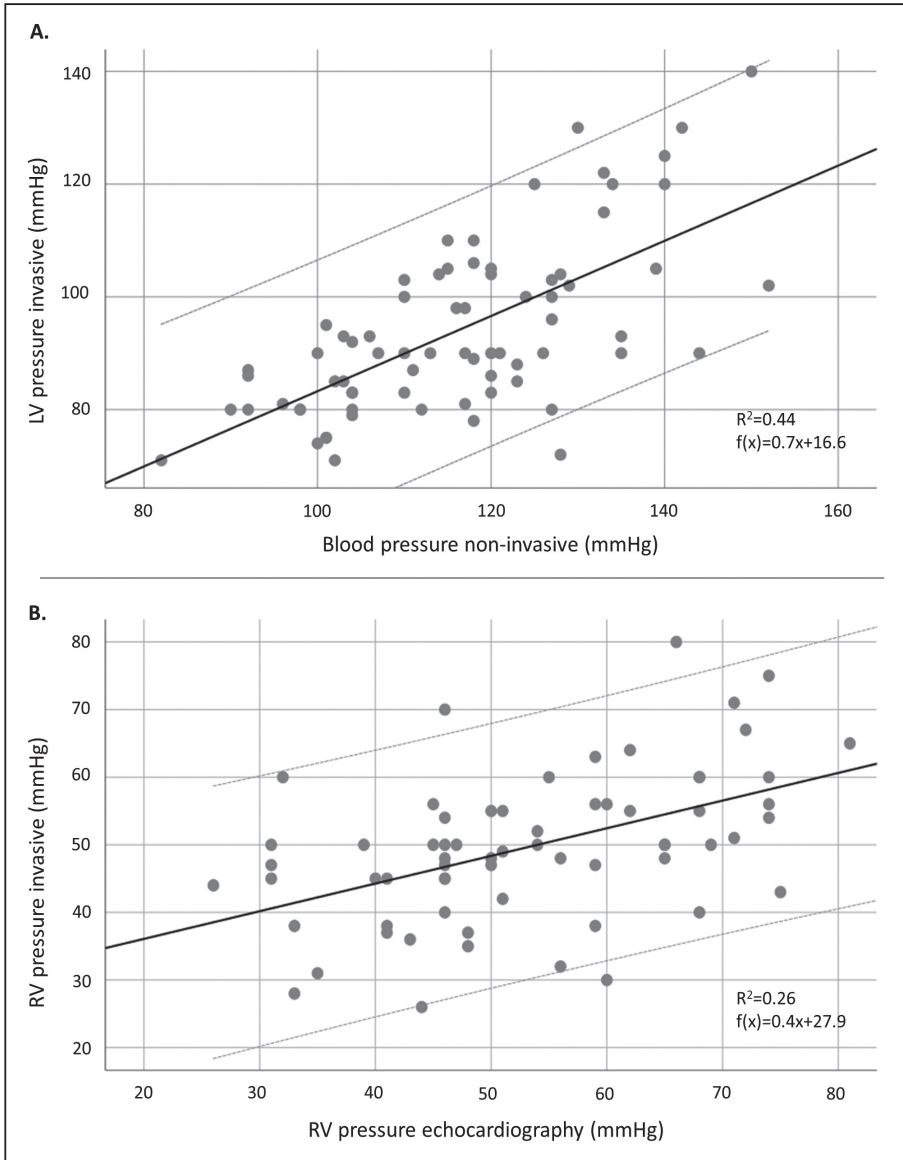


Figure 2 - Correlation between non-invasive and invasive pressure measurements in mmHg.

Each red dot represents one case. In black the linear regression line is added with the 95% confidence interval shown by the grey dotted lines. A: the non-invasive measured systolic blood pressure compared to the invasive systolic left ventricular (LV) pressure. $R^2=0.44$ $f(x)=0.7x+16.6$. B: the systolic right ventricular (RV) pressure measured by cardiac echocardiography compared to the systolic invasive RV pressure. $R^2=0.26$ $f(x)=0.4x+27.9$.

3.6 Post-intervention measurements

The post-intervention baseline RV:LV ratio was available for 11 patients of group 2 ('Intervention'). This ratio decreased significantly from 0.7 to 0.5 ($p=0.002$). The baseline RV pressure was reduced with 18 mmHg to 42 mmHg. The post-intervention epinephrine ratio was available for 2 patients of this group. In one patient the pre-intervention ratio was 0.81 which was decreased to 0.62 post-intervention. The epinephrine ratio went down from 0.7 to 0.48 in the other patient.

Post-intervention pressures were measured in 10 of the 19 patients of group 3 ('Epinephrine indication'). In these patients the baseline RV:LV ratio decreased to 0.37, coming from 0.5 pre-intervention ($p=0.001$). With epinephrine the ratio was 0.74 pre-intervention and 0.46 post-intervention ($p<0.001$). None of these patients had a post-intervention baseline ratio of ≥ 0.6 and 1 patient had a post-intervention epinephrine ratio of ≥ 0.6 (0.63 respectively coming from 0.89). The difference between the pre- and post-intervention RV pressure was 12 mmHg at baseline and 38 mmHg with epinephrine.

3.7 Complications

No epinephrine related complications were seen during or after catheterization. In 8 of the 74 (10.8%) procedures epinephrine unrelated complications were seen. These included blood loss through the catheter, a small dissection of a vessel, a lung bleed and rhythm problems by either the wire or rapid pacing for 3D rotational angiography. After the procedure 5 more complications were seen (6.8%). These complications included re-bleeding, infection and occlusion of the arteria femoralis.

The dosage of epinephrine used to evaluate the RV load depended on the desired IBP based on the NIBP. In over half of the patients (50.7%) 0.2-0.5 $\mu\text{g}/\text{kg}$ epinephrine was administered. In 14.9% of the patients the dosage was less than 0.2 $\mu\text{g}/\text{kg}$ and in 19.4% over 0.7 $\mu\text{g}/\text{kg}$ was provided with a maximum of 1.6 $\mu\text{g}/\text{kg}$. The other 14.9% of the patients received a bolus with 0.2-0.5 $\mu\text{g}/\text{kg}$ epinephrine.

3.8 Follow-up

The mean follow-up time was 21.6 months with a maximum of 91 and a minimum of 0 months. During follow-up 6 patients underwent a re-intervention. In 2 cases the stents needed to be re-dilated due to somatic growth. This was done respectively 23 and 29 months after the first intervention. In 3 other patients a percutaneous pulmonary valve implantation was performed and in 1 patient the Melody valve

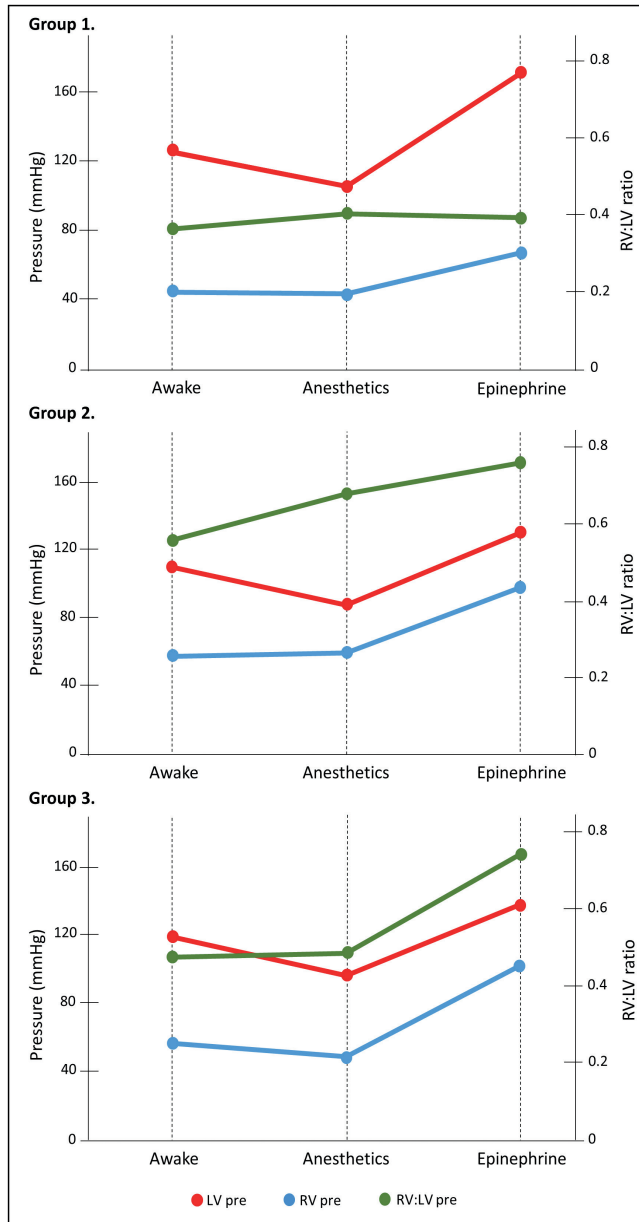


Figure 3 - Pressures under different conditions. The systolic right (RV) and left (LV) ventricular pressures measured non-invasively (awake), under anesthetics (anesthetics) and right after epinephrine (Epinephrine). Group 1: low RV:LV ratio at baseline and after epinephrine (no intervention). Group 2: low baseline RV:LV ratio and high epinephrine RV:LV ratio (intervention). Group 3: high baseline and epinephrine RV:LV ratio (intervention).

implanted during the first intervention needed to be revised. During follow-up 2 patients needed surgery to treat a stenosis in their homograft respectively 36 and 24 months after the first intervention.

4 DISCUSSION

This retrospective study describes our single-center experience with epinephrine provocation in patients with PAS. This is the first study describing the use of pharmacological agents to evaluate RV pressure load in the cathlab. The artificial circumstances caused by general anesthetics result in possible underestimation of RVSP and pressure gradients. This may cause under treatment of PAS in up to 25% of the patients referred to the cathlab. They account for a possible blind spot in the invasive assessment of RV load under general anesthetics.

The hemodynamic condition of a patient with PAS is assessed by echocardiography and/or CMR. During these non-invasive evaluations, the RVSP and pressure gradients over a stenosis are measured in an awake, normotensive patient. When a high pressure gradient and/or an elevated RVSP is found, the patient is referred to the cathlab for invasive evaluation and potential treatment. These invasive evaluations however, are performed in a patient under general anesthesia. This study shows, that the ultimate rest state caused by anesthetics, results in an IBP below the NIBP. Under these circumstances, the invasive measured pressure gradients and RVSP often deviate from the values measured in the awake patient. This makes interpretation of the invasive pressure gradients challenging. It may even lead to uncertainty about the treatment indication. In this study, all patients were referred to the cathlab with an indication for treatment based on non-invasive pressure measurements. Of these patients, 19 (25%) did not have an indication for intervention based on invasive baseline pressure measurements. In these patients the indication for treatment was revealed when the IBP was elevated up to the NIBP. This is the group of patients at risk for under treatment of PAS, and the group that may benefit from epinephrine testing during cardiac catheterization.

Epinephrine has positive chronotropic effects and increases the cardiac output resulting in an increase in systemic arterial blood pressure.⁸ Other possible agents for pharmacological exercise testing include isoproterenol, norepinephrine and dobutamine. Isoproterenol increases the heart rate but has limited effects on

the cardiac output, which may result in an decrease in arterial blood pressure.^{9,10} Dobutamine is well known for its use during stress echocardiography.¹¹ Its use in the cathlab during invasive evaluation, is not yet described. Adverse events that may be associated with epinephrine are ventricular tachycardia or fibrillation. However, in our study no epinephrine related adverse events occurred.

A new approach for RV load evaluation in patients with PAS is proposed in figure 4. The aim is to perform invasive pressure measurements under anesthesia in a normotensive patient. We advise to raise the IBP during catheterization to the awake NIBP. Under these conditions the RV:LV ratio should be evaluated. In cases with morphological severe stenosis, but a low pressure gradient and/or a RV:LV ratio <0.6 , epinephrine exercise testing might be considered. In these patients, the IBP can be further increased using epinephrine to reach a state of high cardiac output mimicking exercise conditions. This may be especially relevant for patients with clinical complaints of exercise intolerance. In the presented study, epinephrine testing was also performed in patients with a baseline RV:LV ratio ≥ 0.6 . In our experience, this can be helpful in determining the RV function but it does not alter the clinical decision making in this group of patients. Therefore, it is not included in the flowchart of figure 4.

The response of the RVSP on the increase in IBP can be subdivided in 3 groups, depending on the degree of PAS. First, there are patients with mild stenosis, with a low baseline and epinephrine RV pressure load (group 1). In these patients an increase in IBP results in minimal elevation of RVSP and RV:LV ratio. The physiological reaction of the RV, is to lower the pulmonary resistance and increase the cardiac output.^{12,13} These patients do not have an indication for intervention. In patients with severe stenosis (group 2), the baseline RV:LV ratio is already high, indicating a heavily challenged RV. A rise in IBP further increases the RV load. The physiological response of lowering the pulmonary resistance is insufficient to maintain an acceptable cardiac output. The RV responds by increasing the arterial pressure. In these patients, the indication for intervention is already confirmed during baseline testing.

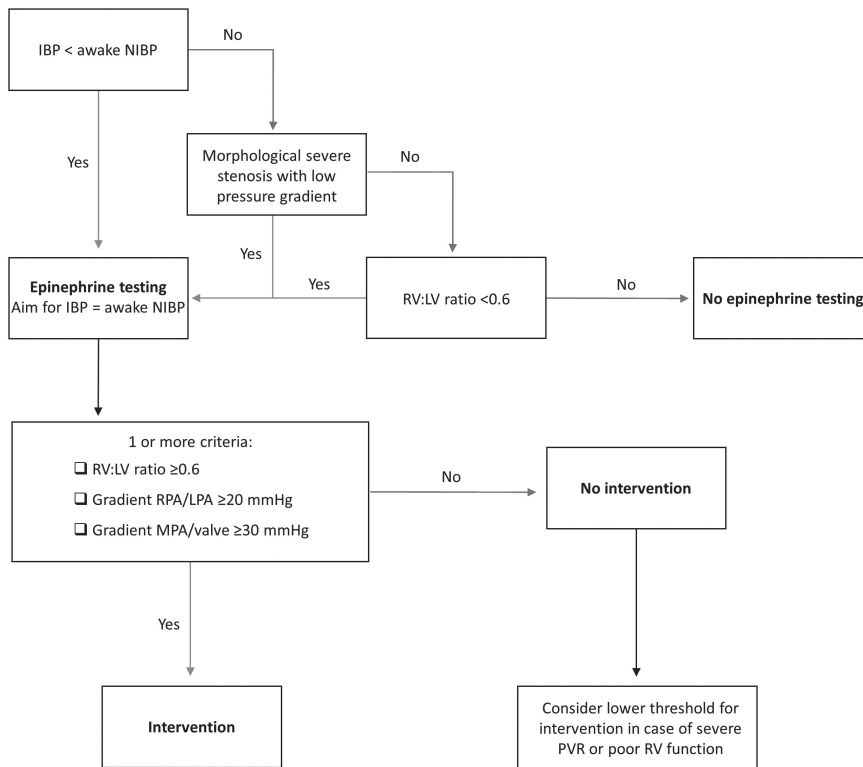


Figure 4 - New approach. The proposed new approach for the invasive evaluation of patients with – suspicion of – PA stenosis in the cathlab. IBP: invasive arterial blood pressure, NIBP: non-invasive arterial blood pressure

Finally, there are patients with a low RV:LV ratio during the hypotensive state caused by anesthetics. During these circumstances the RV is capable of creating a sufficient cardiac output without a rise in arterial pressure. However, when the IBP increases, a threshold is reached after which the RVSP has to rise significantly in order to maintain the cardiac output. It is likely that this threshold is different for each patient - i.e. awake circumstances, mild or heavy exercise - depending on the degree of stenosis. When the threshold is reached, the behavior of the RV is similar to group 2. In this last group of patients, elevating the IBP up to the NIBP is essential to unmask the RV load and PAS. Therefore, we advise treatment of PAS in cases with a baseline or epinephrine ratio ≥ 0.6 . Other indications for intervention include a pressure gradient of ≥ 20 mmHg over a stenosis, or ≥ 30 mmHg over the PV. In cases with severe PV

regurgitation, lower thresholds for intervention may be considered depending on the amount of dilatation of the RV.

4.1 Limitations

The presented study has some limitations. First, as a consequence of the retrospective design the study was highly dependable on the availability of the data. Pre-interventional pressure data was complete for all patients, which allowed for complete evaluation of the pre-interventional conditions. However, post-interventional pressures were not obtained in all patients. Also, this study included a relatively small cohort with 74 cases. Together with the absence of a control group, the level of evidence of this study might be limited. Lastly, the experience presented in this study is subject to a learning curve. The desired IBP was not always reached or sometimes exceeded. This also explains the variety in epinephrine dosage. This might have resulted in an overestimation of the percentage of patients under treated without epinephrine testing. Especially in the patients with a low baseline ratio and low epinephrine ratio (group 1, no intervention), the LV pressure was elevated above the NIBP after epinephrine bolus. As the RVSP remained low in this group, this supports the hypothesis that the RV behaves differently in the absence of stenosis, as compared to the presence of stenosis.

5 CONCLUSION

General anesthetics cause a decrease in systemic and pulmonary pressure. The evaluation of RV pressure load under general anesthesia, may lead to underestimation of the stenosis. This was the case in 25% of the patients included in this study. This patient group is at risk for under treatment. Under treatment can be avoided by performing invasive pressure measurements under conditions similar to the awake state. Epinephrine is a safe and effective agent to counteract the hypotensive properties of anesthetics. We advise to administer a bolus of epinephrine to all patients under anesthetics with an invasive blood pressure below the awake (non-invasive) blood pressure.

REFERENCES

1. Trivedi KR, Benson LN. Interventional strategies in the management of peripheral pulmonary artery stenosis. *J Interv Cardiol*. 2003 Apr;16(2):171-88.
2. Bacha EA, Kreutzer J. Comprehensive management of branch pulmonary artery stenosis. *J Interv Cardiol*. 2001 Jun;14(3):367-75.
3. Anderson IM, Nouri-Moghaddam S. Severe pulmonary stenosis in infancy and early childhood. *Thorax*. 1969 May;24(3):312-26.
4. Cuypers JA, Witsenburg M, van der Linde D, Roos-Hesselink JW. Pulmonary stenosis: update on diagnosis and therapeutic options. *Heart*. 2013 Mar;99(5):339-47.
5. Groh GK, Levy PT, Holland MR, Murphy JJ, Sekarski TJ, Myers CL, Hartman DP, Roiger RD, Singh GK. Doppler echocardiography inaccurately estimates right ventricular pressure in children with elevated right heart pressure. *J Am Soc Echocardiogr*. 2014 Feb;27(2):163-71.
6. Akata T. General anesthetics and vascular smooth muscle: direct actions of general anesthetics on cellular mechanisms regulating vascular tone. *Anesthesiology*. 2007 Feb;106(2):365-91.
7. Meijis TA, Krings GJ, Saad A, Molenschot MMC, Doevendans PA, Voskuil M. Epinephrine stress testing during cardiac catheterization in patients with aortic coarctation. *Am Heart J*. 2020 Jul;225:78-87.
8. Mann SJ, Krakoff LR, Felton K, Yeager K. Cardiovascular responses to infused epinephrine: effect of the state of physical conditioning. *J Cardiovasc Pharmacol*. 1984 Mar-Apr;6(2):339-43.
9. Patel ND, Sullivan PM, Takao CM, Badran S, Ahdoot J, Ing FF. Unmasking the borderline coarctation: the utility of isoproterenol in the paediatric cardiac catheterisation laboratory. *Cardiol Young*. 2018 Jun;28(6):804-810.
10. Kim KS, Eryu Y, Asakai H, Hayashi T, Kaneko M, Kato H. Isoproterenol stress test during catheterization of patients with coarctation of the aorta. *Pediatr Int*. 2012 Aug;54(4):461-4.
11. Lau EMT, Vanderpool RR, Choudhary P, Simmons LR, Corte TJ, Argiento P, D'Alto M, Naeije R, Celermajer DS. Dobutamine stress echocardiography for the assessment of pressure-flow relationships of the pulmonary circulation. *Chest*. 2014 Oct;146(4):959-966.
12. Chia EM, Hsieh CH, Pham P, Vidaic J, Xuan W, Leung D, Thomas L. Changes in Right Ventricular Function with Exercise in Healthy Subjects: Optimal Parameters and Effects of Gender and Age. *J Am Soc Echocardiogr*. 2015 Dec;28(12):1441-51.e1.
13. Kovacs G, Olschewski A, Berghold A, Olschewski H. Pulmonary vascular resistances during exercise in normal subjects: a systematic review. *Eur Respir J*. 2012 Feb;39(2):319-28.

To treat or not to treat pulmonary arteries?



PULMONARY ARTERY STENOSIS AND VALVE INSUFFICIENCY IN TETRALOGY OF FALLOT – A FLOW ANALYSIS PRE AND POST TREATMENT.

Maartje Conijn

Gregor J. Krings

Submitted

ABSTRACT

Background Tetralogy of Fallot (ToF) is the most common form of cyanotic congenital heart disease. Long-term complications include pulmonary valve regurgitation (PR) and pulmonary artery stenosis (PAS). Whether, when and how to treat these is still topic for debate. The aim of this study was to numerically explore the combination of PR and PAS in patients after ToF repair.

Methods Two cases were selected, representing the most common patterns of PAS after ToF repair: one with left PAS and one case with bifurcation stenosis. A 3D model of the patient-specific anatomy was reconstructed. Mass flow was applied at the inlet and a 3-element windkessel at the outlets. For each case 4 scenarios were simulated: with- and without valve, with- and without stenosis.

Results In stenotic arteries high flow velocities are found with pressure gradients and post-stenotic recirculation zones. High wall shear stress is seen in stenotic areas. Stent placement reduces velocity, pressure gradients and wall shear stress. Recirculation zones move towards the branch ostia. Regurgitation increases post-stent placement. Valve placement solves regurgitation and increases diastolic pressures. This results in a decrease in pulse pressure and flow velocities.

Conclusion Stent placement results in an increase in regurgitation in the branches. The effect of stent implantation depends on the diameter, branching angle and origin of the stented artery. Implantation of a valve, reduces pulse pressure thereby decreasing flow velocity and WSS. This study emphasizes the importance of individual decision making in patients with the combination of PR and PAS.

1 INTRODUCTION

Tetralogy of Fallot (ToF) accounts for 5-7% of all congenital heart defects (CHD) and it is thereby one of the most common forms of cyanotic CHD. It involves four cardiac abnormalities including an overriding aorta, a ventricular septal defect, right ventricular (RV) hypertrophy and varying degrees of pulmonary stenosis.¹ The quality of surgical repair for ToF has greatly improved over the last decades. As now most patients grow into adulthood, long-term complications of ToF repair are seen. Pulmonary valve regurgitation (PR) and stenosis of the branch pulmonary arteries are the two most common -late- effects of ToF repair.²

PR is seen in over half of the patients after ToF repair. In severe PR, the increase in RV volume load results in dilatation of the RV and eventually an impaired RV function. The timing of treatment, especially in asymptomatic patients, is still topic for debate.^{2,3} Pulmonary artery branch stenosis (PAS) is seen in up to 20% of the patients with ToF. The most common location is the left pulmonary artery (LPA), followed by a multiple level stenosis of the pulmonary bifurcation.^{4,5} Severe PAS increases pressure load on the RV and, if left untreated, PAS is thought to be unbeneficial for lung development.⁶⁻⁸

Literature is inconclusive and even conflicting, when it comes to the hemodynamic impact of PAS in the presence of PR. On the one side, it is thought that PR is not tolerated well in the presence of PAS, increasing regurgitation and thereby RV volume load.⁹⁻¹¹ It is therefore advised to treat PAS first and then re-evaluate the need for PR. On the other side, the presence of PAS is thought to do the exact opposite. These studies showed the decrease of PR in the presence of PAS. Here, the stenosis protects the RV from volume overload and the presence of PAS delays the need for valve replacement.^{12,13} This makes the combination of PR and PAS after ToF repair a challenge for clinicians. Should one first treat the stenosis or the insufficient valve? And when is the most favorable moment to intervene?

Numerical analysis of the pulmonary arteries after ToF repair allows for detailed evaluation of hemodynamic parameters and flow behavior. Several studies are published using computational fluid dynamics (CFD) for surgical treatment planning and the evaluation of the impact of PAS or PR in ToF patients.¹⁴⁻¹⁹ However, the combination of PAS and PR in patient-specific anatomies has not been computationally explored. The aim of this study was to simulate PR in the most

common patterns of PAS after ToF repair and to explore the hemodynamic impact of stent- and valve placement in these patients.

2 METHODS

2.1 Case selection

Two cases were selected. These cases were representative for the two patterns of PAS most commonly seen after surgical ToF repair. The first case involves a patient with LPA stenosis. It's a 11 year old girl with a body surface area (BSA) of 1.04. The second case represents a bifurcation stenosis with involvement of the main-, right- and left pulmonary artery. This is a 16 year old boy with a BSA of 1.85. Both patients were referred to the cathlab by a multidisciplinary team for evaluation of their PAS. They were both treated by stent placement in the LPA (case 1) and the bifurcation (case 2) respectively. The cases were selected based on the availability of a 3D rotational angiography, as this was considered the highest quality imaging for anatomic reconstruction. Invasive pressure measurements in the pulmonary branches and a CMR with flow measurements needed to be present. In the event of equal suitability, the case with highest quality imaging for anatomic reconstruction was selected. This study was assessed by the institutional ethical committee. Informed consent was waived.

2.2 Anatomic reconstruction

For each case, two different geometries were created (figure 1). First the stenotic, pre-stent anatomy was reconstructed. For this reconstruction, the 3D rotational angiography obtained during cardiac catheterization was used. The pulmonary arteries were segmented with ITK-SNAP software.²⁰ With a non-shrinking method, the 3D-model was smoothed in Meshmixer (Autodesk Inc, San Rafael, USA). Additional branches were removed, after which each geometry consisted of 1 inlet (main pulmonary artery (MPA)) and 3 outlets (1 right, 2 left). A second geometry was created representing the anatomy after stent placement. A virtual stent, with the same dimensions used to treat the actual stenosis, was implanted in the original anatomy. In case 1, a 16x15 mm stent was implanted in the LPA. Case 2 was treated with two stents: a 28x22 mm stent in the right pulmonary artery (RPA) and a 45x24 mm stent in the LPA.

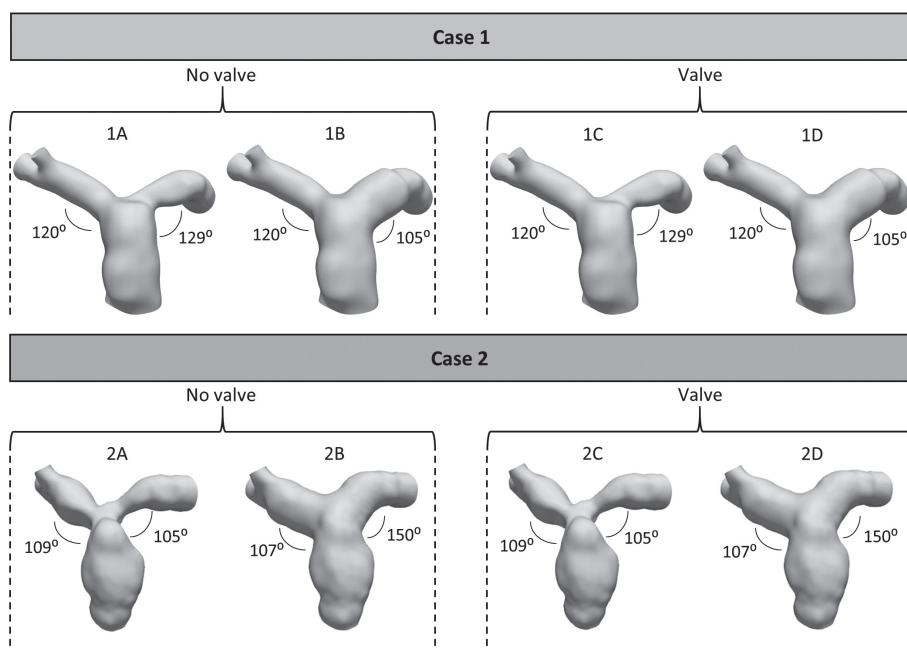


Figure 1 - Anatomies and scenarios. For each case four scenarios were simulated: 1. With stenosis, no valve (1A, 2A), 2. Treated stenosis, no valve (1B, 2B), 3. With stenosis, competent valve (1C, 2C), 4. Treated stenosis, competent valve (1D, 2D). The branching angles (degrees) of the right and left pulmonary artery are displayed.

2.3 Scenarios

For both cases, four different scenarios were simulated (figure 1). Subsequently a total of 8 scenarios were simulated.

1. With stenosis, no valve (1A, 2A)
2. Treated stenosis, no valve (1B, 2B)
3. With stenosis, competent valve (1C, 2C)
4. Treated stenosis, competent valve (1D, 2D)

2.4 Boundary conditions

An overview of the used inlet- and outlet boundary conditions is displayed in figure 2. At the inlet, a mass flow boundary condition was applied. For the valveless scenarios the waveform was based on the CMR measurements in both cases. The percentage of backflow during the diastole was 40%. For the scenarios without PR, a waveform

was created without backflow. This waveform was based on literature.^{21,22} The stroke volume was scaled to fit the BSA of the patient. The netto stroke volume, defined as the forward-, minus the back flow, was equal in all scenarios (table 1). A plug flow inlet velocity profile was used for all scenarios.

At the outlets of the models a 3-element windkessel was applied. The elements included a proximal- and distal resistor and a capacitor. The values for these lumped parameters were calculated as described in appendix 1. The wall was assumed to be a rigid tube. Blood was modelled as a Newtonian fluid with a blood density of 1060 kg/m³ and a viscosity of 0.004 kg/ms. The heart frequency was set to be 80 beats/min.

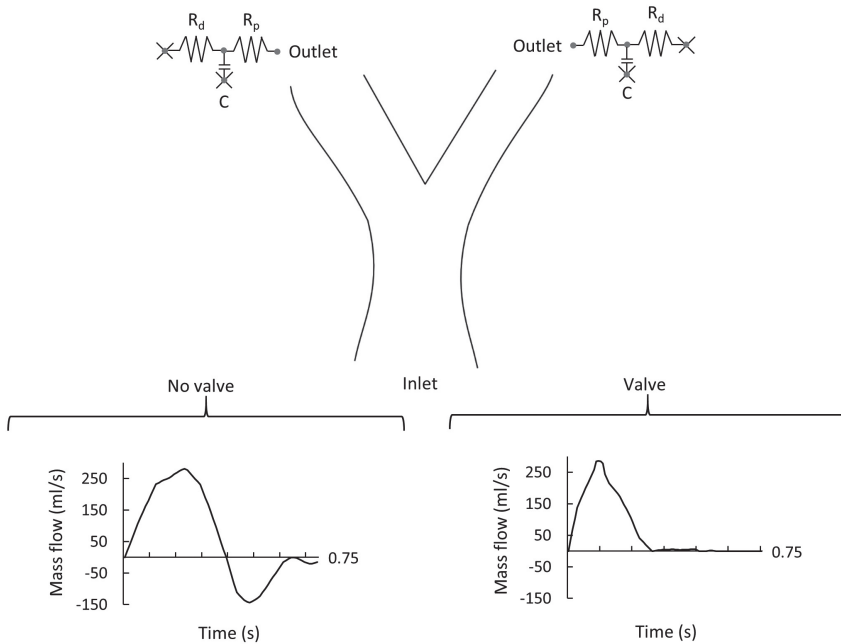


Figure 2 - Boundary conditions. A schematic overview of the applied inlet- and outlet boundary conditions. The flow waveforms for the scenarios with and without pulmonary valve are displayed together with the electrical RCR system applied at the outlets of the models.

2.5 Mesh independence test

The models were meshed using CRIMSON software.²³ A non-structured mesh was constructed, consisting of tetrahedral elements with five boundary layers close to

the wall. For each geometry, multiple meshes were created. Numerical outcomes for these meshes were compared to ensure a grid independent solution. The solution was considered mesh independent, when the results showed a difference of <1 mmHg in pressure, and <1 ml in flow split outcomes. The results of the mesh test were used for both scenarios with the same anatomy (i.e. scenario 1A and 1C). The final mesh for scenario 1A-C consisted of 985.913 elements and the mesh for scenario 1B-D of 1.083.485 elements. Scenario 2A-C was simulated with 1.110.995 elements and Scenario 2B-D with 1.309.729 elements. A total of four cardiac cycles were simulated with a time step size of 0.001s. The solution was assumed to be converged when the residuals dropped below 10^{-4} . Calculations were performed using CRIMSON software. The outcomes of the last cardiac cycle were analysed and used for the results section. For clarity, in the results section the scenarios are indicated with their corresponding numbers between brackets.

3 RESULTS

3.1 Flow distribution

In table 1 the distribution of flow between the RPA and LPA is shown for all scenarios. In the stenotic geometries without a pulmonary valve (1A, 2A) flow distribution was unequal, with a preference for the RPA in both cases. In scenario 1A, the RPA received 73% and the LPA 27% of the flow. The distribution in scenario 2A was 69%:31% for the RPA and LPA respectively.

After stent placement (1B, 2B), flow distribution became more equal in both cases. The proportion of flow to the LPA of case 1 increased to almost 60%. In scenario 2B, 58% of the flow went to the RPA and 42% to the LPA.

Valve placement did not influence the flow distribution in the geometries. In both the stenotic (1C, 2C) and stented (1D, 2D) scenarios, the flow distribution was comparable to the valveless scenarios.

Table 1 - Flow inlet specifications and flow distribution outcomes

Case 1					
No valve			Valve		
Scenario	1A	1B	Scenario	1C	1D
Foward flow	70 ml	70 ml	Foward flow	48 ml	48 ml
Back flow	22 ml	22 ml	Back flow	0 ml	0 ml
Netto flow	48 ml	48 ml	Netto flow	48 ml	48 ml
PR	32%	32%	PR	0%	0%
RPA:LPA flow	73%:27%	41%:59%	RPA:LPA flow	74%:26%	37%:63%
Back flow RPA	14 ml	19 ml	Back flow RPA	0.1 ml	6 ml
Back flow LPA	7 ml	5 ml	Back flow LPA	2 ml	0.2 ml

Case 2					
No valve			Valve		
Scenario	2A	2B	Scenario	2C	2D
Foward flow	123 ml	123 ml	Foward flow	85 ml	85 ml
Back flow	38 ml	38 ml	Back flow	0 ml	0 ml
Netto flow	85 ml	85 ml	Netto flow	85 ml	85 ml
PR	31%	31%	PR	0%	0%
RPA:LPA flow	69%:31%	58%:42%	RPA:LPA flow	69%:31%	52%:48%
Back flow RPA	30 ml	37 ml	Back flow RPA	1 ml	4 ml
Back flow LPA	7 ml	10 ml	Back flow LPA	0.5 ml	0.2 ml

The flow inlet boundary conditions for all scenarios are displayed above the black line. Below the line the flow distribution outcomes are displayed. LPA: left pulmonary artery, PR: pulmonary valve regurgitation, RPA: right pulmonary artery.

3.2 Regurgitation fraction

Prior to stent placement, in both cases there was more back flow in the RPA then in the LPA (1A, 2A). Stent implantation (1B, 2B) resulted in an increase in regurgitation in the RPA. In case 1, the regurgitation in the RPA increased to 19 ml. In case 2, the regurgitation in the RPA increased with 7 ml. After stent placement, the back flow in the LPA was decreased in case 1 and increased in case 2 (1B, 2B).

Valve placement resulted in an overall reduction of both the total regurgitation and the back flow in the branches (1C-D, 2C-D). In case 1, some regurgitation in the RPA remained, while almost no back flow was seen in the LPA (1C). Stenting the LPA

in this case, resulted in a further decrease of LPA back flow and an increase in the RPA regurgitation (1D). In case 2, valve implantation resulted in an almost complete reduction of regurgitation in the branches (2C). When the bifurcation was stented, the regurgitation fractions remained comparable (2D).

3.3 Velocity

In figure 3 slices through the MPA, RPA and LPA are shown with velocity coloring. In scenario 1A and 2A, the stenotic branches caused an acceleration of flow towards the upper wall of the artery. Here, the velocity profile developed the shape of a more axial profile. An area of low flow velocity with recirculation zones was observed behind the stenosis. Acceleration of flow was also seen in the LPA in scenario 1A. This acceleration however was not accompanied by skewness or a post-stenotic recirculation zone.

After stent implantation there was a decrease in flow velocity in the stented areas (1B, 2B). In case 1 the flow velocity in the LPA decreased from 2.5 m/s (1A) to 1 m/s (1B). The stent placement in the LPA also influenced the flow velocity in the RPA. Here the flow velocity decreased from 2.3 m/s (1A) to 1.6 m/s (1B). The maximal flow velocity in the MPA remained unchanged. In case 2 the maximal velocity in the RPA decreased from 4 m/s (2A) to 1.5 m/s (2B). The maximal velocity in the LPA was 3 m/s prior to stenting (2A) and decreased to 1.5 m/s after stent placement (2B). Recirculation zones were still present and developed closer to the branch ostia then before stent placement.

Valve implantation resulted in an overall decrease in maximal flow velocity (1C-D, 2C-D). In the stented scenarios the decrease in flow velocity was less distinct (1D, 2D). The maximal velocity in the LPA of case 1 decreased from 2.5 m/s (1A) to 1.7 m/s (1C). In the RPA there was a decrease of maximal velocity observed, from 2m/s (1A) to 1.5 m/s (1C) respectively. In the RPA of case 2 the maximal velocity dropped from 4.0 m/s (2A) to 3 m/s (2C). In the LPA of case 2 the velocity decreased from 3 m/s (2A) to 2 m/s (2C). The presence of a valve had little to no influence on the velocity profiles in the branches and did not influence the development of recirculation zones. Moving velocity streamlines during the whole cardiac cycle for all scenarios can be viewed in the supplementary materials (movie 1 and movie 2).

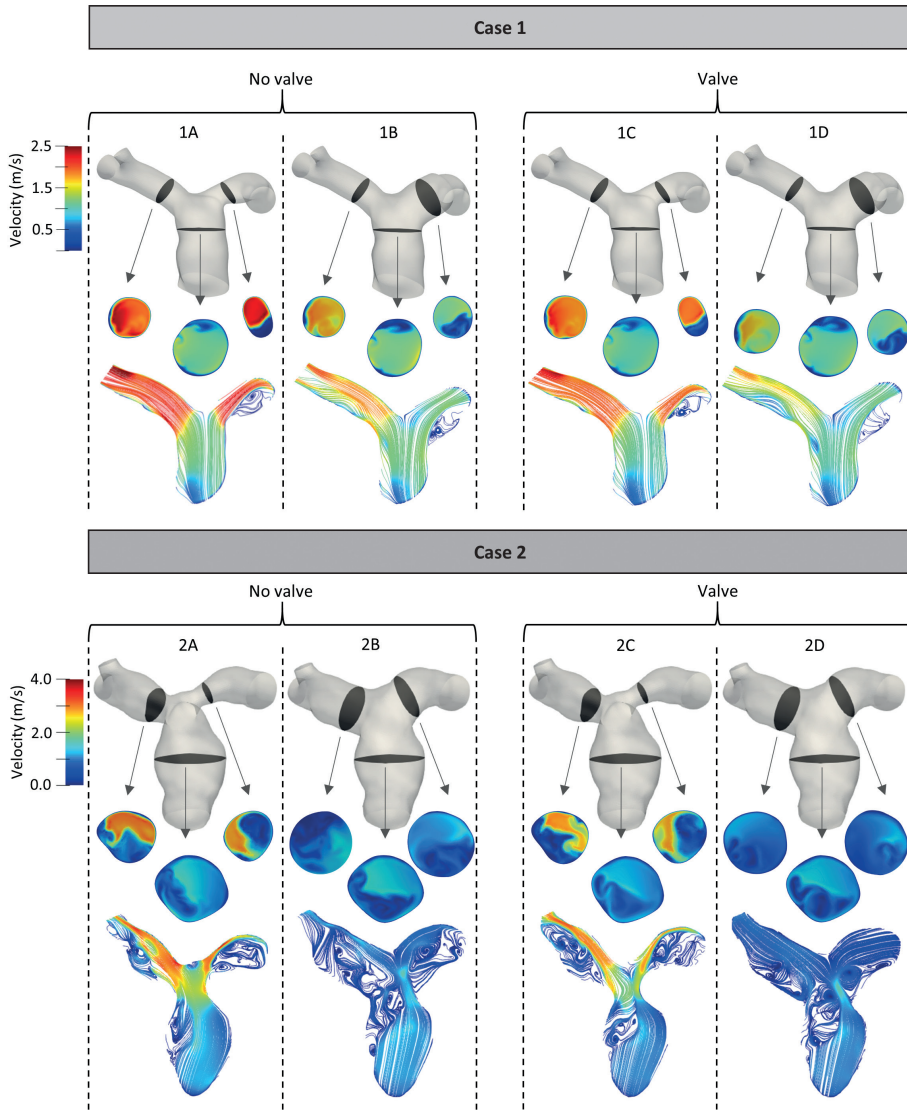


Figure 3 - Cross sections with velocity coloring. Slices through the main-, left- and right pulmonary artery and a longitudinal slice through the geometry. The colors show the velocity as displayed in the legends. The lines in the longitudinal cross sections represent the streamlines with velocity coloring similar to the other cross sections.

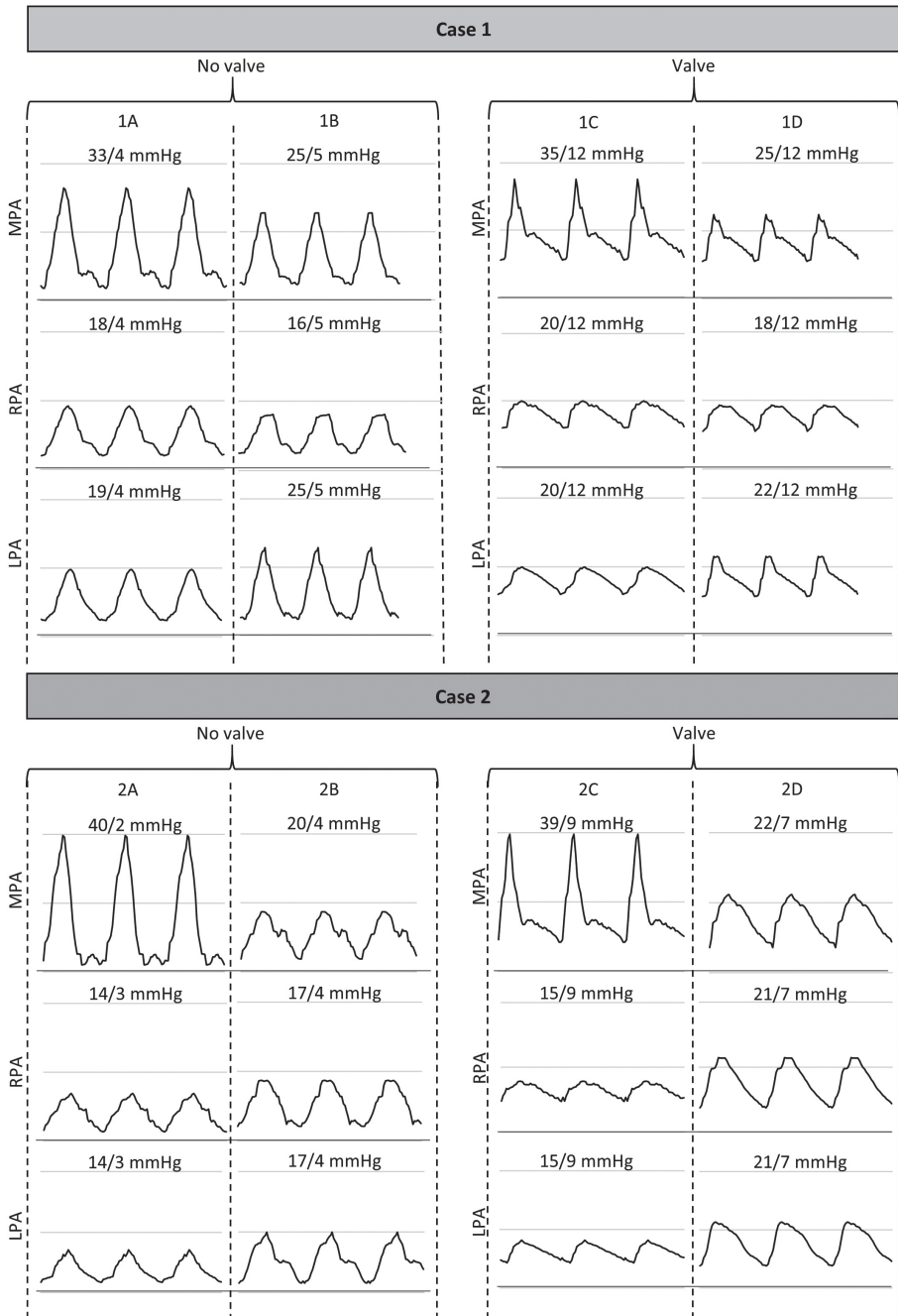


Figure 4 - Pressure results. Pressure curves for all scenarios of case 1 and 2. MPA: main pulmonary artery, RPA: right pulmonary artery, LPA: left pulmonary artery.

3.4 Pressure

As a result of the branch stenosis, there was a high MPA pressure in scenario 1A and 2A (figure 4). In case 1, the systolic pressure was 33 mmHg and in case 2 40 mmHg. In both cases there was a systolic pressure gradient over the RPA and LPA. Stent placement in the stenotic branches resulted in a decrease in MPA pressure and pressure gradients (1B, 2B). In case 1 (1B) the pressure gradient over the LPA dropped to 0 mmHg. Over the RPA, a pressure gradient of 9 mmHg remained. In case 2 (2B) the pressure gradient over both branches was resolved after stent placement. Stent placement did not influence the diastolic pressure.

After valve implantation the diastolic pressure increased while the systolic pressure remained unchanged, resulting in a lower pulse pressure (1C-D, 2C-D). Stent placement in combination with a functioning valve (1D) resulted in a pulse pressure of 13 mmHg. In scenario 2C, the MPA pulse pressure decreased with 8 mmHg to 30 mmHg. After stent placement the pulse pressure was 15 mmHg (2D). Implantation of a valve did not influence the pressure gradients over the branches (1A-B, 2A-B).

3.5 Wall shear stress

In figure 5 the wall shear stress (WSS) distribution during peak systole and maximal WSS values are presented. The values peaked in areas where the stenosis was most severe and close to recirculation zones (1A, 2A). In the LPA of case 1, WSS reached a maximum of 0.96 mmHg during systole (1A). In the hypoplastic RPA, the maximal WSS was 0.74 mmHg. In case 2, WSS values were highest on the ostia of the RPA and LPA, with respectively 1.94 and 1.50 mmHg.

After stent placement, WSS was more equally distributed and peak values decreased (1B, 2B). Valve implantation led to a further decrease in WSS. This decrease was most evident when a valve was implanted in the stented geometries (1D, 2D). Implantation of a valve in the geometries with stenosis had less impact on WSS values (1C, 2C). The areas with highest WSS were similar prior and post valve implantation.

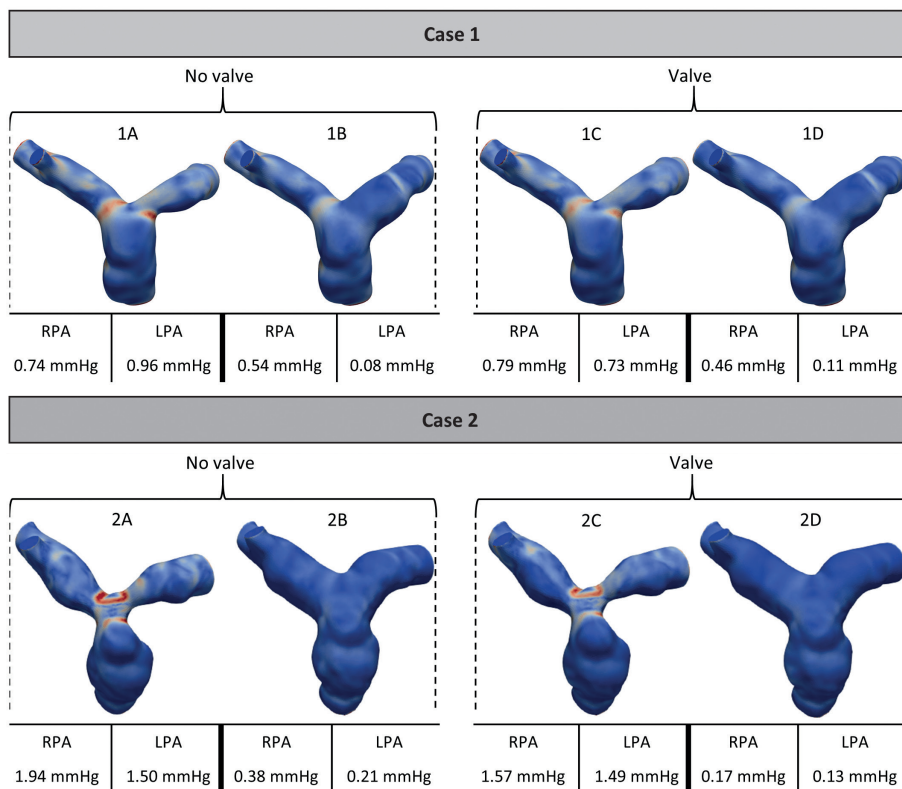


Figure 5 - Wall shear stress outcomes. Wall shear stress distribution in all scenarios during top systole. Maximal values of wall shear stress in the RPA and LPA in mmHg.

4 DISCUSSION

Stenosis is commonly seen in surgically repaired ToF patients. The combination with regurgitation is clinically challenging as there is little evidence on the timing and the sequence of treatment. Studying flow characteristics, can be helpful in increasing insights in the pulmonary circulation of repaired ToF patients. This may provide important answers for clinical decision making in these complex patients. The combination of PR and PAS in patient-specific geometries has not been numerically explored before. Therefore, in this study, the effect of stent and valve placement in the pulmonary arteries of repaired ToF patients with PAS and PR was numerically evaluated. It shows some interesting and important findings on hemodynamics after stent placement and the effect of valve placement in these cases.

4.1 Stent placement

Stent placement resulted in an increase in total branch regurgitation. This supports the hypothesis that a local stenosis prevents backflow in the branches, thereby protecting the RV from further volume load in severe PR.^{12,13} Interestingly, the regurgitation in the RPA increased, while the regurgitation in the LPA decreased. Previous research showed that in stenotic arteries, there is more back flow in the branch with the largest diameter.^{18,19,24} Other factors influencing regurgitation include the angle of the branching artery. Small, acute angles result in more regurgitation while larger angles prevent regurgitation.^{14,15,19} Before stent placement in our cases, the regurgitation in the RPA was larger than in the LPA (figure 1). In both cases the RPA diameter was bigger than that of the LPA. Although the LPA angle was small in both cases, the severity of the local stenosis prevented regurgitation. After stent placement the LPA angle in case 1 increased, while the RPA angle remained unchanged. The absence of a local stenosis resulted in higher back flow, even though the RPA diameter was small due to hypoplasia. In case 2, bilateral stenting resulted in almost equal diameters of the RPA and LPA. In both the RPA and LPA the backflow increased. Due to the significantly smaller RPA branching angle, the amount of regurgitation in the RPA increased more compared to the LPA.

Besides regurgitation, stent placement influences flow velocity and streamlines. Our cases show the well-known acceleration of flow in stenotic arterial branches. The flow is skewed towards the upper part of the arterial wall, and the flow velocity increases as the stenosis becomes more severe. Below these areas of high flow velocity, post-stenotic recirculation zones develop.^{18,24} In these zones the flow particles become trapped, continuously recirculating with low velocity. After stent placement, the overall flow velocity decreases and with the disappearance of the local stenosis, the recirculation zones move more towards the ostia of the RPA and LPA. Extended areas of recirculation are associated with sudden changes in WSS. The recirculation of particles in these zones may lead to platelet activation and thereby intima proliferation.^{19,25,26} In the absence of local stenosis, extensive recirculation zones are found in branches with acute angles and a more proximal origin.^{15,18,19}

4.2 Valve placement

Besides the obvious reduction of PR, valve placement showed three important subsequent findings. First, the diastolic pressure increased and the pulse pressure decreased. Severe PR is associated with a prolonged systolic phase and an increased stroke volume to maintain a sufficient cardiac output.²⁷ The absent or

poorly functioning valve, provides little resistance to diastolic flow resulting in a low diastolic pressure and a wide pulse pressure.²⁷ The low diastolic pressure is seen in our 'no valve' scenarios with diastolic pressures of 4 mmHg and 2 mmHg in the MPA of case 1 and 2 respectively. After valve placement, the diastolic pressure increased to 12 mmHg in case 1 and 9 mmHg in case 2. The increase in diastolic pressure with an unchanged systolic pressure equals a lower pulse pressure.

This smaller difference in systolic and diastolic pressure results in a decrease in overall flow velocity. This effect of valve placement is most distinct in stenotic areas. In the presence of a valve, systolic time reduces and the stroke volume is decreased while the netto stroke volume remains unchanged. In our cases this resulted in a higher peak mass flow for the scenarios with valve. In spite of this, the flow velocity decreases instead of increases, due to the lower pulse pressure. The decrease in flow velocity resulted in a decrease in WSS values and a more equal WSS distribution.

4.3 Limitations

The presented study has some limitations. First, there were several assumptions in the boundary conditions. The artery was assumed to be a rigid tube thereby neglecting compliance of the arterial wall. This could have caused an overestimation of pressure and WSS values.²⁸ However, this assumption is common in similar studies as the arterial wall deformation during the cardiac cycle of the pulmonary arteries is relatively low.^{14,15,18} In this study two patients were selected. This is obviously a relatively low number making the level of evidence limited. However, both of these patients represent a common pattern of PAS after ToF repair allowing for some generalization of the results.

4.4 Clinical perspective

PAS in combination with PR forms a clinical challenge. This study emphasizes the importance of individual decision making in patients with complex congenital heart disease. It shows that the effect of stent implantation on PR not only depends on the relief of obstruction, but also on the angle and origin of the stented branch. Numerical studies may provide a handle on which way to go. The combination of computational studies on generalized, idealized and patient-specific cases, is necessary to provide some applicability to the whole ToF population. Generalization, will however never be possible as each ToF patient has an unique anatomy and varying degrees of PR. The addition of numerical analysis in the work-up for these patients allows for optimal treatment planning in this complex patient group.

5 CONCLUSION

In this study, the effect of stent- and valve placement in the pulmonary arteries of repaired ToF patients with both PAS and PR was numerically evaluated. In general, stent placement results in an increase in regurgitation in the branches. However, the effect of stent implantation on PR depends on the angle and origin of the stented branch as well. Implantation of a valve reduces pulse pressure thereby decreasing flow velocity and WSS. This study emphasizes the importance of individual decision making in patients with the combination of PR and PAS.

REFERENCES

1. Bashore TM. Adult congenital heart disease: Right ventricular outflow tract lesions. *Circulation*. 2007;115(14):1933-1947.
2. Yoo BW, Park HK. Pulmonary stenosis and pulmonary regurgitation: Both ends of the spectrum in residual hemodynamic impairment after tetralogy of fallot repair. *Korean J Pediatr*. 2013;56(6):235-241.
3. de Torres-Alba F, Kaleschke G, Baumgartner H. Impact of percutaneous pulmonary valve implantation on the timing of reintervention for right ventricular outflow tract dysfunction. *Rev Esp Cardiol (Engl Ed)*. 2018;71(10):838-846.
4. Sheikh AM, Kazmi U, Syed NH. Variations of pulmonary arteries and other associated defects in tetralogy of fallot. *Springerplus*. 2014;3:467-1801-3-467. eCollection 2014.
5. Sharma SN, Sharma S, Shrivastava S, Rajani M, Tandon R. Pulmonary arterial anatomy in tetralogy of fallot. *Int J Cardiol*. 1989;25(1):33-37.
6. Pewowaruk R, Hermesen J, Johnson C, et al. Pulmonary artery and lung parenchymal growth following early versus delayed stent interventions in a swine pulmonary artery stenosis model. *Catheter Cardiovasc Interv*. 2020;96(7):1454-1464.
7. Bates ML, Anagnostopoulos PV, Nygard C, et al. Consequences of an early catheter-based intervention on pulmonary artery growth and right ventricular myocardial function in a pig model of pulmonary artery stenosis. *Catheter Cardiovasc Interv*. 2018;92(1):78-87.
8. Takao CM, El Said H, Connolly D, Hamzeh RK, Ing FF. Impact of stent implantation on pulmonary artery growth. *Catheter Cardiovasc Interv*. 2013;82(3):445-452.
9. Petit CJ, Gillespie MJ, Harris MA, et al. Relief of branch pulmonary artery stenosis reduces pulmonary valve insufficiency in a swine model. *J Thorac Cardiovasc Surg*. 2009;138(2):382-389.
10. Davlouros PA, Karatza AA, Gatzoulis MA, Shore DF. Timing and type of surgery for severe pulmonary regurgitation after repair of tetralogy of fallot. *Int J Cardiol*. 2004;97 Suppl 1:91-101.
11. Chaturvedi RR, Kilner PJ, White PA, Bishop A, Szwarc R, Redington AN. Increased airway pressure and simulated branch pulmonary artery stenosis increase pulmonary regurgitation after repair of tetralogy of fallot. real-time analysis with a conductance catheter technique. *Circulation*. 1997;95(3):643-649.
12. Maskatia SA, Spinner JA, Morris SA, Petit CJ, Krishnamurthy R, Nutting AC. Effect of branch pulmonary artery stenosis on right ventricular volume overload in patients with tetralogy of fallot after initial surgical repair. *Am J Cardiol*. 2013;111(9):1355-1360.
13. Kuehne T, Gleason BK, Saeed M, et al. Combined pulmonary stenosis and insufficiency preserves myocardial contractility in the developing heart of growing swine at midterm follow-up. *J Appl Physiol (1985)*. 2005;99(4):1422-1427.
14. Chern MJ, Wu MT, Wang HL. Numerical investigation of regurgitation phenomena in pulmonary arteries of tetralogy of fallot patients after repair. *J Biomech*. 2008;41(14):3002-3009.
15. Chern MJ, Wu MT, Her SW. Numerical study for blood flow in pulmonary arteries after repair of tetralogy of fallot. *Comput Math Methods Med*. 2012;2012:198108.

16. Das A, Gottliebson WM, Karve M, Banerjee R. Comparison of hemodynamic endpoints between normal subject and tetralogy patient using womersley velocity profile and MR based flow measurements. *Mol Cell Biomech.* 2011;8(1):21-42.
17. Rao AS, Menon PG. Presurgical planning using image-based in silico anatomical and functional characterization of tetralogy of fallot with associated anomalies. *Interact Cardiovasc Thorac Surg.* 2015;20(2):149-156.
18. Boumpouli M, Danton MHD, Gourlay T, Kazakidi A. Blood flow simulations in the pulmonary bifurcation in relation to adult patients with repaired tetralogy of fallot. *Med Eng Phys.* 2020;85:123-138.
19. Zhang W, Liu J, Yan Q, Liu J, Hong H, Mao L. Computational haemodynamic analysis of left pulmonary artery angulation effects on pulmonary blood flow. *Interact Cardiovasc Thorac Surg.* 2016;23(4):519-525.
20. Yushkevich PA, Piven J, Hazlett HC, et al. User-guided 3D active contour segmentation of anatomical structures: Significantly improved efficiency and reliability. *Neuroimage.* 2006;31(3):1116-1128.
21. Sloth E, Houliind KC, Oyre S, et al. Three-dimensional visualization of velocity profiles in the human main pulmonary artery with magnetic resonance phase-velocity mapping. *Am Heart J.* 1994;128(6 Pt 1):1130-1138.
22. Cheng CP, Herfkens RJ, Taylor CA, Feinstein JA. Proximal pulmonary artery blood flow characteristics in healthy subjects measured in an upright posture using MRI: The effects of exercise and age. *J Magn Reson Imaging.* 2005;21(6):752-758.
23. Arthurs CJ, Khlebnikov R, Melville A, et al. CRIMSON: An open-source software framework for cardiovascular integrated modelling and simulation. *PLoS Comput Biol.* 2021;17(5):e1008881.
24. Katritsis DG, Theodorakakos A, Pantos I, et al. Vortex formation and recirculation zones in left anterior descending artery stenoses: Computational fluid dynamics analysis. *Phys Med Biol.* 2010;55(5):1395-1411.
25. Farnoush A, Avolio A, Qian Y. Effect of bifurcation angle configuration and ratio of daughter diameters on hemodynamics of bifurcation aneurysms. *AJNR Am J Neuroradiol.* 2013;34(2):391-396.
26. Cunningham KS, Gotlieb AI. The role of shear stress in the pathogenesis of atherosclerosis. *Lab Invest.* 2005;85(1):9-23.
27. Rommel JJ, Yadav PK, Stouffer GA. Causes and hemodynamic findings in chronic severe pulmonary regurgitation. *Catheter Cardiovasc Interv.* 2018;92(3):E197-E203.
28. Kheyfets VO, O'Dell W, Smith T, Reilly JJ, Finol EA. Considerations for numerical modeling of the pulmonary circulation--a review with a focus on pulmonary hypertension. *J Biomech Eng.* 2013;135(6):61011-61015.



THE Y-STENTING TECHNIQUE FOR PULMONARY ARTERY BIFURCATION STENOSIS: INITIAL RESULTS AND MID-TERM OUTCOMES.

Maartje Conijn
Johannes M.P. Breur
Mirella M. Molenschot

Michiel Voskuil
Gregor J. Krings

International Journal of Cardiology
2018; 1;268:202-207

ABSTRACT

Background Treatment for main or peripheral PBS is challenging. An interventional approach is generally preferred as surgical angioplasty often results in residual stenosis. However, there is limited data on the mid- and long-term results of the different interventional approaches. The aim of this study is to report on initial and mid-term results of the Y-stenting technique for pulmonary artery bifurcation stenosis (PBS).

Methods A single centre retrospective study of all Y-stenting procedures for main or peripheral PBS was conducted. Patient and procedural data as well as mid-term outcomes were analysed.

Results 11 Y-stenting procedures were performed, 9 in the main pulmonary bifurcation and 2 in the PA periphery. In 8 patients the bifurcation stents were connected, in 3 patients there was no connection between the stents. Y-stenting creates a geometry close to the physiological PA bifurcation anatomy with complete alignment to the vessel wall without flow separation. Control angiography showed unrestricted blood flow after all procedures. Median right/left ventricle pressure ratio decreased from 0.9 to 0.5. No immediate or delayed adverse events were seen. During a median follow-up of 33.5 months, 2 patients in the non-connected group and 3 patients in the connected group needed a total of 6 re-interventions. No intima proliferation was seen in patients with connected stents.

Conclusion Y-stenting is a safe and effective treatment for PBS. When both bifurcation stents are connected, this may result in lower rates of in-stent intima proliferation in comparison to other PBS stenting techniques.

1 INTRODUCTION

Pulmonary artery (PA) branch stenosis is common in several types of congenital heart disease (CHD) such as Tetralogy of Fallot (TOF), pulmonary atresia and Transposition of the Great Arteries (TGA).^{1,2} When the main or peripheral PA bifurcation is involved, treatment is often challenging. Percutaneous stent implantation is a widely used approach to treat these complex stenosis as surgical angioplasty often results in residual stenosis.^{3,4} In renal, iliac and coronary artery bifurcation stenosis different interventional approaches as kissing stent implantation and V-, T-, or Y-stenting are used depending on the morphology of the stenosis.⁵ Initial and long-term results of these approaches are well known.⁵⁻⁹ The feasibility of similar techniques for pulmonary bifurcation stenosis (PBS) is described but data on long-term results are very limited. The only long-term follow-up data after PBS stenting is published by Stapleton et al. who reported on outcomes after simultaneous (kissing) stent implantation.¹⁰ The Y-stenting technique for PBS was first described by Narayan et al. who reported on the feasibility of this technique in two patients without data on long-term follow-up.¹¹ The aim of this study is to report on our experience with the Y-stenting technique for PBS including the initial and mid-term results.

2 MATERIALS AND METHODS

We retrospectively analysed all Y-stenting procedures at the Wilhelmina Children's Hospital (University Medical Centre, Netherlands).

2.1 Procedure

All procedures were performed under general anaesthesia. Patients received an intravenous Heparin bolus of 100 IU/kg to a maximum of 5000 IU and Cefazolin 50 mg/kg. In all patients single femoral venous and arterial access was obtained. For 3 dimensional rotational angiography (3DRA) acquisition (Siemens Atris Zee DynaCT, Leonardo 3D workstation, Siemens Healthineers, Erlangen, Germany) biventricular contrast injection was performed under rapid pacing and respiratory arrest. The resulting 3D image was post-processed, duplicated and divided into a separate left and right heart dataset. This allowed for optimal understanding of topographic interactions between the PA stenosis and the ascending aorta, coronary arteries and airways.¹² Y-stenting was precluded if the coronary arteries were at high risk for compression during stent placement in the PA bifurcation. If necessary,

balloon interrogation with simultaneous coronary artery injection was performed to ensure coronary artery safety. Following initial hemodynamic assessment and 3D reconstruction the interventional strategy and stenting sequence were defined. The 3D dataset was used for roadmap guidance during the procedure.

The Y-stenting technique was performed as described by Narayan et al.¹¹ In main PBS, a stent was deployed in the MPA extending into either the LPA or RPA (fig 1A). Next, the guidewire was advanced through the stent struts into the contralateral PA branch periphery. Using sequential balloon dilatation the stent struts to the contralateral PA branch were opened after which a second stent was advanced in the contralateral PA branch (fig 1B-H). This second stent can either be a closed or open cell design but preferably a stent with the same mechanical behaviour as the first placed stent (open cell design) was used. The second stent was expanded either with a 3-4 mm overlap to the first deployed stent (connected Y-stenting, fig 1G) or without overlap (non-connected Y-stenting) (figure 2). In peripheral PBS the first stent was deployed jailing the upper or lower lobe side branch after which the stent struts were opened for second stent placement in the PA lobe.

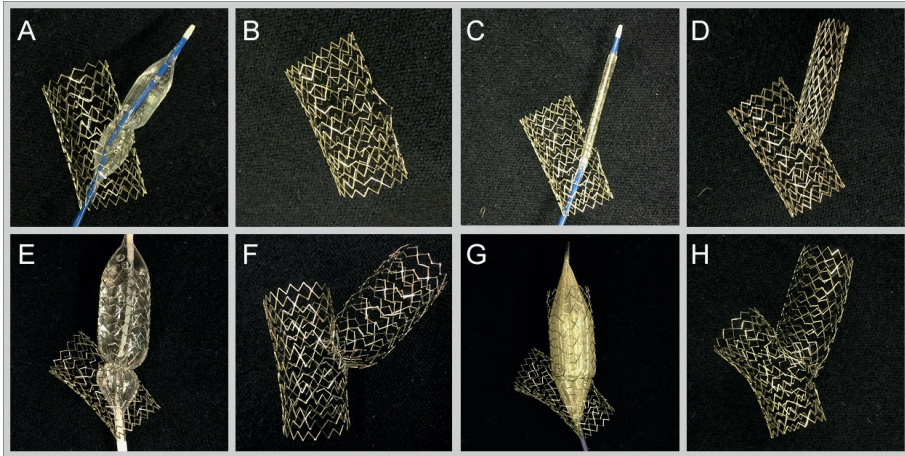


Figure 1 - in vitro Y-stenting (main PA bifurcation): **A:** a stent was placed traversing the 'MPA' into the 'RPA'. Using balloon dilatation the stent struts to the contralateral 'PA' are opened up to 50% of the target vessel diameter. **B:** MPA-RPA stent after stent strut opening. **C:** A second stent is advanced through the stent struts into the 'LPA'. **D:** The second stent is expanded with an overlap with the 'MPA' stent. **E:** Balloon dilatation of the stent entrance. **F:** Both stents are connected. **G:** The 'LPA' stent is flared up to the desired vessel diameter. **H:** Y-stenting results in a natural PA bifurcation anatomy. PA: pulmonary artery, MPA: main pulmonary artery, RPA: right pulmonary artery, LPA: left pulmonary artery.

Control angiography was performed to confirm unrestricted blood flow through the pulmonary arteries and to exclude vessel trauma after all procedures. Hemodynamic assessment was done after main PA bifurcation stenting. After a peripheral procedure morphological results were used to determine successful procedural outcomes. Post-intervention acetylsalicylic acid (3-5 mg/kg 1xday) was started in case of a post-stent PA diameter <8 mm to reduce intima proliferation. All patients were discharged one day post-intervention after cardiac ultrasonography.

2.2 Data collection

Baseline characteristics of all patients as well as the indication for angiography and intervention were collected. We registered catheterization data including interventional time, used materials and amounts of radiation. Vessel diameters and right to left ventricle (RV:LV) ratio's before and after the intervention were obtained. Missing data on hemodynamic assessment before and after stenting was completed by retrospectively evaluating echocardiographic images from the day after the procedure. We registered all adverse events during and after the intervention. Data on survival, re-interventions and cardiac surgeries during follow-up were collected. The indication for re-intervention or surgery and procedural details of the re-intervention and surgery were registered.

Intima proliferation was defined as visible tissue in the initial bifurcation stents or as narrowing of the area between both stents on angiography during re-catheterization. Restenosis due to somatic growth was defined as a smaller diameter of the stented area with regard to the adjacent vessel in the absence of intima proliferation. Data were reported as median with IQR or as mean with standard deviation. Due to the low number of patients included, no comparative analyses were performed.

3 RESULTS

3.1 Demographics

The Y-stenting technique was performed in 11 patients, 8 for main PBS and 3 for peripheral PBS. The first procedure took place in October 2009 and the last in August 2017. All baseline characteristics are shown in table 1. Initial cardiac diagnosis included Tetralogy of Fallot (TOF), truncus arteriosus (TAC) and isolated pulmonary artery stenosis. Age ranged between 4 months and 21 years and weight varied between 7.4 and 62 kg. All but one patient had previous corrective surgery. A total of 6 patients

had previous interventional treatment for MPA/LPA/RPA stenosis by either balloon dilatation (N=5) or stent placement (N=3). Indications for angiographic assessment were echocardiographic findings including elevated RV pressure, increased flow over the PA branches, decreased PA diameters or diminished visibility of the PA branches. Indication for intervention during catheterization was a right to left ventricular (RV/LV) pressure ratio of at least 2/3 with significant narrowing of the pulmonary bifurcation or morphological severe bifurcation stenosis even with a RV/LV pressure ratio below 2/3.

3.2 Procedural details

In all patients 3DRA was used for pre-intervention imaging and overlay during the procedure except for patient E and F. A total of 22 stents was implanted during interventions. The majority of stents were Ev3 Mega LD (Medtronic, Dublin, Ireland) and Cook Formula 535 (Cook Medical, Bloomington, USA) stents. All used stents are displayed in table 2. 8 patients received connected Y-stents while in 3 patients stents were not connected.

Median overall procedural time was 305 minutes (IQR 175) with a median of 101 minutes (IQR 67.4) of fluoroscopy. Median radiation dose during intervention was 1597 yGym² (IQR 4939).

3.3 Hemodynamic assessment pre- and post-intervention

A total of 33 vessels was treated with a mean increase in minimal vessel diameter of 116.4 SD 133.2 %. Median minimal MPA/RPA/LPA diameters increased from 7 mm (IQR 6), 5 mm (IQR 3) and 6 mm (IQR 3.5) to 14 mm (IQR 5.5), 10 mm (IQR 4) and 11 mm (IQR 5) respectively. Median MPA/RPA/LPA Z-scores increased from -4.49 (IQR 3.56), -4.07 (IQR 1.72), -2.78 (IQR 3.49) to -0.45 (IQR 0.635), 1.8 (IQR 1.85) and 1.08 (IQR 1.6) respectively. Median RV/LV pressure ratio decreased from 0.9 (IQR 0.27) to 0.5 (IQR 0.36). Individual patient data on pre- and post-intervention vessel diameters, Z-scores and LV/RV ratio are displayed in figure 2. In patient B no decrease in RV pressure was seen after intervention due to additional (sub-) valvular pulmonary stenosis. In consultation with the cardiac surgeon it was decided to leave this untreated in anticipation of surgical correction. Post-intervention control angiography showed unrestricted PA perfusion without vessel trauma in all patients. 1 patient was started on acetylsalicylic acid due to a stent diameter <8 mm. 2 patients continued anticoagulation as before intervention (acetylsalicylic acid in 1 patient and acetylsalicylic acid and clopidogrel in another patient). In the 8 other patients there was no indication for post-intervention anticoagulation.

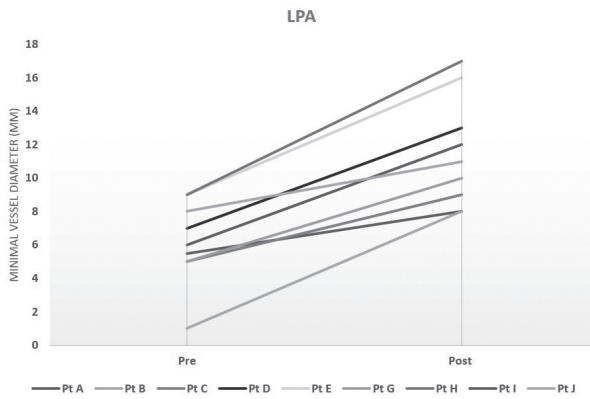
Table 1 - Baseline characteristics

Patient	Diagnosis	Sex	Age	Follow-Up (months)	Weight (kg)	Previous Surgery	Previous Intervention (MPA / LPA / RPA)	
							Balloon dilatation	Stent
A	TOF	M	9 m	56	7.5	Yes	No	No
B	v+svPS	F	4 m	55	7.4	No	No	No
C	DORV	F	16 m	42	9.5	Yes	No	No
D	TAC	F	16 y	15	60	Yes	Yes	No
E	PA	F	7 y	94	21	Yes	No	Yes
F	vPS	M	4 y	71	16.1	Yes	Yes	No
G	TAC	F	30 m	12	14	Yes	No	No
H	ToF	M	19 y	11	62	Yes	Yes	No
I	ToF	M	2.1 y	4	10.8	Yes	No	No
J	TAC	M	5.2 y	4	18	Yes	Yes	Yes
K	PA	V	20 y	0	49	Yes	Yes	Yes

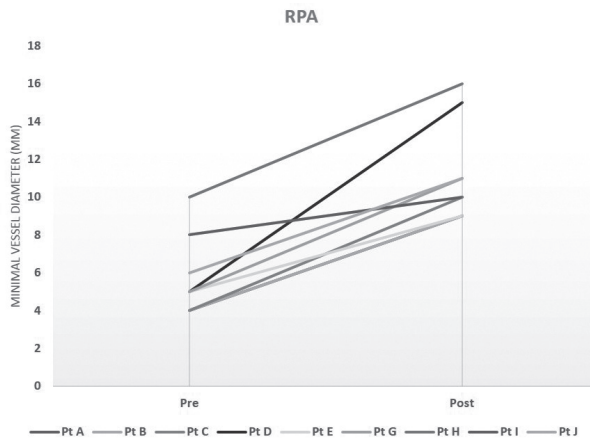
M: Male, F: Female, Age in months (m) or years (y), ToF: Tetralogy of Fallot, vPS: Valvular pulmonary stenosis, sPS: supravulvalar pulmonary stenosis, DORV: Double Outlet Right Ventricle, TAC: Truncus arteriosus communis PA: Pulmonary Atresia, MPA: main pulmonary artery, LPA: left pulmonary artery, RPA: right pulmonary artery.



2A



2B



2C

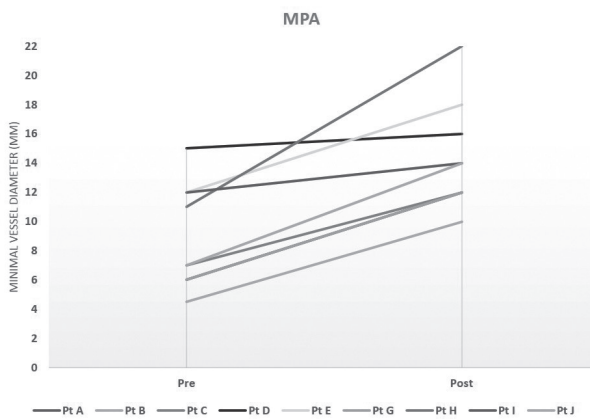
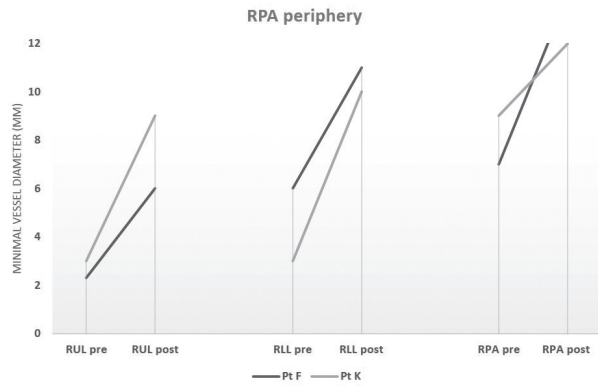
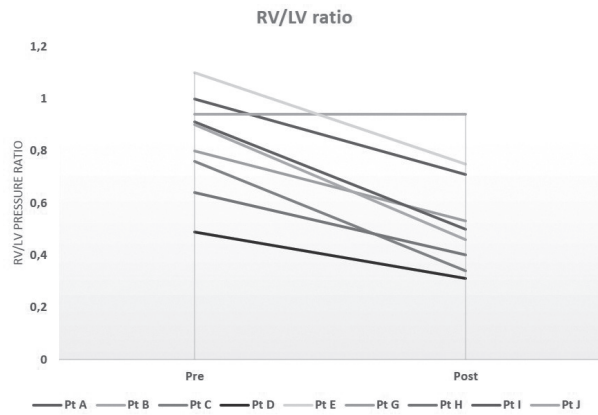


Figure 2 - Pre- and post-interventional PA dm and RV/LV pressure ratio. 2A: minimal LPA diameters (mm) pre- and post-intervention. **2B:** minimal RPA diameters (mm) pre- and post-intervention. **2C:** minimal MPA diameters (mm) pre- and post-intervention.

2D



2E



2F

Patient	Z-scores					
	MPA		RPA		LPA	
	Pre	Post	Pre	Post	Pre	Post
A	-4,49	0,36	-4,07	2,19	-1,51	1,08
B	-6,44	-0,85	-3,99	1,83	-13,22	1,16
C	-3,91	-0,14	-4,69	2,4	-2,78	1,29
D	-2,3	-2,3	-8,61	-0,12	-6	-1,72
E	-2,36	0,48	-5,68	-1,14	-1,39	2,59
G	-6,06	-1,21	-4,28	1,82	-4,07	0,72
H	-5,26	-0,45	-3,15	0,44	-4,21	0,19
I	-0,63	0,45	0,08	1,8	-2,1	2,69
J	-5,72	-0,87	-3,78	0,91	-1,72	0,49

2D: minimal vessel diameters after peripheral PBS stenting in patient F and K. RUL: right upper lobe PA, RLL: right lower lobe. **2E:** pre- and post-intervention RV/LV pressure ratio. **2F:** Z-scores of MPA/RPA and LPA minimal vessel diameters pre- and post-intervention. PA: pulmonary artery, dm: diameter, RV: right ventricle, LV: left ventricle, LPA: left pulmonary artery, RPA: right pulmonary artery, MPA: main pulmonary artery, PBS: pulmonary bifurcation stenosis.

Table 2 - Used material for Y-stenting.

Stent	Cell design	Maximum diameter hole (for second stent passing)	N=	Patient
Ev3 Mega LD	Open	20 mm	9	C, F, G, H, I, J, K, E
Cook Formula 535	Open	16-18 mm	7	A, B, C, G, K
Ev3 Max LD	Open	26 mm	3	D, H
Genesis Medium	Closed	12 mm	1	F
Premounted Genesis Slalom	Closed	12 mm	1	E

3.4 Complications during intervention

In 2 patients the first stent was deformed during stent strut dilatation due to malposition of the wire which was unintentionally positioned on top of the MPA stent instead of in the MPA stent lumen. Therefore, balloon dilatation did not open the stent struts but crushed the stent entrance. The stent lumen was re-entered and balloon dilatation was used to reshape the stent. A second attempt of strut dilatation was successful in both patients. In 1 patient the balloon used for strut dilatation got strangulated. This caused a severe delay in deflation with a prolonged total occlusion of the MPA without clinical consequences. 1 patient got severely hypotensive and bradycardic after first stent deployment with ventricular tachycardia after adrenaline. After 2 shocks with the external defibrillator sinus rhythm returned with satisfactory cardiac output. The post-interventional period was uncomplicated.

3.5 Mid-term follow-up

No patients were lost to follow-up. Median follow-up time was 33.5 months (IQR 49.75). The intervention in patient K was just prior to data collection. Therefore, no mid-term follow-up was available for this patient.

No deaths occurred during follow-up. Patient B had surgical angioplasty of the (sub-)valvular pulmonary stenosis with ASD closure 4 months after the initial procedure. Patient E had cardiac surgery with homograft replacement due to an infected homograft 6 years after the initial intervention. No patients needed cardiac surgery for PA branch stenosis. Follow-up catheterization data is summarized in figure 3. A total of 6 re-interventions was performed in 5 patients. Indications for re-catheterisation and intervention during catheterisation were similar to the indications

for the initial Y-stenting procedure as described above. There were no interventions in vessels other than the MPA, RPA or LPA.

During re-interventions a total of 2 additional stents were placed in one of the previously stented PA branches. 3 patients had balloon angioplasty of one or both of the PA branches and 1 patient had PPVI 4 months after the initial procedure. In the non-connected Y-stent group both patients who received Y-stents in the main pulmonary bifurcation needed re-intervention due to intima proliferation. In one of these patients an additional stent was placed to create a connected Y-stent during re-intervention. The stenosis in the other patient could be treated by balloon angioplasty. In the connected Y-stent group, patient B had a stent fracture (Cook Formula stent) which caused severe intima proliferation in the fractured area which was treated by a stent-in-stent in the RPA. In patient A, the initial stent connection was too weak resulting in disconnection between both stents. During re-intervention 9 months after the initial procedure the gap between both stents showed severe intima proliferation which could be successfully treated by high pressure balloon dilatation. 30 months after the initial procedure this patient was again treated with balloon angioplasty for restenosis due to physical growth. No intima proliferation was seen in other patients receiving connected Y-stents. Median time to re-intervention in both groups was 30 months (IQR 28.5). All re-interventions are shown in figure 3. During re-interventions there were no major or minor complications and branch PA access was without difficulty in all patients.

4 DISCUSSION

In this group of 11 patients, the Y-stenting technique was a safe and effective treatment for main and peripheral PBS. During follow-up a total of 6 re-interventions was necessary in 5 patients. Intima proliferation was seen in patients who received non-connected Y-stents, after stent-fracture or disconnection of initially connected Y-stents. To the best of our knowledge, this is the largest group of patients treated for PBS using the Y-stenting technique. We are the first to report on mid-term outcomes after this procedure.

4.1 Interventional approaches for PBS

All different interventional strategies for bifurcation stenting published so far come with their own advantages and disadvantages.^{10,11,13-15} V-stenting addresses the

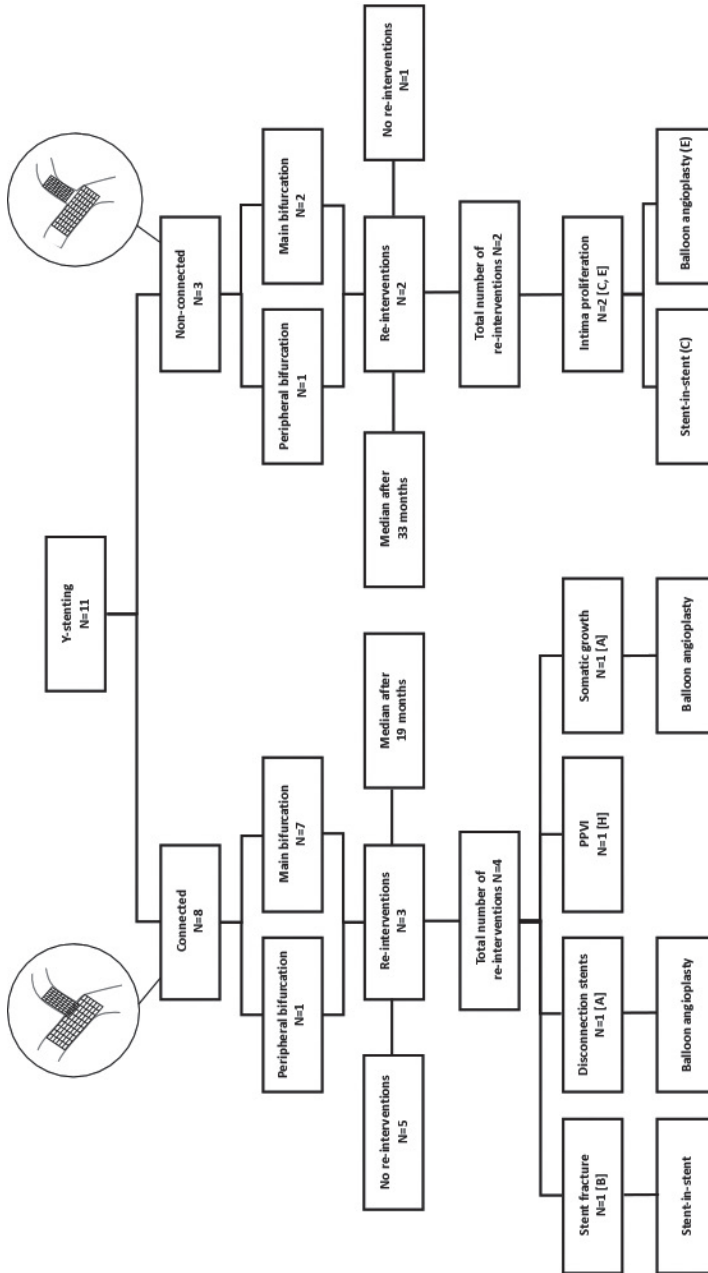


Figure 3 - Flowchart follow-up patients after Y-stenting. PPVI: percutaneous pulmonary valve implantation, N: number

PA branches separately but without reaching into the MPA and is therefore not suitable to treat main PBS with distal MPA involvement. The kissing stent technique treats the three location obstruction by simultaneous bilateral stent implantation via either a double sheath double wire or a single sheath double wire approach.^{10,14,15} However, this demands the use of two separate or one large long sheath which is not favourable in small children or in patients with vessel access difficulties. Also, the kissing stent technique results in a proximal double MPA lumen. Entering this double stent lumen during re-intervention can be difficult especially in PPVI. Y-stenting as described by Narayan et al. creates a stent shape similar to the natural anatomy of the pulmonary bifurcation and leaves a single lumen in the MPA assuring easier access during re-intervention. This lumen also serves as an ideal landing zone for future PPVI which will be necessary in the majority of patients treated for complex PBS.¹¹ This was also seen in one of our patients (K) who underwent PPVI 4 months after the initial Y-stenting procedure. In addition, due to the single wire single sheath approach the Y-stenting technique is preferable in small children. Narayan et al mentioned the possibility of stent fracture after Y-stenting due to weakening of the structural integrity by breaking the stent struts.¹¹ In our study stent fracture occurred in one patient during a median follow-up of 34 months. After bifurcation stenting there is a risk of iatrogenic stent deformation during additional surgery. Thus, surgeons should be informed and aware that iatrogenic stent compression can occur even in simple procedures as placement of epicardiac pacemaker leads.

4.2 Restenosis after bifurcation stenting

The mechanism of re-stenosis after stent implantation in children is multifactorial and not fully understood. Relative stenosis due to physical growth has to be distinguished from intima proliferation causing in-stent stenosis. In some cases, it is caused by aberrant anatomy with external compression of the PA branches (e.g. large diameters of the ascending aorta or a right aortic arch). In single PA stenting, restenosis rates are reported to be around 25%.^{16,17} For bilateral PA stenting, in-stent restenosis rates are higher (52%).¹⁸ Limited data is available on restenosis and intima proliferation after PBS stenting. Stapleton et al. reported 30 repeat catheterizations (68%) with 24 re-interventions (63%) during follow-up of 38 patients after simultaneous (kissing) stent implantation.¹⁰ In 58% of these patients, significant in-stent restenosis of one or both stents was the indication for re-intervention. No differentiation between restenosis caused by intima proliferation or physical growth was made. It has previously been reported that stent over inflation can cause intima proliferation by migration of smooth muscle cells. In addition, stents with greater radial force and

stents with a closed cell design increase the risk for intima proliferation.¹⁸ Patient characteristics can also be a risk factor for intima proliferation. This includes patients with Alagille or Williams syndrome and patients with distal MPA stenosis. Other high risk-patients are patients post-pulmonary bifurcation plasty surgery, post-Contegra valve implantation and post-unifocalization surgery. This accounts for most of the population in need for intervention for PBS as is seen in our study population which – except for patient I - included only high risk patients. Stapleton et al. hypothesized that high rates of re-stenosis after PBS might be explained by a greater exposure to metal due to two implanted stents which causes distortion to the vessel wall. Also, the more turbulent flow at the bifurcation may cause intima proliferation.¹⁰ Although re-intervention rates in our study are also high, we found in-stent restenosis due to intima proliferation only in patients receiving non-contacting Y-stents and after stent-fracture or disconnection of initial contacting Y-stents. Therefore, we hypothesize that inter-stent movement between non-connected Y-stents causes higher proximal shear stress with endothelial trauma (figure 4) (movie 1, supplementary data). This hypothesis is supported by findings in iliacal and coronary artery stenting.^{5,9,19} Kissing stents lack contact between the vessel wall and opposing stents and cause flow separation. This is associated with high variations in wall shear stress which may cause intima proliferation.^{9,19} Y-stenting for PBS with connected stents creates a bifurcation close to the natural geometry with complete alignment to the vessel wall and without flow separation. Therefore, it is likely that connected Y-stents account for lower rates of restenosis than kissing stents. However, long-term follow-up in a larger patient group is necessary to support these findings.

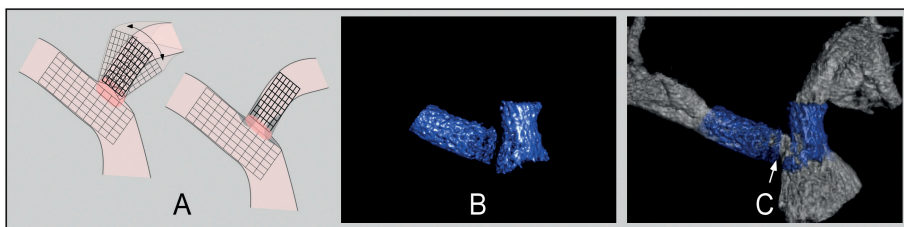


Figure 4 - Intima proliferation in non-connected Y-stents. A: Inter-stent movement between non-connected stents increases the risk for in-stent intima proliferation. **B:** 3DRA image (cranial view) of non-connected bifurcation stents. **C:** 3DRA image demonstrating in-stent and pre-stent intima proliferation in the RPA (vessel lumen in grey, stent in blue, intima proliferation indicated by arrow). 3DRA: 3D rotational angiography. RPA: right pulmonary artery.

5 CONCLUSION

This is the only and largest study reporting on the initial and mid-term follow-up after Y-stenting for PBS. Y-stenting creates a geometry close to the physiological PA bifurcation anatomy with complete alignment to the vessel wall without flow separation. Especially when both stents are connected, Y-stenting may cause lower rates of intima proliferation in comparison to other PBS stenting techniques. However, additional research is recommended to support these findings.

REFERENCES

1. Bacha EA, Kreutzer J. Comprehensive management of branch pulmonary artery stenosis. *J Interv Cardiol.* 2001;14(3):367-375.
2. Hoffman JL, Kaplan S. The incidence of congenital heart disease. *J Am Coll Cardiol.* 2002;39(12):1890-1900.
3. Trant CA, Jr, O'Laughlin MP, Ungerleider RM, Garson A, Jr. Cost-effectiveness analysis of stents, balloon angioplasty, and surgery for the treatment of branch pulmonary artery stenosis. *Pediatr Cardiol.* 1997;18(5):339-344.
4. Luhmer I, Ziemer G. Coarctation of the pulmonary artery in neonates. prevalence, diagnosis, and surgical treatment. *J Thorac Cardiovasc Surg.* 1993;106(5):889-894.
5. Lefevre T, Louvard Y, Morice MC, Loubeyre C, Piechaud JF, Dumas P. Stenting of bifurcation lesions: A rational approach. *J Interv Cardiol.* 2001;14(6):573-585.
6. Rux S, Sonntag S, Schulze R, et al. Acute and long-term results of bifurcation stenting (from the coroflex registry). *Am J Cardiol.* 2006;98(9):1214-1217.
7. Morton AC, Siotia A, Arnold ND, et al. Simultaneous kissing stent technique to treat left main stem bifurcation disease. *Catheter Cardiovasc Interv.* 2007;69(2):209-215.
8. Lorin JD, Hirsh DS, Attubato MJ, Sedlis SP. A dual wire approach to severe ostial bifurcating renal artery stenosis. *Catheter Cardiovasc Interv.* 2006;67(6):956-960.
9. Yilmaz S, Sindel T, Golbasi I, Turkyay C, Mete A, Luleci E. Aortoiliac kissing stents: Long-term results and analysis of risk factors affecting patency. *J Endovasc Ther.* 2006;13(3):291-301.
10. Stapleton GE, Hamzeh R, Mullins CE, et al. Simultaneous stent implantation to treat bifurcation stenoses in the pulmonary arteries: Initial results and long-term follow up. *Catheter Cardiovasc Interv.* 2009;73(4):557-563.
11. Narayan HK, Glatz AC, Rome JJ. Bifurcating stents in the pulmonary arteries: A novel technique to relieve bilateral branch pulmonary artery obstruction. *Catheter Cardiovasc Interv.* 2015;86(4):714-718.
12. Truong UT, Fagan TE, Deterding R, Ing RJ, Fonseca BM. Use of rotational angiography in assessing relationship of the airway to vasculature during cardiac catheterization. *Catheter Cardiovasc Interv.* 2015;86(6):1068-1077.
13. Stumper O, Bhole V, Anderson B, Reinhardt Z, Noonan P, Mehta C. A novel technique for stenting pulmonary artery and conduit bifurcation stenosis. *Catheter Cardiovasc Interv.* 2011;78(3):419-424.
14. McMahon CJ, El-Said HG, Mullins CE. Three new applications of stent technology in a single patient. *Tex Heart Inst J.* 2001;28(2):125-128.
15. Brown SC, Cools B, Boshoff DE, et al. Delivering stents in congenital heart disease using the double-wire technique: Technical considerations. *Catheter Cardiovasc Interv.* 2013;82(7):1156-1163.
16. Hallbergson A, Lock JE, Marshall AC. Frequency and risk of in-stent stenosis following pulmonary artery stenting. *Am J Cardiol.* 2014;113(3):541-545.
17. Krisnanda C, Menahem S, Lane GK. Intravascular stent implantation for the management of pulmonary artery stenosis. *Heart Lung Circ.* 2013;22(1):56-70.

18. Gonzalez I, Kenny D, Slyder S, Hijazi ZM. Medium and long-term outcomes after bilateral pulmonary artery stenting in children and adults with congenital heart disease. *Pediatr Cardiol.* 2013;34(1):179-184.
19. Moore JE, Jr, Timmins LH, Ladisa JF, Jr. Coronary artery bifurcation biomechanics and implications for interventional strategies. *Catheter Cardiovasc Interv.* 2010;76(6):836-843.



**THE HEMODYNAMIC IMPACT OF AN OVAL
VERSUS CYLINDRICAL STENT SHAPE TO
PREVENT COMPRESSION OF ADJACENT
STRUCTURES IN COMPLEX PULMONARY
ARTERY STENTING.**

Maartje Conijn

Gregor J. Krings

Submitted

ABSTRACT

Background In patients with CHD, extensive cardiac surgery may cause an intra-thoracic mass shift resulting in a close vessel-to-airway relation. In these patients, stenting a PA stenosis may result in compression of adjacent structures. Implanting a stent that is oval shaped by the double balloon technique prevents this. Little is known about the hemodynamic impact of non-cylindrical stent shapes. This study aimed to computationally evaluate the differences in pulmonary artery (PA) hemodynamics after cylindrical and oval stent implantation for pulmonary artery (PA) stenosis in patients with congenital heart disease (CHD).

Methods One biventricular and one univentricular case were retrospectively selected. The patient-specific pre-interventional 3D anatomy of the PA's, aorta and airway were reconstructed. Based on this pre-interventional anatomy, a post-interventional oval stent and cylindrical stent anatomy were constructed. On the inlet(s), a mass flow boundary condition and on the outlets a 3-element windkessel boundary condition were applied. A mesh independent test was performed to evaluate grid independence. Computational analysis was performed over four cardiac cycles. Anatomy, flow distribution, velocity and pressure outcomes were compared between the pre-, cylindrical- and oval stent scenario.

Results In both cases, a cylindrical stent resulted in compression of other structures by the left PA. No compression was observed in the oval stent scenarios. Oval and cylindrical stent implantation showed equal results in flow distribution, pressure and velocity outcomes.

Conclusion An oval stent shape prevents airway compression in patients with close vessel-to-airway relation. The oval stent has no hemodynamic disadvantages over a cylindrical stent.

1 INTRODUCTION

Eight of every 1000 live births is born with a congenital heart disease (CHD).¹ On top of the already aberrant anatomy, cardiac surgery to palliate or correct CHD may again impact the anatomy. The intrathoracic mass-shift caused by extensive surgery may result in a complex morphology with limited retro-aortic space. Not seldom this results in compression of the left pulmonary artery (LPA) by the aorta or in airway compression by the LPA. About 2-3% of the patients with CHD will at some point develop a degree of PA stenosis with an incidence up to 20% in patients with Tetralogy of Fallot, Transposition of the Great Arteries and Pulmonary Atresia.^{1,2} To relieve the obstruction, percutaneous stent implantation is generally the treatment of first choice.³⁻⁵ In complex anatomies with close relation between the different anatomical structures, stent placement in the PAs may cause compression of an adjacent vessels or bronchus.⁶⁻⁸

We previously reported on oval stent implantation to prevent airway compression in patients with limited retro-aortic space.⁹ We demonstrated the feasibility, safety and anatomical outcome of this double balloon double wire technique in 11 patients at risk for airway compression by PA stenting. Not much is known about the hemodynamic effects of non-cylindrical stent shapes. The aim of this study was to compare the hemodynamic impact of an oval stent shape to a cylindrical stent shape in bi- and univentricular anatomies with use of computational fluid dynamics.

2 METHODS

2.1 Case selection

A total of 15 oval stent procedures were performed in our institution. These included primary oval stent implantations and secondary oval shaping of prior PA stents. We retrospectively selected two cases – one biventricular and one univentricular. For both cases, pre- and post-interventional 3D rotational angiography (3DRA) imaging was available for anatomic reconstruction (section 3.2.). The cases were selected because of their exceptional anatomy of the PA's and adjacent structures. The oval stenting procedures, including the hemodynamic assessment, imaging and post-processing, were performed as previously described.⁹

The first case concerned a 14-years old girl with aortic valve and aortic arch hypoplasia. When she was 5 months old, she underwent a biventricular repair. The aortic arch reconstruction resulted in an extensive intrathoracic mass shift with the newly reconstructed aorta coursing below the left pulmonary artery (LPA). A left pulmonary artery (LPA) stenosis developed, for which she was interventionaly treated by stent placement when she was 7 and 9 years old. During routine follow-up, non-invasive imaging showed a restenosis in the LPA. She was referred for cardiac catheterization with hemodynamic evaluation. Here, pressure measurements and 3DRA imaging confirmed the LPA stenosis and showed a discrete coarctation of the aortic arch, just caudally to the LPA. To prevent further compression of the aortic arch, an oval stent was primarily horizontal deployed.

The second case was of a 4-years old boy with hypoplastic left heart syndrome (HLHS). Recently, his Fontan circulation was completed by a total cavo pulmonary connection (TCPC). Before the TCPC, he was interventionaly treated for coarctation of the aorta by balloon dilatation. During routine follow-up, non-invasive imaging showed a stenosis in the LPA for which he was referred to the cardiac catheterization room. 3DRA visualized a close relation of the LPA to the main left bronchus. A discrete re-coarctation of the aorta was present. To evaluate the possibilities for stent placement, a balloon interrogation under bronchoscopy was performed. This revealed a clear compression of the left bronchus by the balloon in the LPA. To prevent compression and still be able to treat the LPA stenosis, a cylindrical stent was implanted and ovalized by the double-balloon technique.

2.2 Anatomic reconstruction

To evaluate the hemodynamic differences between a cylindrical and oval stent shape, for each case a total of 3 different scenarios were simulated:

1. The pre-interventional anatomy with LPA stenosis
2. The post-interventional anatomy with a cylindrical stent in the LPA
3. The post-interventional anatomy with an oval stent in the LPA.

Using the 3DRA, the pre-interventional anatomy of both patients was reconstructed. First, the PAs were segmented using ITK-snap (<http://itksnap.org>). In Meshmixer software (Autodesk Inc, San Rafael, USA), the anatomy was manually smoothed and additional branches were removed. The final model consisted of the main pulmonary artery (MPA) with the right and left branch and two to three peripheral

branches on each side. The 3D model was imported into CRIMSON software (Cardiovascular Integrated Modelling and Simulation (CRIMSON; available at <http://www.crimson.software/> accessed 10.6.2020). Here, a mesh was created consisting of tetrahedral elements with a total of five boundary layers. A mesh independent test was performed to ensure a grid independent solution. The final mesh for case 1 (biventricular), consisted of 951.739 elements for the pre-intervention scenario. For the pre-intervention scenario of case 2 (univentricular) the final mesh consisted of 1.319.461 elements.

The pre-intervention anatomy served as the starting point for the reconstruction of the post-interventional anatomies. For both cases, a post-interventional 'empty' 3DRA (3DRA without contrast to visualize airway and stents in situ) was available. Using this scan, the oval shaped stent was segmented. The STL of this stent – with maintenance of the location- was appended to the pre-interventional anatomy. The LPA geometry was then adjusted to fit the oval stent shape in Meshmixer. To reconstruct the post-interventional scenario with a cylindrical stent, a cylinder with a cross sectional area equal to the oval stent was implanted in the pre-interventional anatomy. The resulting post-interventional anatomies were imported in CRIMSON and meshed as described above. The element size of the final pre-interventional scenario was applied to the post-interventional scenarios. For case 1 (biventricular), this resulted in 993.376 elements for the oval stent scenario and 969.512 elements for the cylindrical stent scenario. For case 2 (univentricular) the oval stent scenario consisted of 1.350.857 elements and the cylindrical stent scenario of 1.351.612 elements.

To determine the interaction between the pulmonary anatomy and the adjacent structures, the airway and aorta anatomy were reconstructed. The aorta and the bronchus were segmented in ITK-snap software as described above.

2.3 CFD analysis

The CFD analysis of flow in the pulmonary arteries was performed using CRIMSON software. A mass flow inlet boundary condition was defined. For case 1 (biventricular), the main pulmonary artery (MPA) waveform (ml/s) obtained by cardiac magnetic resonance (CMR) was used. Due to the absence of a second ventricle in case 2 (univentricular), PA perfusion was driven by the alternating intrathoracic pressure caused by breathing. The breath dependent inlet waveform was extracted from echocardiography of the superior vena cava (SVC). This waveform was applied as

the inlet boundary condition for the SVC, inferior vena cava (IVC) and anonyma. The percentages of flow for the three inlets in this case were assumed to be: 60% IVC, 20% SVC and 20% anonyma. A three- element windkessel was coupled to each outlet. The capacitor, proximal- and distal resistance values were calculated as previously described.¹⁰ The wall was set to be rigid and blood was assumed to behave as a Newtonian fluid with a density of 1060 kg/m³ and a viscosity of 0.004 kg/m·s. A total of four cardiac cycles were simulated. For case 1 (biventricular), the time step size was 0.001s, for case 2 (univentricular) the time step size was 0.003s with a total cardiac cycle time of 0.8s and 2.4s for case 1 (biventricular) and case 2 (univentricular). This resulted in a total of 800 time steps per cardiac cycle for each case. The solution was assumed to be converged when residuals dropped below 10⁻⁴.

2.4 Comparison cylindrical versus oval stent

Anatomical outcomes, flow distribution, velocity and pressure outcomes were compared between the three scenarios using Paraview software. The last simulated cardiac cycle was analyzed.

3 RESULTS

3.1 Anatomy

In figure 1, the anatomy for case 1 (biventricular) is shown. In this case, the right pulmonary artery (RPA) was largely oversized. The MPA was generally small, most distinct just prior to the bifurcation. The LPA in this case was small over a long course with a clear stenosis in the area where the aortic arch caudally passes the branch. The left main bronchus is compressed by the overlying arch. The cylindrical stent compressed the aorta arch but the oval stent preserved the aortic space.

In figure 2, the anatomy for case 2 (univentricular) is shown. In this case, both the RPA and LPA were relatively small. The LPA had a local stenosis just proximal to the bifurcation where the aorta passes. The main left bronchus coursed posterior to the LPA. Stenting the LPA with a cylindrical stent resulted in compression of the left main bronchus. There was no compression of the bronchus after oval stent implantation.

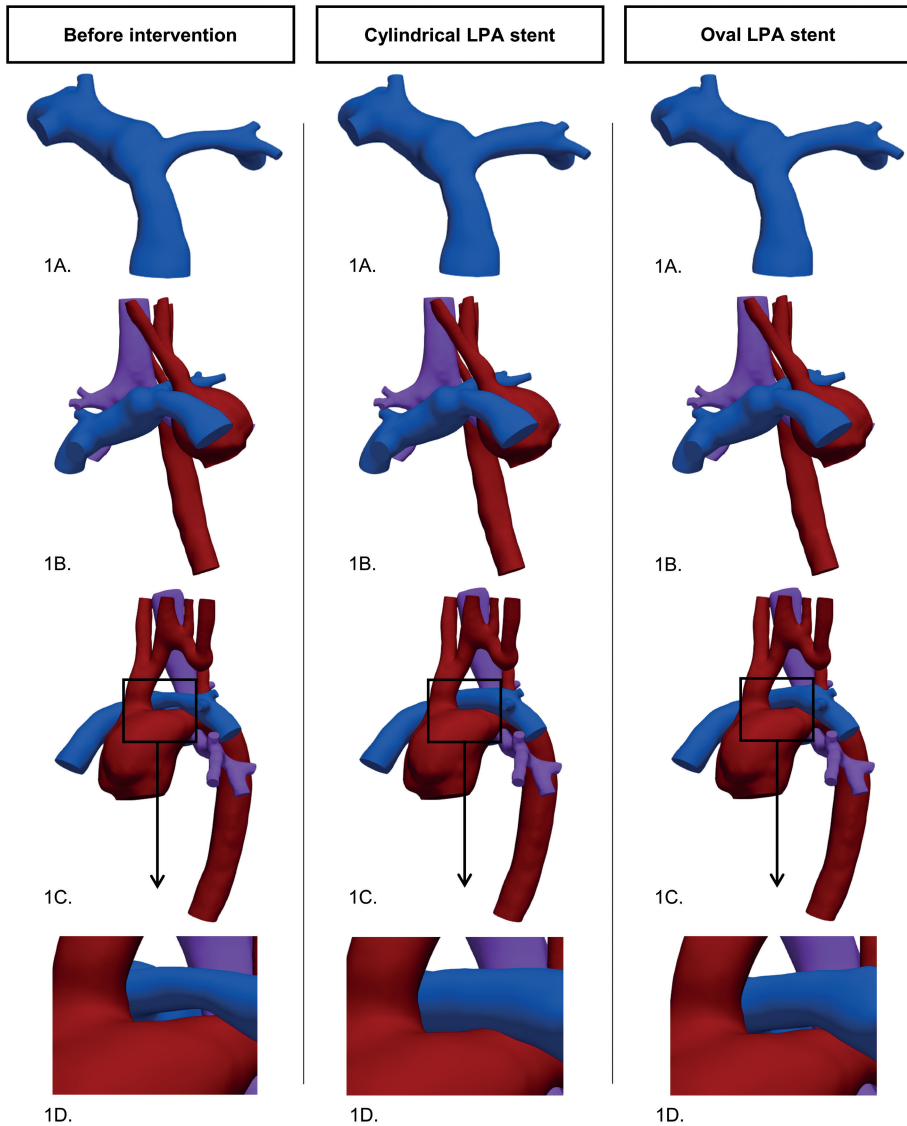


Figure 1 - Anatomy of case 1 (biventricular) before intervention, after cylindrical stent implantation and after oval stent implantation. 1A. The pulmonary artery anatomy. **1B.** The pulmonary arteries (blue), aorta (red) and airway (purple). **1C.** Lateral view of the anatomy and the close relation between the pulmonary arteries and the aorta and the aorta and the left main bronchus. **1D.** Close up of the region of the aorta compressed by the round stent.

3.2 Flow distribution

Before intervention, flow in case 1 (biventricular) went predominantly to the RPA with a RPA:LPA flow distribution of 84%:16%. The implantation of a cylindrical or oval stent had no influence on the flow distribution. Due to the oversized RPA, the post-intervention RPA:LPA flow distribution remained 84%:16% (figure 3A).

In case 2 (univentricular) the pre-intervention RPA:LPA flow distribution was 66%:34% (figure 4A). Post-intervention, the RPA:LPA flow distribution in the cylindrical stent scenario was 35%:65%. In the oval stent scenario the distribution was 34%:66%.

3.3 Pressure

Before intervention, in case 1 (biventricular) there was a gradient of 11 mmHg over the LPA and 8 mmHg over the RPA with a MPA pressure of 29 mmHg (figure 3B). After cylindrical stent implantation, the gradient over the LPA decreased to 8 mmHg. The post-intervention MPA pressure lowered to 27 mmHg. The oval stent had no influence on the gradient over the LPA and the MPA pressure. No difference in RPA gradient was measured between the pre- and post-intervention scenarios. In case 2 (univentricular), there was a pre-intervention gradient of 1 mmHg over the LPA (figure 4B). After stent implantation, the gradient over the LPA was resolved in both the cylindrical and oval stent scenario. There was no gradient over the RPA.

3.4 Velocity streamlines

The top systolic velocity streamlines for case 1 (biventricular) showed an increased velocity over the stenotic part of the MPA, extending into the RPA (figure 3C). The maximal flow in the MPA was 3.5 m/s, in the RPA 3.2 m/s and in the LPA 1 m/s. After cylindrical and oval stent implantation, the maximal velocity in the MPA, RPA and LPA remained unchanged. In all three scenarios, the low flow velocity in the LPA resulted in extensive areas of recirculation. In case 2 (univentricular) there was an acceleration of flow over both the RPA and LPA before intervention (figure 4C). The velocity increased from 0.2 m/s to a maximum of 0.4 m/s in the LPA and 0.5 m/s in the RPA. After implantation of a cylindrical stent, the flow velocity decreased to a maximum of 0.35 m/s in both branches. Oval stent implantation resulted in a maximum velocity of 0.3 m/s in the LPA and 0.35 m/s in the RPA. In the supplementary materials, a movie of the velocity streamlines over the complete cardiac cycle in the three scenarios of both cases can be viewed.

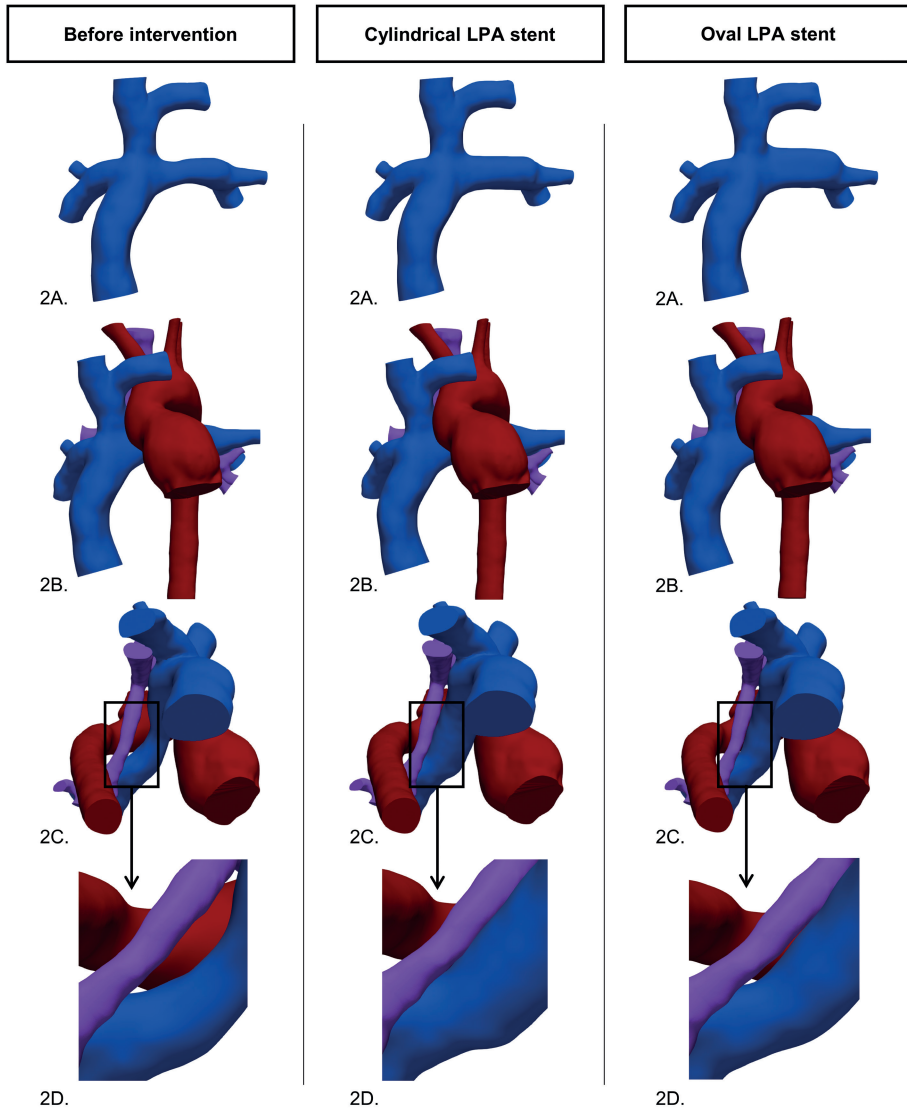


Figure 2 - Anatomy of case 2 (univentricular) before intervention, after cylindrical stent implantation and after oval stent implantation. 1A. The pulmonary artery anatomy. 1B. The pulmonary arteries (blue), aorta (red) and airway (purple). 1C. Caudal view of the anatomy and the close relation between the pulmonary arteries airway. 1D. Close up of the region of the airway compressed by the round stent.

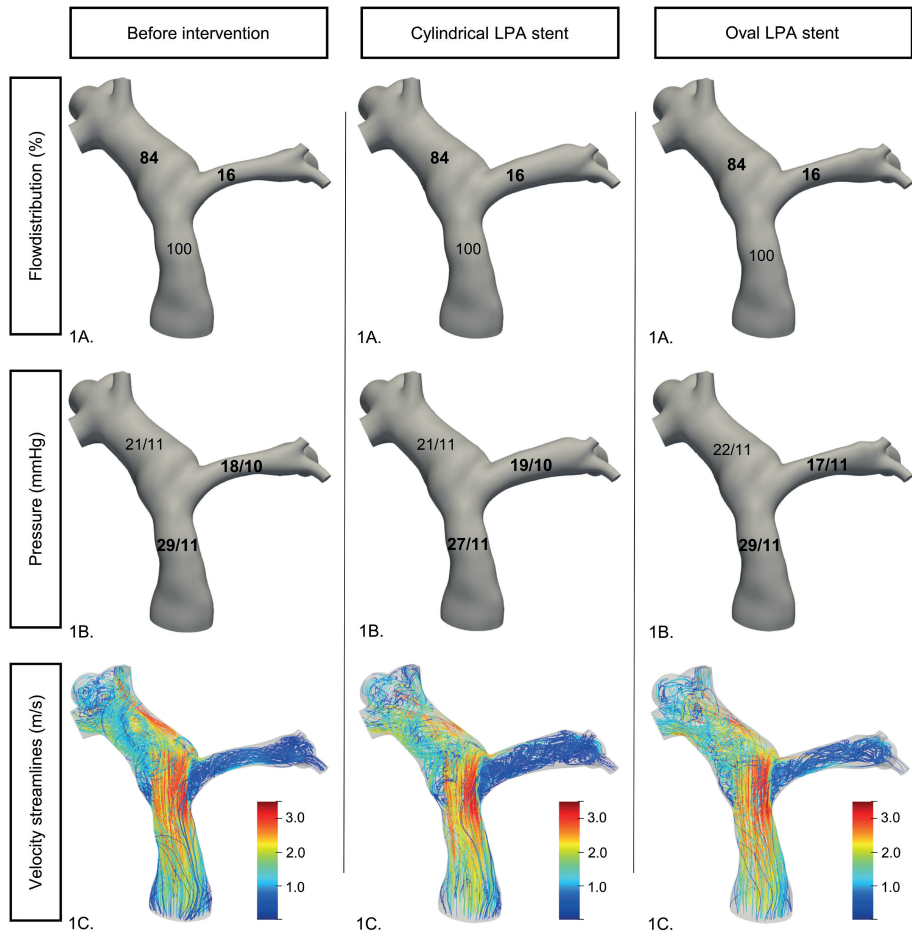


Figure 3 - Computational outcomes of flow distribution (1A), pressure (1B) and velocity (1C) of case 1 (biventricular).

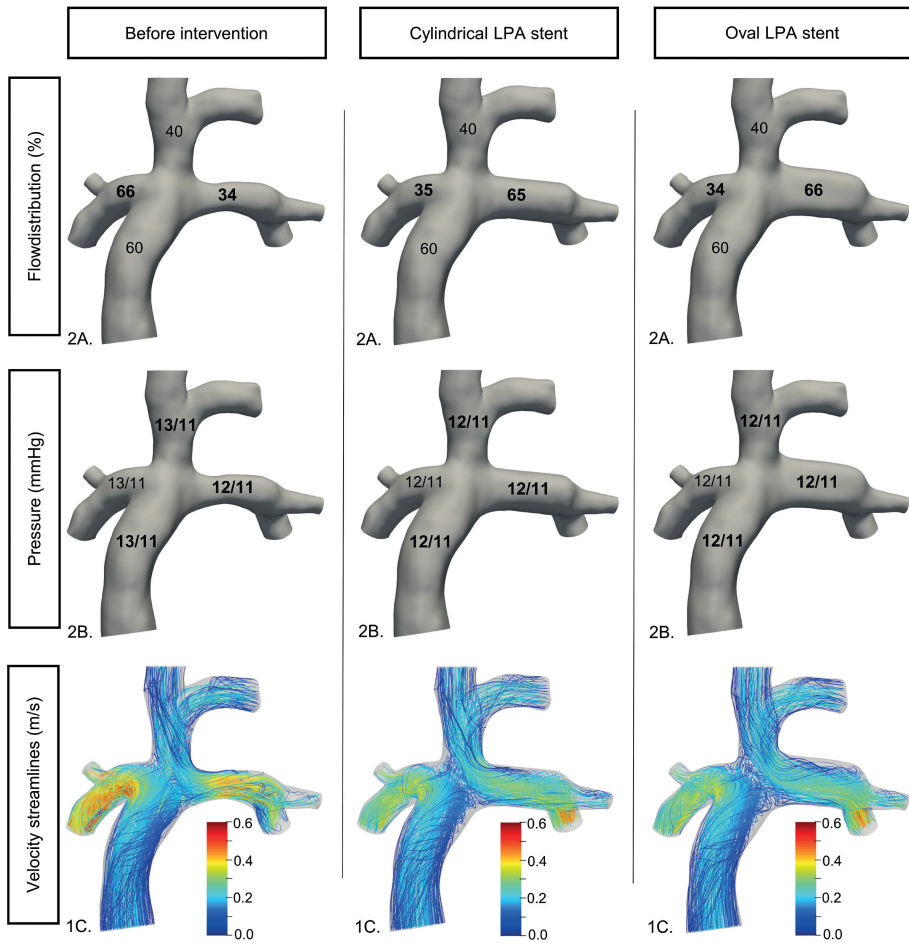


Figure 4 - Computational outcomes of flow distribution (2A), pressure (2B) and velocity (2C) of case 2 (univentricular).

4 DISCUSSION

Surgery on the great arteries of patients with CHD may result in a significant intrathoracic mass shift, completely redefining the anatomy of a patient. This increases the risk for compression of the LPA by the aorta as is seen in a significant portion of patients with an univentricular morphology. In patients with biventricular CHD, extensive surgery on the aortic arch may reduce the subaortic space increasing the risk for LPA stenosis. The patients selected for this study were chosen not because of their representativity of the general PA stenosis population but because of their exceptionality. They represent the complexity of the anatomy in patients with CHD after extensive corrective surgery at risk for collateral damage by stent placement in the LPA. We previously demonstrated the feasibility of implanting a traditional cylindrical stent that is ovally shaped to prevent airway compression. Not much is known about the hemodynamic impact of non-cylindrical stent shapes. This study now shows that an oval stent shape has no hemodynamic disadvantages over a cylindrical stent shape.

In fluid mechanics, cylindrical tubes are essential to enable efficient, low turbulent flow. Compared to squared or triangular tubes, a cylindrical tube is able to withstand higher pressures. On top of that, fluid friction is lowest in cylindrical shaped geometries, allowing for smooth and fast flow. In low pressure systems, a cylindrical shaped geometry has less advantages over other i.e. triangular or oval shapes. By nature, arteries adapt to the adjacent anatomy adopting a tortuous course, and are almost never perfectly cylindrical. In interventional cardiology however, stents are traditionally cylindrical. The hemodynamic impact of other stent shapes is not well known. The results of this study show no hemodynamic benefits of a cylindrical stent over an oval stent with an equal cross sectional area. Pressure, flow distribution and velocity outcomes were similar for the oval and cylindrical stent scenarios. In case 1 (biventricular), the reconstruction of the aorta resulted in the abnormal positioning of the aortic arch below the LPA. This resulted in limited space for the LPA and predominant flow to the RPA. Due to the stenosis in the distal MPA and the oversized RPA there was no difference in pre- and post-interventional flow distribution. In this patient, it may be argued to treat the distal MPA stenosis in order to increase flow to the LPA. In case 2 (univentricular) the flow distribution remained unequal after stent implantation but with an oppositional flow distribution. While pre-intervention there was a preference for the RPA, post-intervention more flow went towards the LPA. In this case, the LPA gradient over the LPA was resolved after stent placement and the

high flow velocity over both the LPA and RPA decreased. The 'unperfect' outcomes of stent placement in both cases show the unpredictability of hemodynamic outcomes of stent placement in patients with complex CHD. It emphasizes the essentiality of 3D (multi-modality) imaging and flow analysis to be able to fully assess the interaction between the different structures in the chest and the effect of stent placement on the hemodynamics in the PAs. The segmented structures in this study represent the fluid domain without vessel wall, the actual compression of the aorta (case 1) and airway (case 2) can therefore be expected to be even more distinct.

4.1 Limitations

The outcomes of this study are limited by the retrospective design and the small number of cases. The large variety in anatomy of CHD makes it difficult to generalize results of patient-specific flow studies. This emphasizes the importance of patient-specific pre-interventional evaluation of the 3D PA-anatomy including the surrounding structures and additional flow analysis to guide the choice between different interventional approaches.

5 CONCLUSION

When the anatomy of patients with CHD is complex and there is a close relation between different structures in the chest, there might be a risk of external airway or vessel compression when a stent is implanted in the PAs. In these patients, the oval stent technique allows for treatment of PA stenosis without compression of adjacent structures. In the two presented cases, an oval stent shape had the same hemodynamic outcomes as the traditional cylindrical stent.

REFERENCES

1. Hoffman JI, Kaplan S. The incidence of congenital heart disease. *Journal of the American College of Cardiology JID* - 8301365.
2. Cuyper JA, Witsenburg M, van der Linde D, Roos-Hesselink JW. Pulmonary stenosis: Update on diagnosis and therapeutic options. *Heart*. 2013;99(5):339-347.
3. Khan A, Ing FF. Catheter interventions for pulmonary artery stenosis: Matching the intervention with the pathology. *Interv Cardiol Clin*. 2013;2(1):131-151.
4. Fujii T, Tomita H, Fujimoto K, et al. Morphological and hemodynamic effectiveness of stenting for pulmonary artery stenosis - subanalysis of JPIC stent survey. *Circ J*. 2016;80(8):1852-1856.
5. Hiremath G, Qureshi AM, Meadows J, Aggarwal V. Treatment approach to unilateral branch pulmonary artery stenosis. *Trends Cardiovasc Med*. 2021;31(3):179-184.
6. Ferandos C, El-Said H, Hamzeh R, Moore JW. Adverse impact of vascular stent "mass effect" on airways. *Catheter Cardiovasc Interv*. 2009;74(1):132-136.
7. Grohmann J, Stiller B, Neumann E, et al. Bronchial compression following pulmonary artery stenting in single ventricle lesions: How to prevent, and how to decompress. *Clin Res Cardiol*. 2016;105(4):323-331.
8. Borik S, Volodina S, Chaturvedi R, Lee KJ, Benson LN. Three-dimensional rotational angiography in the assessment of vascular and airway compression in children after a cavopulmonary anastomosis. *Pediatr Cardiol*. 2015;36(5):1083-1089.
9. Krings GJ, van der Stelt F, Molenschot MMC, Breur JMPJ. Oval stenting in left pulmonary artery stenosis: A novel double balloon technique to prevent airway compression in single ventricle. *EuroIntervention*. 2020;15(13):1209-1215.
10. Conijn M, Krings GJ. Understanding stenotic pulmonary arteries: Can computational fluid dynamics help us out? *Prog Pediatr Cardiol*. 2021:101452.



PART IV



A 3D PRINTED PULMONARY MOCK LOOP FOR HEMODYNAMIC STUDIES IN CONGENITAL HEART DISEASE.

Maartje Conijn

Lieke M. Wintermans

Rutger Metselaar

Janna Ruisch

Eva. A. Bax

Carmen A.W. van Egmond

Ben Nieuwenstein

Evangeline G. Warmerdam

Gregor J. Krings

Submitted

ABSTRACT

Background With the increasing survival of the congenital heart disease population, there is a growing need for in-depth understanding of blood circulation in these patients. Mock loops provide the opportunity for comprehensive hemodynamic studies without burden and risks for patients. This study aimed to evaluate the ability of the presented mock loop to mimic the hemodynamics of the pulmonary circulation with and without stenosis and the MR compatibility of the system.

Methods A pulsatile pump with two chambers, separated by a flexible membrane, was designed and 3D printed. A cough assist device applied an alternating positive and negative pressure on the membrane. One adult, and three pediatric pulmonary bifurcations were 3D printed and incorporated in the setup. Two pediatric models had a 50% stenosis of the left branch. Bilateral compliance chambers allowed for individual compliance tuning. A reservoir determined the diastolic pressure. Two carbon heart valves guaranteed unidirectional flow. The positive pressure on the cough assist device was tuned until an adequate stroke volume was reached with a frequency of 60 bpm. Flow and pressure measurements were performed on the main pulmonary artery and the two branches. The MR compatibility of the setup was evaluated.

Results A stroke volume with a cardiac index of 2L/min/m² was achieved in all models. Physiological pressure curves were generated in both normal and stenotic models. The mock loop was MR compatible.

Conclusion This MR compatible mock loop, closely resembles the pulmonary circulation thereby providing a controllable environment for hemodynamic studies.

1 INTRODUCTION

Congenital heart disease (CHD) is the most common birth defect, with an incidence of 8 per 1000 births.¹ Over the last decades, treatment of patients with CHD has greatly improved. Nowadays, the majority of the patients will survive into adulthood.² All these patients require life-long follow-up, to detect early and late complications of their CHD and/or corrective surgery. With the increased complexity of the surviving CHD population, there is a growing need for in-depth hemodynamic knowledge of CHD.

Stenosis in one of the pulmonary artery branches is frequently seen in patients with CHD, either as a native substrate or as a consequence of corrective surgery.³ Pulmonary artery stenosis significantly alters hemodynamics of the pulmonary circulation by increasing right ventricular afterload and causing under perfusion of the post-stenotic lung segment. Understanding the hemodynamic impact of different types of stenosis, may improve surveillance and treatment of CHD patients with or at risk of pulmonary artery stenosis.

The construction of mock loops has greatly contributed to the understanding of the often complex hemodynamics in CHD.⁴⁻⁶ Mock loops have been a great tool in the development of novel treatment strategies, since they can be used to investigate new surgical approaches and cardiovascular devices.⁴⁻¹⁰ They allow for extensive hemodynamic experiments in a controllable environment without burden and risks for a patient. There are several characteristics that are essential for a useful mock loop: it needs to resemble the actual physiological human circulation as close as possible, with adjustable settings for mimicking different conditions of load (i.e. rest and exercise) and varying patient sizes (i.e. adult and pediatric). Moreover, the ideal mock loop should enable the assessment of a wide range of hemodynamic parameters, combined with the possibility of investigation with clinical modalities (i.e. Magnetic Resonance (MR) imaging).

The aim of this study was to construct a MR compatible mock loop of the pulmonary circulation for hemodynamic investigation of pulmonary anatomies of adult and pediatric CHD patients with and without pulmonary artery stenosis.

2 METHODS

2.1 The mock loop

The mock loop consisted of seven components (figure 1). The artificial ventricle was constructed of two equal sized hemispheres (150 cm^3) separated by a flexible polyurethane membrane (OpSite Incise Theatre Incise Drape, Smith & Nephew, Auckland, New Zealand). The lower hemisphere contained fluid, while the upper hemisphere contained air (figure 2A). An alternating positive and negative air pressure was applied on the membrane by a cough assist device (Emerson Philips Respiroics CA3000 Cough Assist Device, Philips, Eindhoven, NL). The alternating pressures on the membrane effectuated a pulsatile flow, directed by a unidirectional 20mm valve (Sorin Bicarbon bileaflet valves). After leaving the ventricle, the flow entered a patient-specific, 3D printed anatomy (section 2.3). The fluid then continued to flow into two compliance chambers of 30x10 cm constructed from Plexiglas cylinders. The total air volume in the compliance chambers could be adjusted for individual compliance tuning. The outlets of the compliance chambers were connected to a Plexiglas reservoir of 20x20x30 cm. This reservoir provided a head pressure and allowed for adjustment of the diastolic pressure. After passing another 20 mm carbon valve, the fluid re-entered the ventricle.

The different components of the mock loop were connected through flexible non-compliant PVC tubes. To connect the left pulmonary artery (LPA) and right pulmonary artery (RPA) to the compliance chambers, 10 mm tubes were used. In small anatomies with entrance diameters of 10 mm or smaller, these 10 mm tubes were also used to connect the valve to the anatomy. For all other connections, 20 mm tubes were used. Several connectors were used to ensure smooth transitions between tubes with varying diameters. The compliance chambers and the reservoir were connected to the tubes with brass tube fittings. All other connectors were custom-made and 3D printed (section 2.3). To maintain MR compatibility, nylon screws were used instead of iron screws.

Flow and pressure measurements were possible on multiple locations in the loop. For flow measurements, the SonoTT FlowComputer (Em-tec GmbH, Finning, Germany) was used. The SonoTT Clamp-On Transducers 1/16" (Em-tec GmbH, Finning, Germany) could be clamped on 10 mm tubes. In small anatomies (entrance below 10mm), flow in the main pulmonary artery (MPA), LPA and RPA could be measured. In larger anatomies (entrance bigger than 10mm), flow in the LPA and

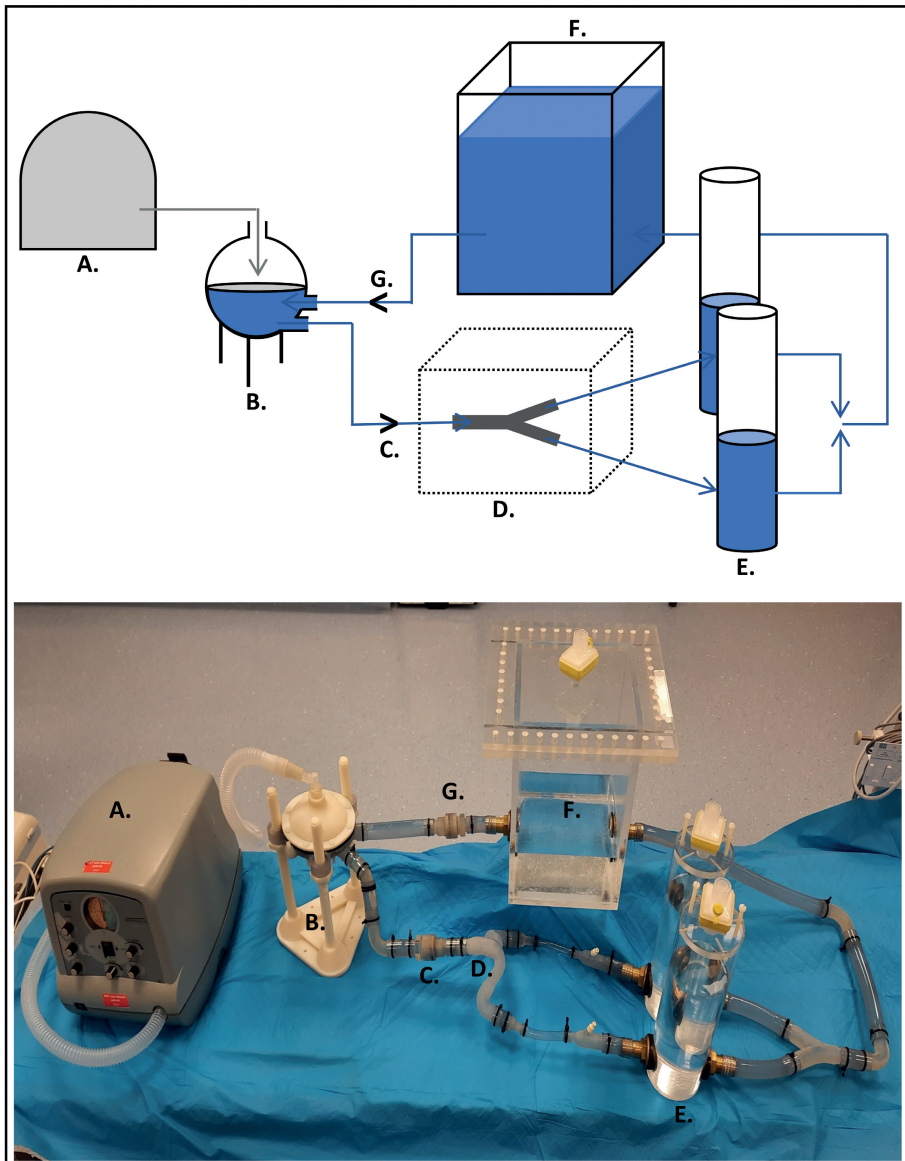


Figure 1 - The constructed mock loop schematic (upper) and real setup (lower). A. Cough assist device, B. Ventricle, C. Unidirectional carbon valve, D. Pulmonary artery bifurcation, E. Compliance chambers, F. Reservoir, G. Unidirectional carbon valve. Flow direction: from B to G.

RPA could be measured. For pressure measurements, two custom made connectors were 3D printed (section 2.3.). These allowed for the introduction of a sheath, wire and catheter to perform invasive pressure measurements (figure 2B). The pressure measurements were performed in the cardiac catheterization room using an endhole multipurpose diagnostic catheter (4 Fr, Cardinal health, Dublin, OH) connected to a Siemens Sensis Hemodynamic monitoring unit (Siemens Healthineers, Erlangen, Germany).

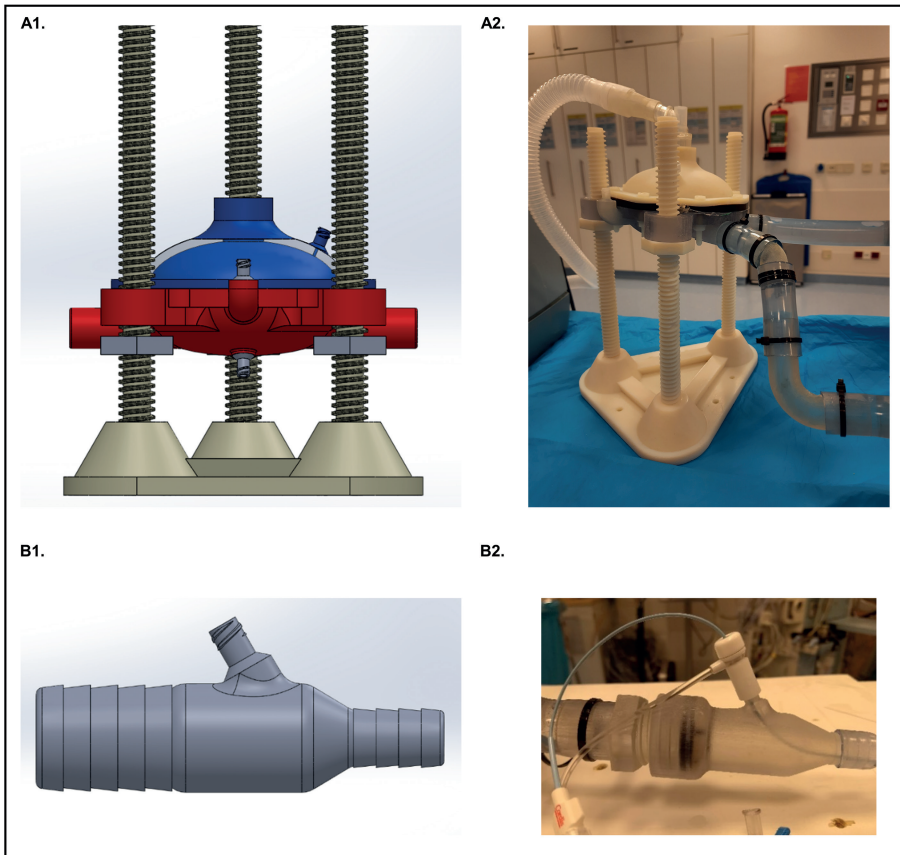


Figure 2 - Detail of custom designed ventricle and pressure measurement connector. A1. Schematic display of the designed ventricle with air hemisphere (blue) and fluid hemisphere (red) separated by a flexible polyurethane membrane. A2. Final result of 3D printed ventricle incorporated in the setup. B1. Schematic display of connector between anatomy and compliance chambers. B2. Final result of 3D printed connector. The luer lock on top of the connector allows for the introduction of sheaths and wires in the mock loop for invasive pressure measurements.

2.2 3D printing

The use of 3D printing allowed for complete avoidance of metal in the mock loop making the system suitable for future MR studies. The 3D printed parts included the ventricle (except for the membrane), several connectors and four reconstructed pulmonary bifurcations. The ventricle and connectors were custom designed using SolidWorks (Dassault Systèmes SolidWorks Corporation, Waltham, MA) software. The final 3D model was printed using the Objet30 Prime 3D printer (Stratasys, Eden Prairie, MN). The print material used for the ventricle was Rigur (RGD 450, Stratasys, Eden Prairie, MN). All connectors were printed in VeroClear (RGD 810, Stratasys, Eden Prairie, MN). To ensure a waterproof connection to the compliance chambers and reservoir, a total of 6 O-rings were printed using TangoBlack (FLX 973, Stratasys, Eden Prairie, MN) material. The four anatomic models for the below described in vitro experiment, were 3D printed using VeroClear material (RGD 810, Stratasys, Eden Prairie, MN).

2.3 In vitro experiment

To determine the mock loops' capability of mimicking the pulmonary circulation, an in vitro experiment with different anatomies was conducted. This experiment aimed to evaluate the capability of the mock loop to simulate physiological circumstances in different anatomical sizes, with and without stenosis of one of the pulmonary branches. One patient case was used to reconstruct an adult size pulmonary artery bifurcation after which this model was modified to design three pediatric size pulmonary bifurcations, with and without stenosis. This resulted in a total of four pulmonary artery bifurcation models (figure 3):

- A. An adult size pulmonary bifurcation without stenosis (MPA dm 18 mm)
- B. A pediatric pulmonary bifurcation without stenosis (MPA dm 10 mm)
- C. A pediatric pulmonary bifurcation with 50% LPA stenosis of 6 mm length (MPA dm 10 mm)
- D. A pediatric pulmonary bifurcation with 50% LPA stenosis of 12 mm length (MPA dm 10 mm)

The adult size geometry (case A) was reconstructed of a 16-year old patient (body surface area 1.2 m²) without pulmonary artery stenosis undergoing left cardiac catheterization. During the procedure, a 3D rotational angiography (3DRA) was routinely acquired. As this is a high-resolution imaging source, the DICOM images of this 3DRA were used for anatomic reconstruction of the pulmonary bifurcation.

Using ITK-SNAP software the pulmonary arteries were segmented (<http://itksnap.org>). This segmentation resulted in a 3D model of the fluid domain of the pulmonary arteries. In Meshmixer software (Autodesk Inc, San Rafael, USA), the 3D model was smoothed and additional branches were removed until the model consisted of the MPA, RPA and LPA. Next, an artery wall was extruded, creating a hollow model with a wall thickness of 2 mm. At the inlet and outlets of the constructed model, connection parts were added to avoid turbulent flow by the transition from model to tube. The resulting 3D model of the adult size bifurcation was 3D printed as described above (section 2.2). For the pediatric bifurcation, the fluid domain of the patient was scaled to a pediatric size with a MPA diameter of 10 mm. Then, an artery wall was extruded and connection parts were added similar to the adult model. The pediatric model was altered in Meshmixer by introducing a stenosis in the LPA. Two pediatric models with different LPA stenosis lengths were reconstructed resulting in a 50% LPA stenosis with a length of 6 mm starting in the ostium of the LPA in case C and a 50% LPA stenosis with a length of 12 mm in case D.

The four models were alternately integrated into the mock loop. The adult anatomy (case A) was connected to the valve using a 20 mm tube. The pediatric anatomies (case B-D) were connected with a 10 mm tube. For this experiment, the mock loop was filled with water until the desired diastolic pressure of 10 mmHg was reached. The frequency of the cough assist device was set to 60 breaths/min with a positive pressure of 20 mmHg and a negative pressure of -7 mmHg. The positive and negative pressure on the cough assist device were adjusted until the desired stroke volume was reached. The aim was to obtain a stroke volume fitting a cardiac index (CI) of ± 2.0 L/min/m².

During testing of the mock loop, multiple pressure and flow measurements were performed. Invasive pressures values were obtained in the MPA, LPA and RPA. In case of a stenosis, the pressure was measured directly post-stenosis, to determine the pressure gradient over the stenosis. When no stenosis was present, the pressure in the branches was measured approximately 10 mm distal to the bifurcation. The MPA pressure was measured 10 mm proximal to the bifurcation. The flow transducers were clamped on the MPA, LPA and RPA of the pediatric size anatomies (case B-D). In the adult size anatomy, no flow measurements on the MPA were possible due to restrictions in transducer size. Therefore, the sum of the left and right branch flow was used to determine the MPA flow. During testing of the normal adult size anatomy, two angiographic images were obtained with the Siemens Artis Zee biplane

system (Siemens Healthineers, Erlangen, Germany). To visualize the movement of the membrane a lateral angulated angiography of the ventricle was performed. Using a cranial angulated angiography, the course of the fluid through the ventricle was recorded. For this last image, contrast was injected using a Covidien Power Injector (Medtronic, Minneapolis, MN) filled with Optiray 300 contrast (Guerbet, Villepinte, France).

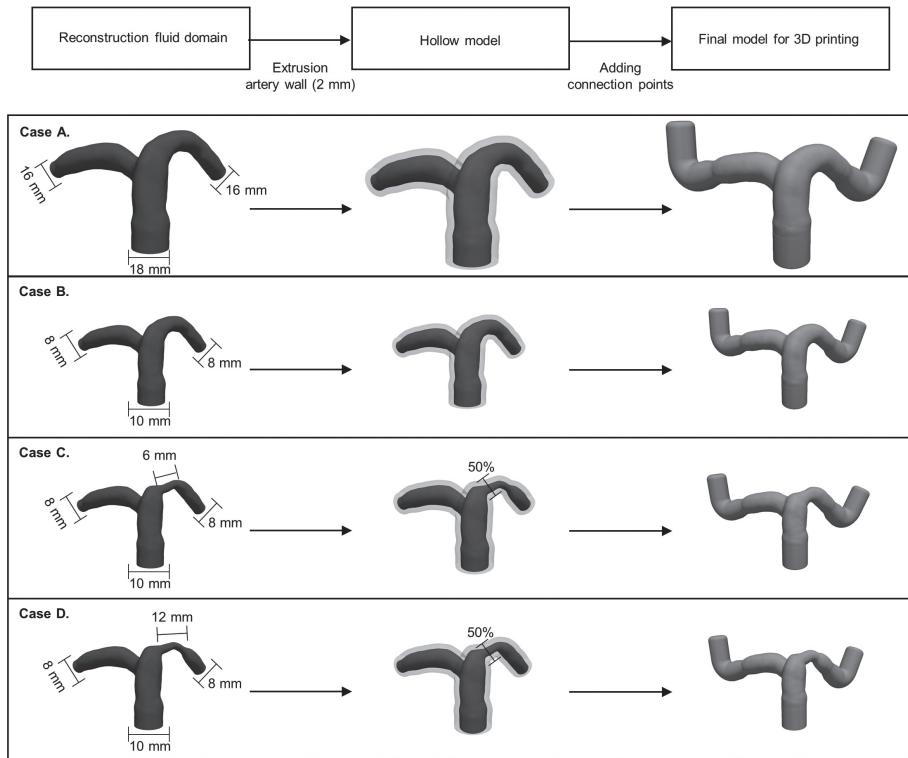


Figure 3 - The method for reconstruction of the pulmonary bifurcations used for testing the mock loop. First, the fluid domain was reconstructed through segmentation from DICOM images of a patient specific case. Next, an artery wall of 2 mm was constructed by extrusion resulting in a hollow model. Finally, connection points were added and the model was 3D printed. Case A is the original case, Case B-D were scaled to a pediatric size. In case C and D a stenosis was constructed in the LPA of 6 mm (case C) and 12 mm (case D) in length and 50% of the diameter of the original branch.

2.4 Magnetic Resonance scan

To evaluate the feasibility of using the mock loop for MR studies, a 3.0T clinical MR scan (Igenia, Phillips, Eindhoven, The Netherlands) of the complete system was acquired (Igenia, Phillips, Eindhoven, The Netherlands). The setup, with exclusion of the cough assist device, was free of iron and thus MR compatible. The cough assist device is able to build adequate pressures over a length of over 6 meters and could therefore be placed outside the MR room. For this experiment, a Plexiglas box filled with 1% agar-agar was built around the pediatric anatomies to obtain a strong MR signal (figure 4A). Hydrophobic filters were placed on top of the reservoir and compliance chambers to prevent fluid leakage while allowing free flowing of air for maximal compliance. The fluid was put in motion by the cough assist device after which a 2D non-contrast MR scan was acquired. Settings for the MR acquisition were as follows: pixel size $2.5 \text{ mm}^2 \times 2.5 \text{ mm}^2$, slice thickness 8.0 mm, echo time 2.6 ms, flip angle 10° , 30 heart phases per cycle with retrospective triggering using an external trigger.

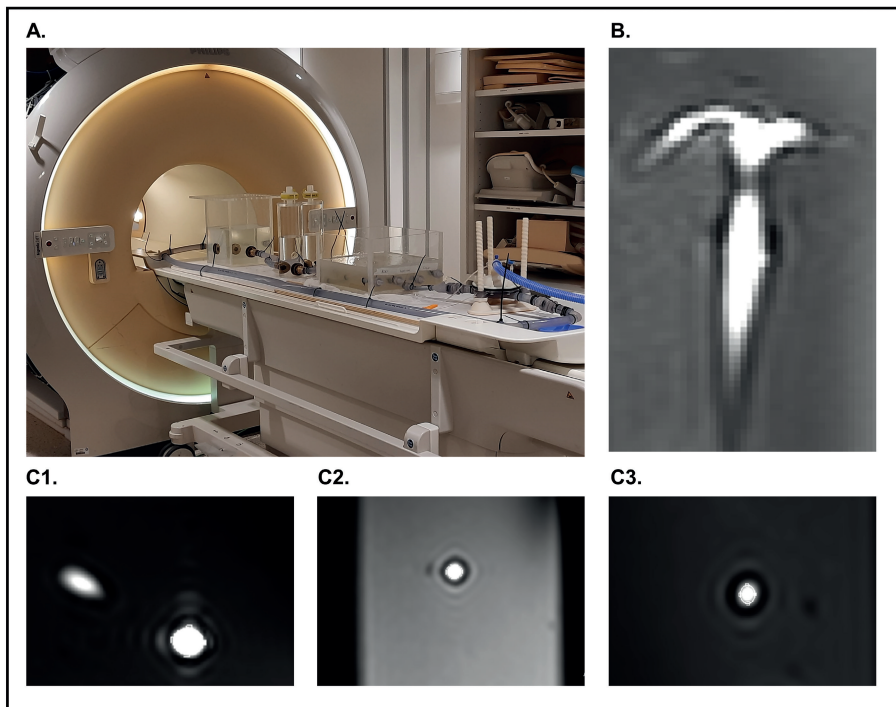


Figure 4 - The MR compatibility of the mock loop was tested in a 3T MR scanner. A. The mock loop setup on the MR table prior to a scan. B. A 2D scan in coronal plane showing the anatomy of case D with the long stenosis in the LPA. C. 2D images in axial plane of the main branch (C1), right branch (C2) and left branch (C3) of case D.

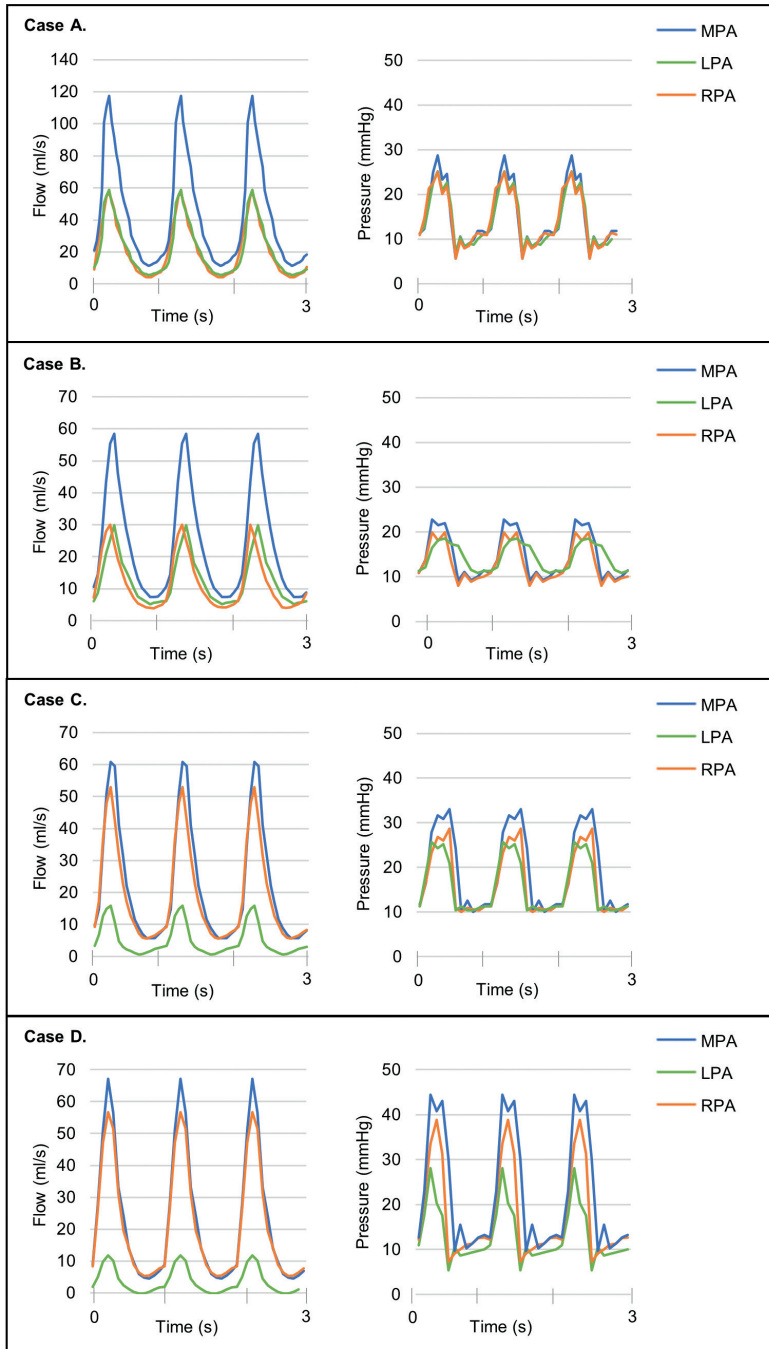


Figure 5 - The acquired flow and pressure measurements for the four cases (A-D). MPA: main pulmonary artery, LPA: left pulmonary artery, RPA: right pulmonary artery.

3 RESULTS

3.1 Flow measurements

Flow and pressure curves are presented in figure 5. In all cases, the reached CI was above 2.0 L/min/m². In the cases without stenosis (case A and B), flow distribution between the RPA and LPA was equal (table 1). In the pediatric anatomy with a short LPA stenosis (case C), 20% of the flow went towards the LPA and 80% to the RPA. As the length of the stenosis increased (case D), the flow distribution became more unequal. To maintain the desired stroke volume, the positive pressure on the cough assist device needed to be increased when a stenosis was introduced (Table 1). The systolic:diastolic ratio was 0.65s:0.35s. Zero flow was not obtained during diastole.

3.2 Pressure measurements

The pressure measurements showed physiological pressure in the MPA of the adult and pediatric anatomy without stenosis (case A and B). No relevant pressure gradients were measured over the branches in these cases (3.5 mmHg). When introducing the anatomy with a short stenosis (case C), the MPA pressure increased to 33 mmHg. In this case, a gradient of 4.3 mmHg was measured over the RPA while a gradient of 7.3 mmHg was measured over the LPA. The long stenosis (case D) increased the gradient over the LPA to 16.3 mmHg. The gradient over the RPA was 5.5 mmHg with a MPA pressure of 44.4 mmHg.

Table 1 - Case details.

	Case A	Case B	Case C	Case D
BSA (m ²)	1.2	±0.6	±0.6	±0.6
HF (beats/min)	60	60	60	60
Positive pressure (mmHg)	20	20	30	35
Negative pressure (mmHg)	-7	-7	-10	-12
SV (ml)	43.4	23.6	22.3	22.8
CO (l/min)	2.6	1.4	1.3	1.4
CI (L/min/m ²)	2.2	2.4	2.2	2.3
SV RPA (%)	49.7	49.0	79.8	85.4
SV LPA (%)	50.3	51.0	20.2	14.6

BSA: body surface area, HF: heart frequency, Positive pressure: applied positive pressure on the membrane by the cough assist device, Negative pressure: applied negative pressure on the membrane by the cough assist device, SV: stroke volume, CO: cardiac output, CI: cardiac index, SV RPA: stroke volume in the right pulmonary artery branch, SV LPA: stroke volume in the left pulmonary artery branch.

3.3 Angiography

The movement of the polyurethane membrane in the ventricle was visualized by fluoroscopy with contrast from a lateral projection during the whole cycle. As a result of the positive pressure generated by the cough assist device, the membrane moved towards the bottom of the ventricle thereby pushing the fluid actively out. When the negative pressure moved the membrane upwards, fluid was actively and passively pulled into the ventricle. The angiography with contrast visualizes the in-, and outflow of fluid over the cycle directed by the unidirectional carbon valves. The angiographic movies can be found in the online supplementary materials (movie 1 and 2).

3.4 MR acquisition

Figure 4 demonstrates the acquired MR scan of case B, C and D. These models of pediatric size with- and without stenosis provide a clear signal with the ability to acquire flow measurements (figure 4B-D). This shows the feasibility of using this mock loop for MR studies.

4 DISCUSSION

In this study we present a MR compatible hydro-pneumatic driven mock loop, consisting of 3D printed components. This study aimed to evaluate the capability of the mock loop to mimic the hemodynamics of the human pulmonary artery circulation. Four 3D printed bifurcations of different sizes, with and without stenosis, were incorporated into the system. The mock loop was capable of creating physiological stroke volumes, pressures and flow distribution in normal and stenotic anatomies of pediatric and adult size. The use of non-ferro elements with 3D printed parts and PVC tubing created a completely MR compatible system.

The in-house creation of our mock loop allowed for constant tuning of the setup. The dimensions and properties of all elements including the ventricle, the elastic membrane and the in- and outflow elements were adapted to fit the hemodynamic needs of the mock circulation. This resulted in a system in which models of different sizes could be incorporated and evaluated. The use of a cough assist device as pump for a mock loop is unique. This device provides an artificial cough impulse, by applying an alternating positive (inhale) and negative (exhale) pressure. It is frequently used in patients with weakening of the respiratory muscles, to help evacuate mucus from the lungs. In our mock loop, the alternating positive and negative air pressure applied

by the cough assist device in combination with the valves allowed for a pulsatile unidirectional circulation. The cough frequency could be adjusted with the possibility of tuning the exhale (diastolic) and inhale (systolic) duration. Also, the inhale (positive) and exhale (negative) pressures could be individually programmed with a maximum of ± 80 mmHg. The cough assist device produced the defined pressure, independent of the length over which it needs to build this pressure. The distance between the cough assist device and the ventricle did therefore not influence the functioning of the system. This allowed for a flexible system, deployable in situations with varying setup requirements, i.e. placement of the cough assist device outside the MR scan room for MR studies or close to the ventricle in the cardiac catheterization room.

The flow and pressure curves measured in the system closely resembled the physiological state of the pulmonary circulation with and without stenosis. In anatomies without stenosis it produced an almost 50%:50% flow distribution between the branches, whereas in anatomies with branch stenosis it produced an unequal distribution. Similar to the *in vivo* circulation, pressure gradients occurred when a stenosis was introduced and gradients increased with the length of stenosis.¹¹ A number of differences between the physiological circulation and the artificial setup were noted. First, a low constant flow was observed during the diastole caused by the constant filling pressure of the reservoir. Second, the systole:diastole ratio in the system was set to be 0.65:0.35s. A physiological ratio would have a longer diastole and a shorter systole. However, in the mock loop this caused a significant decrease in stroke volume, warranting an increase of positive pressure to maintain the desired stroke volume. This resulted in high, non-physiological, pressures throughout the entire system. Increasing the duration of the diastole, while maintaining the duration of the systole resulted in a heart frequency below 60 beats per minute which was considered undesirable.

During the experiments, pediatric and adult pulmonary bifurcations were evaluated. The MPA sizes of 18 mm and 10 mm in diameter fit a body surface area of 1.2m^2 and 0.6m^2 respectively. This corresponds to a 10 kg pediatric and a 50 kg adult patient. The size range of the incorporated models was limited by the diameter of the valve connected to the anatomy. The 20 mm carbon valve prevented adequate stroke volumes in anatomies with an inlet greater than 20 mm. However, the maximal diameter of 20 mm was considered to be sufficient, as no changes in hemodynamic behavior were expected in larger bifurcations. All models with a diameter below 20 mm could be incorporated into the system without limitations. For this study,

the minimal diameter used in a model was a 10 mm inlet to allow for MR imaging. With a spatial resolution of $2.5 \text{ mm}^2 \times 2.5 \text{ mm}^2$, a branch diameter of 8 mm with a 50% stenosis resulted in imaging of a single pixel at the site of the stenosis. A diameter below 4 mm at any location in the incorporated anatomy would therefore be undesirable for the purpose of MR studies.

4.1 Limitations

The presented experiment has several limitations. First, the system was filled with water, instead of a more blood analogue fluid. However, the use of water as flowing medium is frequently seen in comparable studies with mock loop systems.^{6,7,9,10} As during our experiments the hemodynamics in large vessels were evaluated, the influence of viscosity was considered to be relatively low. We therefore hypothesized that the use of water would not significantly influence our results. Further research to conform this hypothesis is warranted. Second, the build-in bifurcations were not patient specific in the stenotic cases. The system pressure could therefore not be compared to the actual invasive pressure measurements. Lastly, clamp-on flow meters used in this study were only available in a single size, making measurements of flow in the MPA of the adult anatomy not possible. This could have been solved by using a small tube prior to the anatomy. However, this would subsequently result in insufficient stroke volumes. Since no stenosis were present in the MPA, flow in the MPA was assumed to be equal to the sum of flow in both branches.

5 CONCLUSION

In this study we evaluated the capacity of an in-house build MR compatible hydro-pneumatic driven mock loop to mimic the in vivo pulmonary circulation. Using 3D printed components, anatomies of different sizes and with or without stenosis were evaluated. The mock loop created physiological stroke volumes, pressures and flow distribution in all evaluated cases. The presented mock loop is MR compatible and the ability to incorporate anatomies of different sizes allows for a wide range of hemodynamic studies.

REFERENCES

1. Hoffman JI, Kaplan S. The incidence of congenital heart disease. *J Am Coll Cardiol.* 2002;39(12):1890-1900.
2. Oster ME, Lee KA, Honein MA, Riehle-Colarusso T, Shin M, Correa A. Temporal trends in survival among infants with critical congenital heart defects. *Pediatrics.* 2013;131(5):e1502-8.
3. Cuypers JA, Witsenburg M, van der Linde D, Roos-Hesselink JW. Pulmonary stenosis: Update on diagnosis and therapeutic options. *Heart.* 2013;99(5):339-347.
4. de Leval MR, Kilner P, Gewillig M, Bull C. Total cavopulmonary connection: A logical alternative to atriopulmonary connection for complex fontan operations. experimental studies and early clinical experience. *J Thorac Cardiovasc Surg.* 1988;96(5):682-695.
5. Figliola RS, Giardini A, Conover T, et al. In vitro simulation and validation of the circulation with congenital heart defects. *Prog Pediatr Cardiol.* 2010;30(1-2):71-80.
6. Roldán-Alzate A, García-Rodríguez S, Anagnostopoulos PV, Srinivasan S, Wieben O, François CJ. Hemodynamic study of TCPC using in vivo and in vitro 4D flow MRI and numerical simulation. *J Biomech.* 2015;48(7):1325-1330.
7. Knoops PGM, Biglino G, Hughes AD, et al. A mock circulatory system incorporating a compliant 3D-printed anatomical model to investigate pulmonary hemodynamics. *Artif Organs.* 2017;41(7):637-646.
8. Bonhoeffer P, Boudjemline Y, Saliba Z, et al. Transcatheter implantation of a bovine valve in pulmonary position: A lamb study. *Circulation.* 2000;102(7):813-816.
9. Biglino G, Cosentino D, Steeden JA, et al. Using 4D cardiovascular magnetic resonance imaging to validate computational fluid dynamics: A case study. *Front Pediatr.* 2015;3:107.
10. David A, Le Touze D, Warin-Fresse K, et al. In-vitro validation of 4D flow MRI measurements with an experimental pulsatile flow model. *Diagn Interv Imaging.* 2019;100(1):17-23.
11. Lipscomb K, Hooten S. Effect of stenotic dimensions and blood flow on the hemodynamic significance of model coronary arterial stenoses. *Am J Cardiol.* 1978;42(5):781-792.



GENERAL DISCUSSION.

A stenosis in one of the pulmonary branches affects the hemodynamics of the pulmonary circulation. It causes an unequal flow distribution over the right and left lung and increases the pressure load of the right ventricle (RV).^{1,2} On top of that, a stenosis may disturb the normal, laminar flow of blood. It is thought that the abnormal flow caused by a stenosis contributes to diminished cardiovascular functioning on the long-term.³ To improve our understanding of the hemodynamic impact of a stenosis, it is important to extensively study flow patterns and hemodynamic parameters. This thesis describes the hemodynamics of pulmonary artery (PA) stenosis in three compartments: in vivo, in silico and in vitro.

It is estimated that 2-3% of all CHD patients develops some degree of PA stenosis with an incidence up to 20% in Tetralogy of Fallot, pulmonary atresia and Transposition of the Great Arteries.^{4,5} There is a large heterogeneity in location, severity and cause of PA stenosis in congenital heart disease (CHD).^{6,7} This is reflected in the cohort that is described in **chapter 2** of this thesis. The patients in this chapter were all percutaneously treated by stent placement or balloon angioplasty during often comprehensive and complex procedures. PA stenosis was diagnosed in patients with over 11 different diagnosis, including univentricular and biventricular hearts. Although the cohort was relatively young (mean age 9.8 years), the vast majority of the patients had prior surgery and three quarter of the patients had a prior catheterization. In a quarter of the studied population, a bilateral or bifurcation intervention was performed and 30% of the patients required a combination of interventional techniques (i.e. stent placement and balloon angioplasty).

Indications for treatment of PA stenosis include a gradient of 20 mmHg or higher over a stenosis, a right to left ventricular pressure ratio of 0.6 or higher, and less than 40% flow to the affected branch.⁸ Defining the severity and hemodynamic impact of a PA stenosis can be challenging. Often multiple imaging modalities are required to determine whether there is an indication for treatment.⁹ Echocardiography is routinely performed in all patients with CHD. It allows for visualization of the proximal pulmonary arteries, measurement of flow velocity in the PA branches and estimation of RV pressure load. However, the pulmonary arteries can be difficult to visualize and RV pressure measurements highly depend on the quality of the tricuspid valve regurgitation signal.¹⁰ If necessary, Computed Tomography Angiography (CTA) and Cardiac Magnetic Resonance (CMR) scans provide additional information on the anatomy of the pulmonary arteries. CMR flow measurements can inform on the distribution of flow over the right and left pulmonary artery, maximal flow velocities

and RV function. Disadvantages of CMR include the low spatial and temporal resolution, the often long acquisition time and the inability of measuring flow after stent implantation due to metal artefacts.¹¹ For determination of the distribution of flow over the right and left PA branch, a ventilation-perfusion (VP) scan can be obtained. This scan visualizes and quantifies the possible ventilation perfusion mismatch caused by PA stenosis. Its main disadvantage is the relative high dosage of radiation required for this scan which is undesirable in the young CHD population.¹²

When the non-invasive evaluation reveals signs of a significant PA stenosis, a patient is referred by a multidisciplinary team to the cathlab for invasive hemodynamic assessment and treatment. In **chapter 6** we discuss that invasively obtained pressure levels and gradients are often in disagreement with the non-invasive measurements. In 64% of the cases, the invasive measured RV pressure was below the echocardiographic RV pressure. Almost half of the patients referred to the cathlab for treatment of PA stenosis had no indication based on invasive pressure measurements. When invasive and non-invasive measurements are in disagreement, which measurement is 'true' and should be adopted as indication for treatment? Invasive pressure measurements are generally obtained in patients under general anaesthetics. We argue that the properties of the used anaesthetics result in hypotension, low vascular resistance and low cardiac output which may lead to underestimation of the severity of a stenosis. To anticipate this, invasive assessment of hemodynamics should be performed in a normotensive patient. We describe our experience in counteracting the hypotensive properties of general anaesthetics with epinephrine. The aim of epinephrine administration is to achieve a condition of load similar to the state of the non-invasive evaluation. This way, the hemodynamic impact of the stenosis can be evaluated in the most common condition of load: the normotensive resting state. In a quarter of the patients without an indication for treatment based on the invasive pressure measurements, epinephrine altered the clinical decision making and revealed an indication for treatment.

Early diagnosis and treatment of PA stenosis has shown to be beneficial for lung development.^{1,13,14} Especially in young pre-school children, increasing flow to the lungs promotes growth of the pulmonary arteries and the underlying lung tissue.^{15,16} But when treating the young CHD population, a balance needs to be pursued between early treatment of a stenosis and the risk of re-interventions. In **chapter 2** we found that 25% of the percutaneously treated patients required a re-intervention during follow-up. In half of these cases, the reason for re-intervention

was a relative restenosis due to somatic growth. The majority of the patients in need for a re-intervention were below 10 years of age at the initial intervention. On top of that, in small patients with stent diameters below 8 mm, the highest rates of intima proliferation were found. Remarkable is the finding that the risk for re-intervention can be significantly reduced by obtaining a 3D Rotational Angiography (3DRA) during cardiac catheterization. A 3DRA enables real-time 3D reconstruction of the chest anatomy through rotation of the C-arm of the angiographic system. This allows for optimal understanding of the anatomy of the pulmonary arteries and adjacent structures. After post-processing, the 3D anatomy can be used as overlay on live fluoroscopy for interventional guidance.¹⁷ On top of the safety, feasibility and applications of this technique, previous research has shown a reduction in total radiation dose when 3DRA is used as overlay during intervention.^{18,19} In addition to all these benefits we found that the use of 3D imaging during the procedure also has long-term advantages. When a 3DRA is obtained, patients have a two times lower risk of re-intervention in the future. We hypothesize that this is caused by the 3D understanding of the pulmonary anatomy prior to the intervention in combination with the optimal positioning of the balloon or stent during the intervention.

Now that the anatomy of patients can be visualized in 3D with all the associated benefits, there is a growing interest in visualizing blood flow inside the arteries of patients with CHD. One of the modalities widely studied for this purpose is Computational Fluid Dynamics (CFD).^{20,21} It allows for simulation of blood flow in a reconstructed 3D fluid domain. In **chapter 3** the applicability of CFD in CHD is described. Among others it is used for treatment planning, simulating different conditions of load and research on common complications after surgery or intervention. The available CFD studies on hemodynamics of the pulmonary arteries are reviewed showing the wide variety of used methods for CFD analysis and the limited clinical validation of the results. In **chapter 4** we describe our own CFD method and compare the outcomes of three numerical cases to CMR and cardiac catheterization measurements. We demonstrate the good agreement between CFD and clinical (non-invasive) modalities and the impressive amount of hemodynamic information obtained by CFD studies.

In **chapter 5**, outcomes of CFD analysis were compared to outcomes of 4D flow CMR. Instead of evaluating flow in a 2D plane in a single direction, 4D flow CMR is currently the only imaging modality able to analyse and quantify blood flow over an entire volume.²² Disadvantages of 4D flow CMR are the low spatial and temporal

resolution and the inability of using 4D flow CMR when a stent is implanted.²³ We compared both techniques on the clinical parameters of flow distribution and velocity over the pulmonary arteries. Three patients with Transposition of the Great arteries and one patient with normal pulmonary arteries were computationally evaluated after 4D flow CMR acquisition. The results showed the agreement on flow distribution over the branches and maximal flow velocities in stenotic pulmonary arteries. The cases also demonstrated the limitation of 3D reconstruction of an anatomy based on CMR. Due to the low spatial resolution, segmentation of the pulmonary arteries, especially in small children, is challenging and may result in uncertainties about the accuracy of the reconstruction. As the outcomes of CFD analysis highly depend on the reconstructed anatomy, a high resolution image source, i.e. high resolution CTA or 3DRA is preferred for segmentation.

In part III of this thesis, we apply our CFD method on patient-specific cases. Based on these *in silico* experiments, advanced interventional techniques for the treatment of PA stenosis and clinical dilemmas on timing and approach of treatment are discussed. We show the possibilities of simulating different treatment options in individual cases with use of CFD. All the described *in silico* cases emphasize the importance of tailor made treatment approaches in patients with CHD.

In **chapter 7** the clinical challenge of PA stenosis in combination with pulmonary valve regurgitation is computationally explored. Does a PA stenosis increase or decrease regurgitation? What is the hemodynamic impact of PA stenosis with or without a competent pulmonary valve? We find that stent placement increases branch regurgitation while valve placement reduces pulse pressure, maximal velocities and wall shear stress. In agreement with previous research, outcomes of stent placement depend on the branch angle and diameter of the branching artery.^{24,25} In **chapter 8**, an advanced stent technique is introduced. We describe eleven patients with complex pulmonary bifurcation stenosis treated with the Y-stenting technique. This technique allows for bifurcation stenting with respect for the natural geometry of bifurcating arteries.²⁶ A stent is implanted in the main branch, extending into one of the branching arteries. A second stent is deployed in the contralateral branch through the stent struts of the first stent. The resulting single lumen in the main artery allows for easier access in future interventions. Also, due to complete alignment of the Y-stent to the vessel wall, there is no flow separation. Y-stenting causes less turbulent flow compared to the kissing stent technique thereby reducing the risk of intima proliferation in these patients. In our patients, intima proliferation was only found

in the cases in which the stents were not connected. The disconnection between both stents allows for movement of both branches relative to each other. This so called 'kinking movement', increases the risk for intima proliferation.⁶ To prevent this both stents should always be carefully connected by creating an overlap in the main branch.

Chosen for their exceptionality, the two cases in **chapter 9** represent the challenge of stenting pulmonary arteries in close approximation to other adjacent structures. The intra-thoracic mass shift caused by extensive surgery on the great arteries in these patients, may cause an intimate relation between the pulmonary arteries, the airway and the aorta.²⁷ Implanting a cylindrical stent to relief PA stenosis may result in compression of the airway or aorta.^{28,29} Oval shaping of a traditional cylindrical stent allows for stenting of the pulmonary arteries without compression of the adjacent structures.³⁰ We found that an oval stent shape has no hemodynamic disadvantages over the traditional cylindrical stent shape when an equal cross sectional area is reached. The cases also point out that treating the obvious stenosis in complex anatomies does not always lead to obvious hemodynamic results. Simulating treatment options in these cases is beneficial in understanding the origin of gradients and high flow velocities.

In addition to the in silico experiments, a set-up for in vitro hemodynamic experiments is presented in **chapter 10**. In this chapter we describe the design and construction of a MR compatible mock loop with custom made 3D printed components. The circulation of flow in this hydro-pneumatic set-up is driven by a cough assist device connected to a ventricle filled with fluid. Anatomies of different sizes (i.e. paediatric and adult), can be 3D printed and incorporated in the system. The mock loop mimics the human pulmonary circulation with physiological pressure curves and waveforms in anatomies with and without stenosis. The controllable and adjustable environment of the mock loop creates opportunities for studying hemodynamics without the burden and risks for patients. In the future, this mock loop can be used for investigating different treatment approaches, the impact of a stenosis and for validation of CFD analysis.

CONCLUSION

This thesis shows that patients with PA stenosis often require comprehensive and repetitive percutaneous interventions to relieve the obstruction. The heterogeneity and complexity of PA stenosis calls for a tailor made treatment approach for each individual patient. The use of advanced 3D imaging during cardiac catheterization benefits the initial and long-term outcomes of an intervention. Obtaining a 3DRA significantly reduces the risk for re-interventions. Computational studies on the hemodynamics of pulmonary arteries are a great tool to increase our knowledge on the causes and effects of a PA stenosis in CHD. This applies to general knowledge on the hemodynamic disturbance of a stenosis but also to patient-specific cases in which CFD studies can be useful in the discussion on the timing and approach of -interventional- treatment.

REFERENCES

- Razavi H, Stewart SE, Xu C, et al. Chronic effects of pulmonary artery stenosis on hemodynamic and structural development of the lungs. *Am J Physiol Lung Cell Mol Physiol*. 2013;304(1):L17-28.
- Hiremath G, Qureshi AM, Meadows J, Aggarwal V. Treatment approach to unilateral branch pulmonary artery stenosis. *Trends Cardiovasc Med*. 2021;31(3):179-184.
- Vanderlaan RD, Caldarone CA, Backx PH. Heart failure in congenital heart disease: The role of genes and hemodynamics. *Pflugers Arch*. 2014;466(6):1025-1035.
- Hoffman JL, Kaplan S. The incidence of congenital heart disease. *J Am Coll Cardiol*. 2002;39(12):1890-1900.
- Bacha EA, Kreutzer J. Comprehensive management of branch pulmonary artery stenosis. *J Interv Cardiol*. 2001;14(3):367-375.
- Khan A, Ing FF. Catheter interventions for pulmonary artery stenosis: Matching the intervention with the pathology. *Interv Cardiol Clin*. 2013;2(1):131-151.
- Hoeffel JC, Henry M, Jimenez J, Pernot C. Congenital stenosis of the pulmonary artery and its branches. *Clin Radiol*. 1974;25(4):481-490.
- Feltes TF, Bacha E, Beekman RH, 3rd, et al. Indications for cardiac catheterization and intervention in pediatric cardiac disease: A scientific statement from the American Heart Association. *Circulation*. 2011;123(22):2607-2652.
- Truong UT, Kutty S, Broberg CS, Sahn DJ. Multimodality imaging in congenital heart disease: An update. *Curr Cardiovasc Imaging Rep*. 2012;5(6):481-490.
- Groh GK, Levy PT, Holland MR, et al. Doppler echocardiography inaccurately estimates right ventricular pressure in children with elevated right heart pressure. *J Am Soc Echocardiogr*. 2014;27(2):163-171.
- Puranik R, Muthurangu V, Celermajer DS, Taylor AM. Congenital heart disease and multi-modality imaging. *Heart Lung Circ*. 2010;19(3):133-144.
- Prakash A, Powell AJ, Geva T. Multimodality noninvasive imaging for assessment of congenital heart disease. *Circ Cardiovasc Imaging*. 2010;3(1):112-125.
- Hiremath G, Qureshi AM, Prieto LR, et al. Balloon angioplasty and stenting for unilateral branch pulmonary artery stenosis improve exertional performance. *JACC: Cardiovascular Interventions*. 2019;12(3):289-297.
- Pewowaruk R, Hermsen J, Johnson C, et al. Pulmonary artery and lung parenchymal growth following early versus delayed stent interventions in a swine pulmonary artery stenosis model. *Catheter Cardiovasc Interv*. 2020;96(7):1454-1464.
- Bates ML, Anagnostopoulos PV, Nygard C, et al. Consequences of an early catheter-based intervention on pulmonary artery growth and right ventricular myocardial function in a pig model of pulmonary artery stenosis. *Catheter Cardiovasc Interv*. 2018;92(1):78-87.
- Takao CM, El Said H, Connolly D, Hamzeh RK, Ing FF. Impact of stent implantation on pulmonary artery growth. *Catheter Cardiovasc Interv*. 2013;82(3):445-452.
- Kang SL, Armstrong A, Krings G, Benson L. Three-dimensional rotational angiography in congenital heart disease: Present status and evolving future. *Congenit Heart Dis*. 2019;14(6):1046-1057.

18. Minderhoud SCS, van der Stelt F, Molenschot MMC, Koster MS, Krings GJ, Breur JMPJ. Dramatic dose reduction in three-dimensional rotational angiography after implementation of a simple dose reduction protocol. *Pediatr Cardiol.* 2018;39(8):1635-1641.
19. Peters M, Krings G, Koster M, Molenschot M, Freund MW, Breur JM. Effective radiation dosage of three-dimensional rotational angiography in children. *Europace.* 2015;17(4):611-616.
20. DeCampi WM, Argueta-Morales IR, Divo E, Kassab AJ. Computational fluid dynamics in congenital heart disease. *Cardiol Young.* 2012;22(6):800-808.
21. Gerrah R, Haller SJ. Computational fluid dynamics: A primer for congenital heart disease clinicians. *Asian Cardiovasc Thorac Ann.* 2020;28(8):520-532.
22. Lewandowski AJ, Raman B, Banerjee R, Milanesi M. Novel insights into complex cardiovascular pathologies using 4D flow analysis by cardiovascular magnetic resonance imaging. *Curr Pharm Des.* 2017;23(22):3262-3267.
23. Dyverfeldt P, Bissell M, Barker AJ, et al. 4D flow cardiovascular magnetic resonance consensus statement. *J Cardiovasc Magn Reson.* 2015;17(1):72-015-0174-5.
24. Chern MJ, Wu MT, Wang HL. Numerical investigation of regurgitation phenomena in pulmonary arteries of tetralogy of fallot patients after repair. *J Biomech.* 2008;41(14):3002-3009.
25. Zhang W, Liu J, Yan Q, Liu J, Hong H, Mao L. Computational haemodynamic analysis of left pulmonary artery angulation effects on pulmonary blood flow. *Interact Cardiovasc Thorac Surg.* 2016;23(4):519-525.
26. Narayan HK, Glatz AC, Rome JJ. Bifurcating stents in the pulmonary arteries: A novel technique to relieve bilateral branch pulmonary artery obstruction. *Catheter Cardiovasc Interv.* 2015;86(4):714-718.
27. Ferandos C, El-Said H, Hamzeh R, Moore JW. Adverse impact of vascular stent "mass effect" on airways. *Catheter Cardiovasc Interv.* 2009;74(1):132-136.
28. Takeuchi K, Srivastava A, Steed DR. Bronchial compression as adverse effect of right pulmonary artery stenting in a patient with truncus arteriosus communis and interrupted aortic arch. *Ann Pediatr Cardiol.* 2019;12(1):66-68.
29. Grohmann J, Stiller B, Neumann E, et al. Bronchial compression following pulmonary artery stenting in single ventricle lesions: How to prevent, and how to decompress. *Clin Res Cardiol.* 2016;105(4):323-331.
30. Krings GJ, van der Stelt F, Molenschot MMC, Breur JMPJ. Oval stenting in left pulmonary artery stenosis: A novel double balloon technique to prevent airway compression in single ventricle. *EuroIntervention.* 2020;15(13):1209-1215.



APPENDIX

NEDERLANDSE SAMENVATTING

Aangeboren hartafwijkingen is de overkoepelende naam voor aandoeningen die vanaf de geboorte aanwezig zijn en waarbij sprake is van een abnormale anatomie of functie van het hart. In Nederland worden ieder jaar 1500 kinderen geboren met een aangeboren hartafwijking. Als een longslagader (pulmonaal arterie) vernauwd is, spreken we van een pulmonaal arterie (PA) stenose. Twee tot drie procent van de kinderen met een aangeboren hartafwijking krijgt vroeg of laat te maken met een PA stenose.¹ In dit proefschrift wordt de hemodynamica van normale en vernauwde pulmonaal arteriën bestudeerd en beschreven.

In **hoofdstuk 1** wordt een inleiding gegeven over PA stenose en de uitdagingen in de diagnostiek en behandeling van deze groep patiënten. PA stenose is een zeer heterogene laesie met veel variatie in oorzaak, ernst en locatie van de vernauwing.² Een PA stenose wordt meestal gevonden in combinatie met andere cardiale afwijkingen maar het kan ook de enige afwijking zijn. De vernauwing kan al vanaf de geboorte aanwezig zijn of later in het leven ontstaan als gevolg van – vaak uitgebreide – operaties ter correctie van de aangeboren hartafwijking. Vernauwingen kunnen op één of op meerdere locaties in de PA anatomie voorkomen variërend in ernst van mild tot zeer ernstig. Een significante PA stenose leidt tot een verhoogde rechter ventrikel (RV) druk met uiteindelijk RV hypertrofie en verminderde RV functie. Onbehandeld kan PA stenose resulteren in verminderde inspanningstolerantie, onderontwikkeling van de longen, ritmestoornissen en zelfs plotselinge hartdood.³ Tijdens de follow-up van patiënten met aangeboren hartafwijkingen worden verschillende beeldvormende technieken gebruikt om de pulmonaal arteriën in beeld te brengen en eventuele vernauwingen op te sporen. Als er een indicatie is voor behandeling van een PA stenose, wordt de patiënt doorverwezen voor een hart katheterisatie. Tijdens deze procedure worden invasieve drukken gemeten en kan de stenose percutaan behandeld worden door middel van ballon dilatatie of stent plaatsing.⁴ De indicaties voor behandeling van PA stenose zijn onder andere: een rechter:linker ventrikel druk ratio van boven de 0.6, een gradient over de stenose van 20 mmHg of meer en minder dan 40% bloedstroom naar het longsegment achter de vernauwing.⁵

Met de huidige mogelijkheden voor 3D beeldvorming (o.a. CT, MRI en 3D rotatie angiografie) kan een goed beeld verkregen worden van de cardiale anatomie van patiënten met een aangeboren hartafwijking. Echter, hoe het bloed stroomt in die bloedvaten kan minder goed gevisualiseerd worden. Het bestuderen van die

bloedstroom is essentieel om onze kennis over -de gevolgen van- aangeboren hartafwijkingen te vergroten en de diagnostiek en behandeling verder te verbeteren. De laatste jaren is er daarom steeds meer aandacht voor de ontwikkeling van technieken die de bloedstroom kunnen visualiseren en kwantificeren. Eén van deze technieken is Computational Fluid Dynamics (CFD). Door het reconstrueren van de 3D anatomie van een bloedvat kan aan de hand van wiskundige- en natuurkundige formules de bloedstroom in het vat gesimuleerd worden.⁶ Door de hoge resolutie en de mogelijkheden voor het simuleren van inspanning en verschillende behandelopties, is CFD een waardevolle aanvulling op de huidige diagnostische mogelijkheden voor PA stenose.⁷

In deel I, **hoofdstuk 2** van dit proefschrift geven we een overzicht van de uitkomsten van de percutane behandeling van PA stenose over de afgelopen 10 jaar. We laten zien dat een groot deel van de patiënten, na een eerste hartkatheterisatie, in de toekomst opnieuw een ingreep nodig heeft ter behandeling van een restenose. Omdat het gaat om relatief jonge patiënten, die veel lichamelijke groei doormaken, is de reden voor re-interventie in de helft van de gevallen een relatieve restenose door somatische groei. In dit hoofdstuk tonen we aan dat het risico op een re-interventie verlaagd kan worden door het gebruik van 3D beeldvorming tijdens een hartkatheterisatie. Patiënten bij wie een 3D rotatie angiografie (3DRA) is gemaakt tijdens de procedure, hebben twee keer minder kans op een re-interventie in de toekomst. Door inzicht in de 3D anatomie van de patiënt, wordt de PA stenose beter begrepen en kan de behandeling beter gepland worden. Daarnaast kan een 3DRA gebruikt worden als overlay op de reguliere angiografie. Hierdoor kunnen stents en ballonnen optimaal gepositioneerd worden tijdens de uiteindelijke behandeling van de stenose.

In **hoofdstuk 3** geven we een inleiding over het gebruik van CFD voor het simuleren van de bloedstroom in pulmonaal arteriën van patiënten met aangeboren hartafwijkingen. Door het evalueren van alle beschikbare literatuur over dit onderwerp laten we de groeiende interesse in deze techniek en de brede toepasbaarheid zien. Zo wordt CFD bijvoorbeeld gebruikt voor onderzoeksdoeleinden maar ook voor diagnostiek van PA stenose en het bepalen van de behandelstrategie. In de literatuur is er een enorme verscheidenheid in de gebruikte workflow en aannames voor CFD studies. Daarnaast zijn er weinig studies beschikbaar die uitkomsten van de simulaties klinisch valideren. Dit maakt de huidige klinische toepasbaarheid en betrouwbaarheid van CFD beperkt. In deel II van dit proefschrift, **hoofdstuk 4 en 5**,

zetten we onze methode voor CFD studies uiteen. We valideren de uitkomsten van onze numerieke studies door ze te vergelijken met uitkomsten van klinische onderzoeken waaronder echocardiografie, MRI, hartkatheterisatie (hoofdstuk 4) en 4D flow MRI (hoofdstuk 5). We laten zien dat CFD studies van pulmonaal arteriën met en zonder stenose een betrouwbare indruk kunnen geven van de snelheid van de bloedstroom, de druk in het bloedvat, de gradiënt over een stenose en de distributie van bloed over de beide longen.

Deel III van dit proefschrift bevat een viertal hoofdstukken waarin klinische vraagstukken en dilemma's rondom de diagnostiek en behandeling van PA stenose verder worden uitgediept. In **hoofdstuk 6** laten we zien dat invasieve druk metingen tijdens een hartkatheterisatie vaak afwijken van niet-invasief gemeten drukken. Door de algehele anesthesie die gebruikt wordt tijdens een hartkatheterisatie daalt zowel de systemische als de pulmonale bloeddruk. Deze hypotensie kan leiden tot onderschatting van de ernst van de stenose. De hypotensieve eigenschappen van anesthetica kunnen worden tegen gegaan door het geven van epinephrine. We beschrijven onze ervaring met het geven van epinephrine tijdens hartkatheterisaties om de bloeddruk te verhogen. Het doel is om de bloeddruk van de patiënt te verhogen tot de waarde gelijk aan de non-invasieve bloeddruk meting bij de wakkere patiënt voorafgaand aan de hartkatheterisatie. In een kwart van onze patiënten zonder indicatie voor behandeling onder anesthesie, was er na de epinephrine gift wel een indicatie voor behandeling. We pleiten er dan ook voor om invasieve druk metingen onder narcose uit te voeren tijdens normotensie. In het stroomschema gepresenteerd in hoofdstuk 6, laten we zien hoe dit bereikt kan worden en wanneer epinephrine toegediend kan worden.

De combinatie van PA stenose en klep insufficiëntie in patiënten met Tetralogy van Fallot is een klinische uitdaging. Wordt de regurgitatie erger of minder erg door een stenose? En is het daarom belangrijk om een vernauwing op te heffen, of stelt de stenose juist de noodzaak van klepvervanging uit? De literatuur over dit onderwerp is inconclusief. In **hoofdstuk 7** bestuderen we aan de hand van CFD simulaties het effect van stent plaatsing bij een functionerende en bij een afwezige klep. We laten zien dat stentplaatsing regurgitatie verergert maar dat het effect grotendeels afhankelijk is van de patiënt specifieke anatomie. De casus in dit hoofdstuk zijn een mooi voorbeeld van de toegevoegde waarde van CFD bij het beoordelen van de impact van een PA stenose. CFD simulaties kunnen in dit soort casus bijdragen aan het plannen van de optimale behandeling voor de individuele patiënt.

In **hoofdstuk 8** beschrijven we de Y-stent methode voor het behandelen van complexe vernauwingen van de pulmonaal bifurcatie. Tijdens een Y-stent procedure wordt er een stent geplaatst in de pulmonaal arterie bifurcatie die uitsteekt vanuit de hoofdtak in de rechter of linker zijtak. Door ballon dilatatie van de stent struts kan een tweede stent geplaatst worden in de contralaterale tak. Deze stent methode respecteert de natuurlijke Y-vorm van de arteriële bifurcatie zonder dat de flow gesplitst wordt zoals bij de conventionele kissing stent techniek. We beschrijven het gebruik de Y-stent methode in 12 patiënten met een aangeboren hartafwijking. We laten de haalbaarheid en veiligheid van deze techniek zien en tonen aan dat een stevige connectie tussen de beide stents van belang is ter voorkoming van intima proliferatie.

De afwijkende anatomie die veroorzaakt wordt door aangeboren hartafwijkingen en de bijbehorende operatie(s) zorgt niet zelden voor een complexe anatomie waarbij de verschillende structuren in de borstholte een nauwe onderlinge relatie hebben. Indien er sprake is van een PA stenose die behandeld moet worden door middel van stent plaatsing kan dit leiden tot compressie van de luchtwegen of de aorta. Door de conventionele cilindrische stent een ovale vorm te geven, kan compressie van omliggende structuren voorkomen worden. Deze zogenaamde oval stent methode was eerder al beschreven.⁸ Er is weinig bekend over het effect van niet-ronde stents op de bloedstroom. In **hoofdstuk 9** vragen wij ons daarom af of de ovale vorm van een stent een negatieve invloed heeft op de hemodynamica van de pulmonaal arteriën. De studie in dit hoofdstuk is de eerste die laat zien dat een ovaal gevormde stent gelijke hemodynamische uitkomsten geeft als de traditionele ronde stent.

Het laatste deel van dit proefschrift bevat **hoofdstuk 10**. In dit hoofdstuk wordt de mock loop geïntroduceerd die we ontwikkeld hebben voor het uitvoeren van in-vitro studies. Dankzij deze set-up kan de hemodynamica in de pulmonaal circulatie bestudeerd worden zonder dat patiënten hiervan hinder of risico's ondervinden. Onze mock loop is uniek door de hydro-pneumatische koppeling en het uitgebreide gebruik van 3D geprinte onderdelen. Hierdoor is het systeem geheel MRI-compatibel. Hoofdstuk 10 laat zien dat de mock loop geschikt is voor het uitvoeren van een grote hoeveelheid toekomstige hemodynamische studies in een controleerbare omgeving.

CONCLUSIE

Dit proefschrift laat zien dat patiënten met PA stenose vaak uitgebreide en veelvuldige percutane interventies nodig hebben om de vernauwing te behandelen. De heterogeniteit en complexiteit van PA stenose roept om een op maat gemaakt behandelplan voor iedere individuele patiënt. Het gebruik van geavanceerde 3D beeldvorming tijdens hartkatheterisaties is gunstig voor zowel de initiële als de lange termijn uitkomsten van een interventie. Het maken van een 3DRA tijdens de procedure vermindert het risico op een re-interventie significant. CFD studies van de hemodynamica in de pulmonaal arteriën zijn een prachtige mogelijkheid om onze kennis van de oorzaken en effecten van PA stenose in aangeboren hartafwijkingen verder te vergroten. Dit geldt zowel voor de hemodynamische verstoring van een stenose in z'n algemeenheid als voor patiënt-specifieke casus waarin CFD de discussie over timing en aanpak van behandeling kan begeleiden.

REFERENCES

1. Trivedi KR, Benson LN. Interventional strategies in the management of peripheral pulmonary artery stenosis. *J Interv Cardiol.* 2003;16(2):171-188.
2. Baum D, Khoury GH, Ongley PA, Swan HJ, Kincaid OW. Congenital stenosis of the pulmonary artery branches. *Circulation.* 1964;29:680-687.
3. Hiremath G, Qureshi AM, Prieto LR, et al. Balloon angioplasty and stenting for unilateral branch pulmonary artery stenosis improve exertional performance. *JACC: Cardiovascular Interventions.* 2019;12(3):289-297.
4. Patel AB, Ratnayaka K, Bergersen L. A review: Percutaneous pulmonary artery stenosis therapy: State-of-the-art and look to the future. *Cardiol Young.* 2019;29(2):93-99.
5. Feltes TF, Bacha E, Beekman RH,3rd, et al. Indications for cardiac catheterization and intervention in pediatric cardiac disease: A scientific statement from the american heart association. *Circulation.* 2011;123(22):2607-2652.
6. Morris PD, Narracott A, von Tengg-Kobligh H, et al. Computational fluid dynamics modelling in cardiovascular medicine. *Heart.* 2016;102(1):18-28.
7. DeCampli WM, Argueta-Morales IR, Divo E, Kassab AJ. Computational fluid dynamics in congenital heart disease. *Cardiol Young.* 2012;22(6):800-808.
8. Krings GJ, van der Stelt F, Molenschot MMC, Breur JMPJ. Oval stenting in left pulmonary artery stenosis: A novel double balloon technique to prevent airway compression in single ventricle. *EuroIntervention.* 2020;15(13):1209-1215.

LIST OF PUBLICATIONS

M. Conijn, J.M.P. Breur, M.M. Molenschot, M. Voskuil, G.J. Krings. The Y-stenting technique for pulmonary artery bifurcation stenosis: Initial results and mid-term outcomes. *Int J Cardiol.* 2018;268:202-207.

M. Conijn, G. J. Krings. Computational Analysis of the Pulmonary Arteries in Congenital Heart Disease: A Review of the Methods and Results. *Comput Math Methods Med.* 2021;2021:2618625.

M. Conijn, G. J. Krings. Understanding Stenotic Pulmonary Arteries: Can Computational Fluid Dynamics Help Us Out? *Progress in Pediatric Cardiology.* 2021 sept 30 [Epub ahead of print].

M. Conijn, T.H.P.M. Dekkers, M.M. Molenschot, J.M.P. Breur, M.G. Slieker, F. Haas, G.J. Krings. To treat or not to treat pulmonary arteries? Epinephrine provocation to unmask right ventricular load. *Int J Cardiol – CHD.* 2022;7:100306.

M. Conijn, G.J. Krings. Pulmonary artery stenosis and valve insufficiency in Tetralogy of Fallot - A flow analysis pre and post treatment. Submitted.

M. Conijn, E.G. Warmerdam, J.J.M Westenberg, F. Haas, T. Leiner, J. Sotelo, S. Uribe, A.A.W. Roest, F.M. Rijnberg, H.J. Lamb, M. Voskuil, G. Krings, H.B. Grotenhuis. Flow distribution and velocity measurements in transposition of the great arteries: a comparison between computational fluid dynamics and four-dimensional flow cardiac magnetic resonance. Submitted.

M. Conijn, M.G. Slieker, T.H.P.M. Dekkers, J.M.P. Breur, M.M. Molenschot, M. Voskuil, G.J. Krings. 10-years' single center experience in percutaneous treatment of pulmonary artery stenosis in congenital heart disease: initial results, long-term outcomes and lessons learned. Submitted.

M. Conijn, G.J. Krings. The hemodynamic impact of an oval versus cylindrical stent shape to prevent compression of adjacent structures in complex pulmonary artery stenting. Submitted.

M. Conijn, L.M. Wintermans, R. Metselaar, J. Ruisch, E.A. Bax, C.A.W. van Egmond, B. Nieuwenstein, E.G. Warmerdam, G.J. Krings. A 3D printed pulmonary mock-loop system for hemodynamic studies in congenital heart disease. Submitted.

REVIEW COMMITTEE

Prof. dr. J.A. van Herwaarden
Afdeling vaatchirurgie
Universitair Medisch Centrum Utrecht, Nederland

Prof. dr. S. Schievano
Afdeling bio engineering
University college London, Groot-Brittannië

Prof. dr. D. Bonnet
Afdeling kindercardiologie
Université de Paris, Frankrijk

Prof. dr. P. van der Harst
Afdeling cardiologie
Universitair Medisch Centrum Utrecht, Nederland

Dr. F. Pluchinotta
Afdeling bio engineering
Politecnico di Milano, Italië

DANKWOORD / ACKNOWLEDGEMENTS

En zo komt er een eind aan mijn promotietraject en daarmee ook aan mijn tijd bij de kindercardiologie. Een tijd van hard werken, vallen en opstaan en heel veel nieuwe dingen leren. Ik ben dank verschuldigd aan een heleboel mensen. Met het risico om iemand te vergeten, doe ik hierbij een poging om de mensen te benoemen die belangrijk zijn (geweest) in mijn promotietraject en daar buiten. Zonder een ieder van jullie was dit alles nooit zo leuk geweest en vooral ook nooit gelukt.

Om te beginnen met mijn promotoren. Met in gedachten het verdrietige voortijdige overlijden van **Prof. dr. F. Haas († 2022)** kort na de afronding van dit proefschrift. Prof. dr. F. Haas, Felix, dank voor de vrijheid om dit traject vorm te geven en uit te voeren zoals Gregor en ik dat in gedachten hadden. Dank voor het behouden van het overzicht en het sturen op de grote lijnen. Het was altijd fijn om weer terug bij de kern te komen. **Dr. J.M.P. Breur**, Hans, dank voor het inspringen tijdens de afronding van dit traject. Zeven jaar geleden begon ik met onderzoek doen onder jouw supervisie. Dat jij in de laatste maanden ook weer betrokken was, maakt de cirkel rond.

Mijn copromotor: **dr. G.J. Krings**. Gregor, waar moet ik beginnen.. De afgelopen jaren heb ik mogen werken aan een project uit jouw koker. Ik denk dat we allebei niet helemaal wisten waar we aan begonnen. We hebben het toch maar mooi voor elkaar gekregen. Met jouw niet aflatende energie, creativiteit en vastberadenheid was er altijd weer een andere optie of een nieuwe weg. Onze gezamenlijke neiging om het beter te willen weten leverde regelmatig goede discussies op. Gelukkig heb ik altijd (vooruit, meestal...) gelijk. Dank dat je altijd vertrouwen in mij hebt. Ik ga jouw mentorschap en onze samenwerking enorm missen.

Prof. dr. J.A. van Herwaarden, Prof. dr. S. Schievano, Prof. dr. D. Bonnet, Prof. dr. P. van der Harst and dr. F. Pluchinotta, thank you for reviewing and approving this thesis. I'm grateful for such an experienced and inspiring review committee.

Zonder de financiële ondersteuning vanuit het **Suerman stipendium** had ik dit promotietraject niet kunnen beginnen. Dank dat jullie mij de beurs toevertrouwen. **Lisan van Os**, bedankt voor jouw begeleiding en de inspirerende masterclasses. Onze persoonlijke gesprekken hebben veel voor me betekend. **Paul Coffey**, dank voor het meedenken en bijsturen waar nodig tijdens de voortgangsgesprekken en daarbuiten. Mijn mede-Suermanners: **Eelco, Jasmijn, Anneloes, Mimount, Tobias**,

Wouter, Suze, Arjan, Marijke en Floris, bedankt voor alle gezelligheid, herkenning en inspiratie tijdens de masterclasses. Ik kijk uit naar ons volgende 'weekend op de hei'.

Alle kindercardiologen en thorax chirurgen in het WKZ (die nog niet genoemd zijn): **Mirella Molenschot, Christiaan Blank, Heynric Grotenhuis, Martijn Sliker** (dank voor jouw statistische hulp!), **Gabriëlle van Iperen, Trinette Steenhuis, Henriëtte ter Heide, Lianne Geerdink, Kim ten Dam, Henk Schipper, Paul Schoof, Bram van Wijk, Hanna Talacua**. Toen ik als student op de afdeling begon, eerst voor een onderzoeksstage en later ook in de kliniek, voelde ik me direct thuis. Dank voor jullie gezelligheid en interesse over de afgelopen jaren.

Mijn mede-onderzoekers bij de kindercardiologie. **Rinske**, wat was het fijn om jou als collega te hebben. Ik mis nog steeds onze koffietjes en lunches met een goed gesprek en de nodige humor. **Evangeline**, dank voor de fijne samenwerking en gezelligheid. **Femke**, met jou als collega weet je altijd precies wat er speelt en waar je moet zijn. Super leuk dat we nu bijna tegelijk ons boekje hebben afgerond. **Renee**, bedankt voor jouw gezelschap de laatste maanden. Veel succes de komende jaren met jouw project.

Veel dank ben ik verschuldigd aan de verschillende studenten die hebben meegewerkt aan mijn projecten. Niet alleen voor het harde werken, maar ook voor de gezelligheid. **Lieke, Rutger, Eva, Janna en Carmen**, dank voor jullie hulp bij het bouwen van de pomp. Naast alle uitdagingen die dit project met zich meebracht heeft het ook veel lol opgeleverd als we moesten rennen voor het water. **Dorita**, dank voor jouw hulp bij het opzetten van de database die de basis vormde voor twee hoofdstukken van dit proefschrift.

Het ontwerpen en bouwen van de mock loop was nooit succesvol geweest zonder de hulp van de medische technologie in het WKZ en het UMC en in het bijzonder van **Ben Nieuwenstein**. Dank voor jouw praktische en theoretische ondersteuning en het meedenken in netwerk en materialen.

Dank aan de **perfusionisten in het UMC** voor het iedere keer weer uitlenen van de flowmeters voor het testen van de mock loop.

Simona Boessenkool en **Hanneke Bosveld-Heijt**, dank voor jullie praktische ondersteuning waar nodig en het goochelen met agenda's om een gaatje te vinden voor besprekingen.

Prof. dr. J. Frenkel. Joost, jij was degene die mij na mijn coschap kindergeneeskunde aanmoedigde om onderzoek te gaan doen bij de kindercardiologie. Een schot in de roos. Dank ook voor de kans om vanuit de geneeskundeopleiding als ANIOS aan de slag te gaan in het WKZ en de enorm leerzame en inspirerende tijd die dit heeft opgeleverd. **Kinderartsen en arts-assistenten WKZ**, dank voor jullie begeleiding, collegialiteit en gezelligheid tijdens mijn ANIOS tijd in het WKZ.

Samen begonnen aan de studie, ruim 10 jaar verder en nog steeds super dankbaar voor onze vriendschap: **Nanda, Hanneke, Willemijn en Nienke**. Ver weg of dichtbij, lang niet gezien of elkaar iedere dag spreken: het blijft als vanouds.

Joyce, we go way back. Dankjewel voor onze vriendschap, die is me heel veel waard. **Anke**, buuf, zigzag raakt nooit uit de mode. Wat is het bijzonder als je elkaar al zolang kent en samen bent opgegroeid. **Mara**, never a dull moment met Mara in de buurt. Het is altijd weer een feest met jouw energie en drive. **Charlotte**, dankjewel voor jouw vriendschap, dat je altijd klaar staat voor een goed advies en met een luisterend oor. **Barberieke**, mijn 'kroonvriendin'. Ik ben super dankbaar dat we elkaar al zolang in het vizier houden. Wat zijn we van ver gekomen!

Anne-Rose, Karel, Roderick, Valerie, Steve, Mia en Evie, liefste schoonfamilie, bedankt dat jullie er zijn en voor alle gezelligheid. Wat is het toch een luxe om in Zeeland te kunnen uitwaaien!

Mijn schoonzusjes, **Hilde** en **Nathalie**, bedankt voor jullie gezelligheid en interesse. **Jan** en **Bas**, lieve broeders, mijn paranimfen. Ik ben zó trots dat jullie straks achter me staan tijdens mijn verdediging. Ik had me geen betere ondersteuning kunnen wensen. Dankjewel dat jullie er altijd voor me zijn en dat we elkaar steeds weer weten te vinden.

Mijn ouders, bedankt dat jullie altijd 100 procent achter me staan. Zonder jullie basis en jullie vertrouwen had ik dit alles nooit kunnen doen. **Mijn vader**, mijn held, die we vlak voor de start van dit traject zo plots moesten verliezen en die ik zo immens mis. Dank voor alles wat je me hebt gegeven. **Mijn moeder**, mijn heldin, die altijd en

overal voor mij en voor ons klaarstaat en die zo ontzettend sterk is. Dankjewel voor alles wat je bent en doet.

En dan mijn gezin. Jullie zijn me alles waard. Lieve, allerliefste **Hugo**, met jou erbij is alles leuker. Dankjewel dat ik jouw mama mag zijn. Je bent mijn grote trots. **Wijnand**, mijn liefde. Samen staan we sterk. Dankjewel dat jij, jij bent. Jouw rol tijdens dit traject mag niet onderschat worden. Bij jou kom ik thuis.

CURRICULUM VITAE

Maartje Conijn was born on the 19th of June, 1991, in Sint-Oedenrode, the Netherlands. With two brothers, she grew up in Son en Breugel. She attended secondary education at the Eckart College in Eindhoven from which she graduated in 2009. After finishing the AALO courses on physical training and exercise, she started medical school at the Utrecht University in 2011. At the end of the first year she developed a special interest in cardiology and started doing research at the department of cardiology. Here, she studied the pathology of heart failure in patients after myocardial infarction. Before starting her medical internships, she paused her study to be on the executive committee of the KNMG Studentenplatform (national representation of the Dutch medical students). After this year of fulltime management she started her clinical internships. Enthusiastic after an inspiring pediatric internship she continued her research ambitions at the pediatric cardiology department under supervision of Hans Breur and Gregor Krings. Here, the interventional cardiology, advanced imaging and the complexity of pediatric cardiology stole her heart. During the last year of medical school she spent 6 months at the pediatric cardiology department for both clinical and research internships. Together with Gregor Krings, she wrote a research proposal and applied for the Alexander Suerman Stipendium. She was granted the scholarship which provided the opportunity for continuation of her research during a PhD. Before starting her PhD she gained clinical experience as a pediatric resident (not in training) at the Wilhelmina Children's Hospital. In October 2018 she started her PhD resulting in the work presented in this thesis.

